Modeling of Saturated Cylindrical-Rotor Synchronous Machines

A Thesis

Submitted to the College of Graduate Studies and Research

in Partial Fulfillment of the Requirements

For the Degree of

Master of Science

in the Department of Electrical Engineering

University of Saskatchewan

Saskatoon, Saskatchewan

by

Elemer Demeter

July 1998

Permission To Use

In presenting this thesis in partial fulfillment of the requirements for a Postgraduate degree from the University of Saskatchewan, the author has agreed that the Libraries of this University may make it freely available for inspection. The author further has agreed that permission for copying of this thesis in any manner, in whole or in part, for scholarly purposes may be granted by the professor or professors who supervised this thesis work or, in their absence, by the Head of the Department or the Dean of the College in which this thesis work was done. It is understood that any copying or publication or use of this thesis or parts thereof for financial gain shall not be allowed without the author's written permission. It is also understood that due recognition shall be given to the author and to the University of Saskatchewan in any scholarly use which may be made of any material in this thesis.

Request for permission to copy or to make other use of material in this thesis in whole or part should be addressed to:

Head of the Department of Electrical Engineering
University of Saskatchewan
57 Campus Drive
Saskatoon, Saskatchewan, Canada
S7N 5A9

Abstract

It has been recognized recently that the magnetic coupling between the direct and quadrature axes of saturated synchronous machines (cross-magnetizing phenomenon) plays an important role in their analysis using the two-axis frame models. To determine the parameters which represent this cross-magnetizing effect, the machine saturation curves in the various intermediate axes are needed.

If a synchronous machine has two windings: one in the direct axis and the other in the quadrature axis, saturation curves in the intermediate axes can be obtained by exciting the machine from both these windings simultaneously under open-circuited condition. However, there is usually no field winding in the quadrature axis of industrial synchronous machines and, thus, the saturation curves in the intermediate axes cannot be obtained by the open-circuit test. This thesis presents an analytical method for determining the saturation curves in the intermediate axes of cylindrical-rotor synchronous machines from their measured d- and q-axis saturation curves. The accuracy of this method is verified by comparing the measured saturation curves in the intermediate axes of a specially-designed cylindrical-rotor synchronous machine, which has d- and q-axis field windings, with those calculated using the proposed method. The thesis also presents a method for determining the parameters representing the cross-magnetizing effect from the calculated intermediate-axis saturation curves of synchronous machines. By applying these methods also to the cases of salient-pole synchronous machines, their generality is demonstrated.

Moreover, a modified two-axis frame model of saturated synchronouns machines which includes the cross-magnetizing effect is presented in this thesis. The accuracy of this modified model is verified by comparing the measured active and reactive power/load angle curves of a cylindrical-rotor and a salient-pole synchronous generators with the curves obtained analytically by applying the proposed modified two-axis frame model.

Acknowledgements

The author would like to express his gratitude to Dr. A.M. El-Serafi for his continuous guidance and encouragement during this research. Without his support, this work would not have been possible.

Financial assistance provided by the Natural Sciences and Engineering Research Council of Canada under Grant No. OGP0007115 is thankfully acknowledged.

Table Of Contents

List of Tables

List of Figures

List of Symbols

AT	ampere-turns
AT_d	d-axis ampere-turns
AT_q	q-axis ampere-turns
AT_d^b	base value of the d-axis ampere-turns
AT_q^b	base value of the q-axis ampere-turns
B	air-gap magnetic flux-density
B_1	fundamental component of the air-gap magnetic flux density
B_d	amplitude of the d-axis component of B_1
B_q	amplitude of the q-axis component of B_1
E_f	electromotive force produced by the field winding
E_{qd}	reduction in the induced e.m.f. due to Φ_{dq}
E_{dq}	reduction in the induced e.m.f. due to Φ_{qd}
F	magnetomotive force
I_a	armature current
I_a^b	base value of the armature current
I_d	d-axis component of the armature current
I_q	q-axis compoment of the armature current
I_{fd}^b	base value of the d-axis field current
I_{fq}^b	base value of the q-axis field current
I_f	field current
K	generic saturation factor

K_d	d-axis saturation factor
K_q	q-axis saturation factor
N_d	effective number of turns of the d-axis field winding
N_q	effective number of turns of the q-axis field winding
P	active power
Q	reactive power
R_a	armature resistance
S_b	base value of power
S_d	saturation function in the unslotted areas
S_q	saturation function in the slotted areas
V_t	terminal voltage
V_{td}	d-axis component of the terminal voltage
V_{tq}	q-axis component of the terminal voltage
V_t^b	base value of the terminal voltage
Z_b	impedance base value
X_d	d-axis synchronous reactance
X_{du}	unsaturated d-axis synchronous reactance
X_{ds}	saturated d-axis synchronous reactance
X_q	q-axis synchronous reactance
X_{qu}	unsaturated q-axis synchronous reactance
X_{qs}	saturated q-axis synchronous reactance
X_{md}	d-axis mutual reactance
X_{mdu}	unsaturated d-axis mutual reactance
X_{mds}	saturated d-axis mutual reactance
X_{mq}	q-axis mutual reactance
X_{mqu}	unsaturated q-axis mutual reactance
X_{mqs}	saturated q-axis mutual reactance

X_l leakage reactance

X_p Potier reactance

k_B constant dependent on the machine dimensions

k_Φ constant dependent on the machine dimensions

m number of measured points

α constant used to modify the equivalent permeability values

α_{0d} slope of the d-axis open-circuit characteristic

α_{0q} slope of the q-axis open-circuit characteristic

α_{dsc} slope of the d-axis short-circuit characteristic

α_{qsc} slope of the q-axis short-circuit characteristic

β the ratio of the unslotted region width over one pole to the pole pitch

δ load angle

δ' angle between the air-gap magnetic flux and direct axis

ϵ average error per measurement

μ equivalent permeability

θ displacement angle from the pole axis to a point in the air-gap

ζ angle between the air-gap magnetic flux and direct axis

Φ magnetic flux

Φ_d air-gap magnetic flux when the machine is excited from its direct axis only

Φ_{du} unsaturated value of Φ_d

Φ_{ds} saturated value of Φ_d

Φ_f flux produced by the excitation current

Φ_j measured values of the air-gap magnetic flux

Φ_j^c calculated values of the air-gap magnetic flux

Φ_R resultant air-gap magnetic flux

Φ_{Rd} d-axis component of Φ_R

Φ_{Rq} q-axis component of Φ_R

Φ_t total air-gap magnetic flux

Φ_{td} d-axis component of Φ_t

Φ_{tq} q-axis component of Φ_t

Φ_q air-gap magnetic flux when the machine is excited from its quadrature axis only

Φ_{qu} unsaturated value of Φ_q

Φ_{qs} saturated value of Φ_q

Φ_{dq} d-axis cross-magnetizing effect

Φ_{qd} q-axis cross-magnetizing effect

List of Abbreviations

c.m.e.	cross-magnetizing effect
e.m.f.	electromotive force
e.m.fs.	electromotive forces
m.m.f.	magnetomotive force
m.m.fs.	magnetomotive forces
o.c.c.c.	open-circuit characteristic curve
o.c.c.cs.	open-circuit characteristic curves
s.c.c.c.	short-circuit characteristic curve
s.c.c.cs.	short-circuit characteristic curves
z.p.f.c.	zero-power-factor characteristic

Chapter 1

Introduction

1.1 General

During the last few decades, the tendency to exploit the available sources of electrical energy at maximum level has increased. To achieve this, the accurate determination of the characteristics of the electrical energy sources, i.e. synchronous generators, has become of paramount importance.

The characteristics of synchronous generators are affected by many factors. Among these factors is the saturation of the iron paths of the machines [1-6]. Under saturated operation, the machine parameters are no longer constant, but dependent on the loading conditions [2, 7, 8]. Power system researchers have concluded that the saturation in synchronous generators is one of the most important causes for the changes in the machine's behavior [9, 10, 11]. An accurate and reliable representation of the saturation phenomena in synchronous generator models can thus help in the prediction of their accurate operating characteristics [12, 13, 14]. Moreover, this can be useful

during the design process of the generators and their excitation systems.

1.2 Methods of representing saturation in synchronous machine models

The choice of the models for investigating the performance of saturated synchronous machines depends to a large extent on the objectives of the investigation. If, for example, the purpose of the investigation is to determine the magnetic flux distribution in specific parts of the machine's magnetic circuit (air-gap, armature, teeth), complex models are usually required, and the time consuming finite difference or finite element approaches have to be applied [15]. On the other hand, the analysis of large power systems involving large number of generators need models which are simple, efficient in computing time, and yet, sufficiently accurate [2, 16].

1.3 The two-axis frame model

In the analysis of synchronous generators and power systems, the two-axis frame models, represented by the phasor diagram of Fig.(1.1), are commonly used [12, 13, 17]. In such a model, it is usually assumed that there is no magnetic coupling between the direct and the quadrature axes and thus, each axis has its own electro-magnetic relationships. Also, in these models, it is assumed that the saturation affects only the mutual flux paths while the leakage flux paths are not affected by it [18]. Based on these assumptions, various models of saturated synchronous machines have been proposed. In all of these models, the saturation is basically represented by modifying

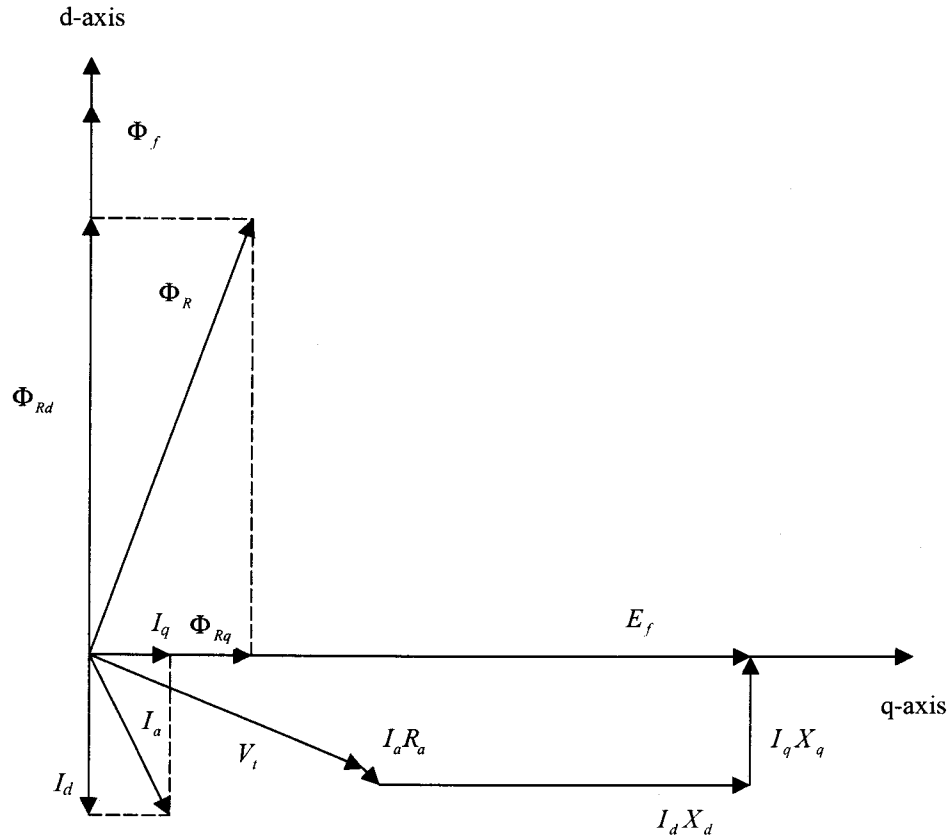

Figure 1.1: Phasor diagram of a synchronous generator

the machine's synchronous reactances. These synchronous reactances can be written as:

$$X_d = X_{md} + X_l \tag{1.1}$$

$$X_q = X_{mq} + X_l \tag{1.2}$$

where X_d and X_q are the d- and q-axis synchronous reactances, X_{md} and X_{mq} are the corresponding mutual reactances, and X_l is the leakage reactance. The saturated

values of the d- and q-axis synchronous reactances, X_{ds} and X_{qs}, can be expressed as follows:

$$\begin{aligned} X_{ds} &= X_{mds} + X_l \\ &= K_d X_{mdu} + X_l \end{aligned} \tag{1.3}$$

$$\begin{aligned} X_{qs} &= X_{mqs} + X_l \\ &= K_q X_{mqu} + X_l, \end{aligned} \tag{1.4}$$

where X_{mds} and X_{mqs} are the saturated d- and q-axis mutual reactances, X_{mdu} and X_{mqu} are the unsaturated d- and q-axis mutual reactances, and K_d and K_q are the d- and q-axis saturation factors, respectively.

The values of the saturation factors K_d and K_q are obtained from the relationships between the ampere-turns AT and the magnetic flux Φ for the direct and quadrature axes, respectively. In both axes, the relationship between Φ and AT has similar variation, and can be depicted as in Fig.(1.2). For each axis, the value of the unsaturated mutual reactance X_{mu} is proportional to the slope of the air-gap line AC of the respective axis. With a well designed per-unit system, the value of the unsaturated synchronous reactance X_{mu} in p.u. can be made equal to the slope of this line:

$$X_{mu} = \frac{CF}{AF}, \tag{1.5}$$

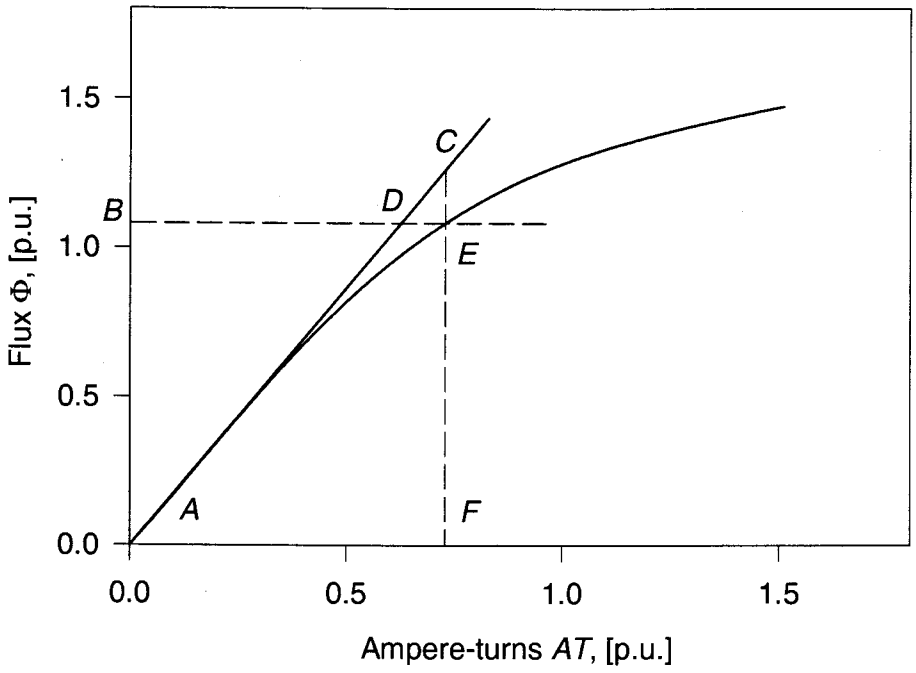

Figure 1.2: Defining the saturation factors using the saturation curves

and its saturated value can be expressed as follows:

$$X_{ms} = \frac{EF}{AF}. \tag{1.6}$$

From Eqs(1.3) to (1.6), the following relationships can be obtained:

$$X_{ms} = X_{mu}\frac{EF}{CF}, \tag{1.7}$$

$$K = \frac{EF}{CF}. \tag{1.8}$$

It can be also found from Fig.(1.2) that the saturation factor K can also be expressed

as follows:

$$K = \frac{BD}{BE}. \tag{1.9}$$

The differences between all the two-axis frame models of saturated synchronous machines, which have been used till recently, are related to the choice of the values of these saturation factors.

For the cases of saturated salient-pole synchronous machines, several researchers have assumed that the saturation in the quadrature axis is negligible, i.e. $K_q = 1$, and only the direct axis saturation is to be taken into account [5, 13]. However, several other researchers do not agree with this assumption since it leads usually to inaccurate results [4, 19]. In fact, experiments have shown that the quadrature axis saturated in certain salient-pole synchronous machines at least as much, and even more, as the direct axis [20, 21]. For the cases of saturated cylindrical-rotor synchronous machines, the assumption of neglecting the saturation in the quadrature axis is in general not valid. If the q-axis saturation curves are not available, it is usually assumed that $K_q = K_d$. In reference [4], polynomial representations have been derived for K_d and K_q as a function of the total air-gap magnetic flux and it was found that, for different sized machines, the changes of these saturation factors have similar patterns as depicted in Fig.(1.3). As this figure shows, there are noticeable differences between the values of K_d and K_q in the saturated region. In more recent papers [19], it has been found that, instead of using the total air-gap magnetic flux as a factor which determines the saturation level, it is more convenient to use the total ampere-turns.

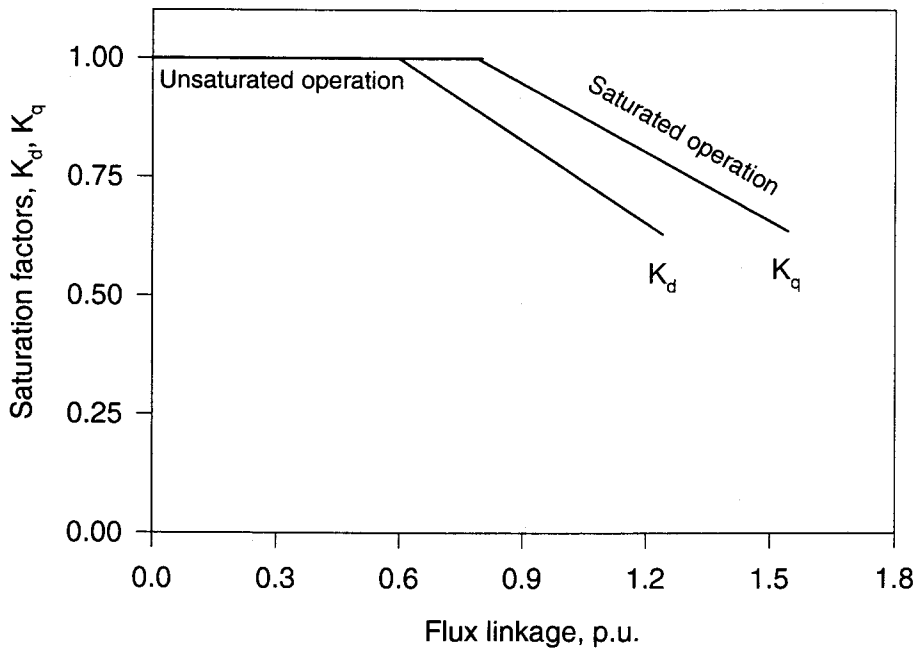

Figure 1.3: Saturation factors as functions of the flux linkage

Other researchers [13, 16, 22] have defined the polynomials representing K_d and K_q using only the d- and q-axis components of the total air-gap magnetic flux or of the total ampere-turns, respectively. As it has been proven [7, 8], this approach can lead to considerable discrepancies between the measured and calculated operating characteristics.

1.4 The cross-magnetizing phenomenon

In the classical two-axis frame model representation of synchronous machines, the assumption is made that there is no magnetic coupling between their direct and quadrature axes [23]. However, experiments [16, 19] and magnetic field plotting [15, 24] have

shown that a magnetic coupling between the direct and quadrature axes of saturated synchronous machines exists, and that the magnitude of this coupling depends on how the saturation phenomena are modeled. Due to this magnetic coupling, the d- and q-axis components of the air-gap magnetic flux are affected by both the ampere-turns in the direct and quadrature axes. This magnetic coupling effect is usually called in the literature as the cross-magnetizing phenomenon [7, 8, 25].

In general, this cross-magnetizing phenomenon is the result of two causes [19]. One of the causes is the difference between the saturation levels in the axis of the total air-gap ampere-turns and those in the direct and quadrature axes. The magnetic saliency in the synchronous machines is the second cause for this phenomenon. In the cases of cylindrical-rotor synchronous machines, the cross-magnetizing effect is mainly due to the first cause while, in the case of salient-pole synchronous machines, the magnetic saliency has a relatively larger contribution to this effect.

1.5 The objectives of the thesis

Researchers have recognized for some time that the two saturation factors approach does not represent adequately the saturation effect in synchronous machine models. Using this approach, discrepancies up to 21 percent have been reported between the measured and calculated power/load angle characteristics of synchronous generators [12, 19, 26]. Since the two-axis approach to synchronous machines modeling is a widely used procedure, any modification aimed to improve the accuracy of these

models should still be made in the same d- and q-axis frame in order to maintain their previously used mathematical representation.

In an attempt to obtain more accurate representation of saturation in the two-axis frame models of synchronous machines, El-Serafi et. al. [7, 8] have introduced two new parameters to represent the cross-magnetizing phenomenon. For determining these parameters, the saturation curves in the intermediate axes of synchronous machines and the corresponding phase angles of the total magnetic fluxes are needed. Since this information cannot be obtained experimentally for industrial synchronous machines, Wu [18] has proposed an analytical approach for determining such information for salient-pole synchronous machines from their measurable d- and q-axis saturation curves. In his approach, an equivalent permeability magnetic model for the salient-pole synchronous machines has been used to determine the intermediate-axis saturation curves and the phase angles of the total air-gap magnetic fluxes of these machines. However, this magnetic model does not represent the magnetic relationships in the cylindrical-rotor synchronous machines and, thus, cannot be used in the cases of these types of machines.

In this context, the main objectives of this thesis are focused on the following aspects:

- To obtain a new magnetic model which could be used to calculate the intermediate-axis saturation curves and the phase angles of the total magnetic fluxes of cylindrical-rotor synchronous machines;

- To verify experimentally the accuracy of this model;
- To determine the parameters representing the cross-magnetizing phenomenon in cylindrical-rotor synchronous machines using this developed model, and to verify the accuracy of these parameters using measured results;
- To modify the two-axis frame model of cylindrical-rotor machines to include the cross-magnetizing effect;
- To verify the accuracy of the modified two-axis frame model for the cases of cylindrical-rotor synchronous generators;
- To verify if the proposed magnetic model is also applicable to the cases of salient-pole synchronous generators.

Chapter 2

Saturation curves in the intermediate axes of cylindrical-rotor synchronous machines

As mentioned in Chapter 1, the intermediate-axis saturation curves of saturated synchronous machines and the corresponding angles of the magnetic fluxes are needed to determine the parameters representing the cross-magnetizing effect. However, these saturation curves and the angles of the magnetic fluxes cannot be obtained experimentally, unless the synchronous machine has also an auxiliary excitation winding in its interpole axis (i.e. quadrature axis). In this chapter, an analytical method for determining the saturation curves in the intermediate axes of cylindrical-rotor synchronous machines from their measured d- and q-axis saturation curves will be presented. This method allows also for the determination of the angles of the total air-gap magnetic fluxes. The method is so general that it can be also applied to the cases of salient-pole synchronous machines.

2.1 Description of the method

In the proposed method, an equivalent permeability is used for the magnetic paths of the synchronous machine. Moreover, considering the rotor structure of cylindrical-

rotor synchronous machines (Fig.(2.1)), it is assumed that, under unsaturated condition, the equivalent permeability along the rotor periphery has the form shown in Fig.(2.2), where μ is the value of the equivalent permeability between $\theta = -\beta\frac{\pi}{2}$ and $\theta = \beta\frac{\pi}{2}$ corresponding to the unslotted region of the rotor, and $\alpha\mu$ is the value of the equivalent permeability between $\theta = -\frac{\pi}{2}$ and $\theta = -\beta\frac{\pi}{2}$ and between $\theta = \beta\frac{\pi}{2}$ and $\theta = \frac{\pi}{2}$ corresponding to the slotted region of the rotor. The equivalent permeability under one pole pitch can thus be expressed mathematically as:

$$\mu(\theta) = \begin{cases} \mu & \text{for } -\beta\frac{\pi}{2} < \theta < \beta\frac{\pi}{2} \\ \alpha\mu & \text{for } -\frac{\pi}{2} < \theta < -\beta\frac{\pi}{2} \text{ and } \beta\frac{\pi}{2} < \theta < \frac{\pi}{2} \end{cases} \tag{2.1}$$

Under saturated condition, the values of the equivalent permeabilities along the rotor periphery are obtained by modifying their unsaturated values by using appropriate saturation functions. For cylindrical-rotor synchronous machines, the saturation can adequately be represented by two saturation functions $S_d(\theta)$ and $S_q(\theta)$. The saturation function $S_d(\theta)$ represents the saturation in the unslotted region of the rotor, while the saturation function $S_q(\theta)$ represents the saturation in the slotted region of the rotor. Thus, the saturation functions can be represented as follows:

$$S(\theta) = \begin{cases} S_d(\theta) & \text{for } -\beta\frac{\pi}{2} < \theta < \beta\frac{\pi}{2} \\ S_q(\theta) & \text{for } -\frac{\pi}{2} < \theta < -\beta\frac{\pi}{2} \text{ and } \beta\frac{\pi}{2} < \theta < \frac{\pi}{2} \end{cases} \tag{2.2}$$

The value of the saturation function $S(\theta)$ at a given point θ away from the pole axis depends on the value of the total ampere-turns $F(\theta)$ at this point. A polynomial representation of this saturation function is a convenient way to represent this

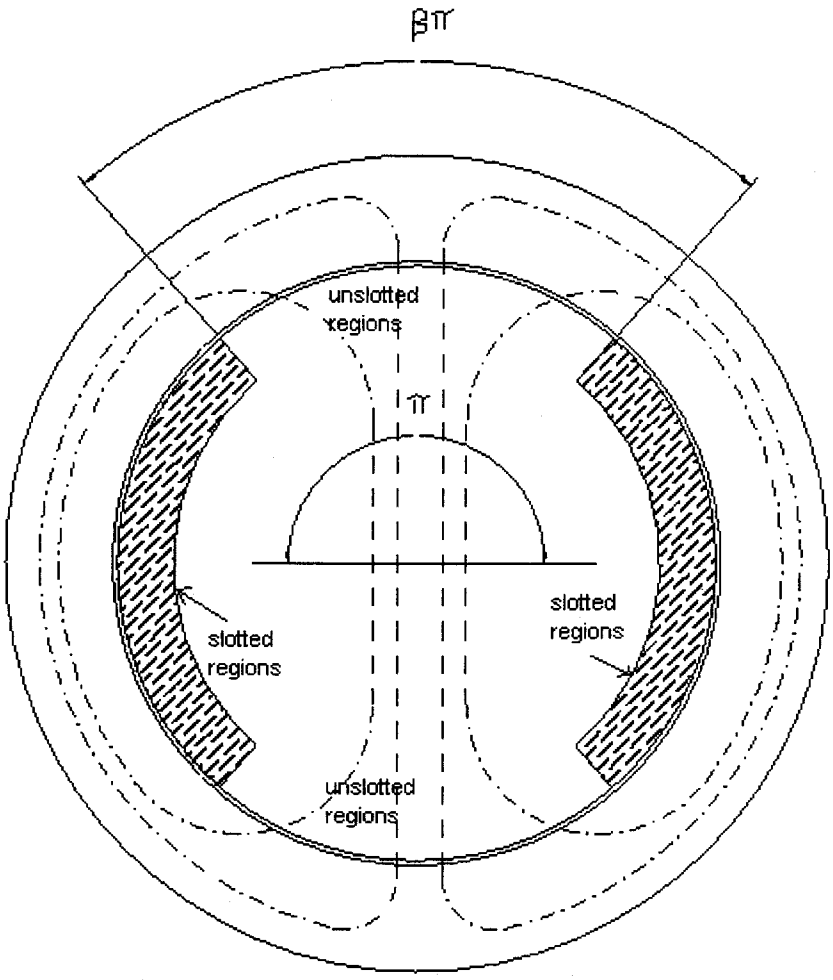

Figure 2.1: Rotor structure of a cylindrical-rotor synchronous machine

dependency. Under this assumption, the saturation function can be written as:

$$S(\theta) = \begin{cases} 1.00 - \sum_{i=1}^{n} a_{id} |F(\theta)|^i & \text{for} \quad -\beta\frac{\pi}{2} < \theta < \beta\frac{\pi}{2} \\ 1.00 - \sum_{i=1}^{n} a_{iq} |F(\theta)|^i & \text{for} \quad -\frac{\pi}{2} < \theta < -\beta\frac{\pi}{2} \text{ and } \beta\frac{\pi}{2} < \theta < \frac{\pi}{2} \end{cases} \tag{2.3}$$

where a_{id} and a_{iq} have constant values for a given machine.

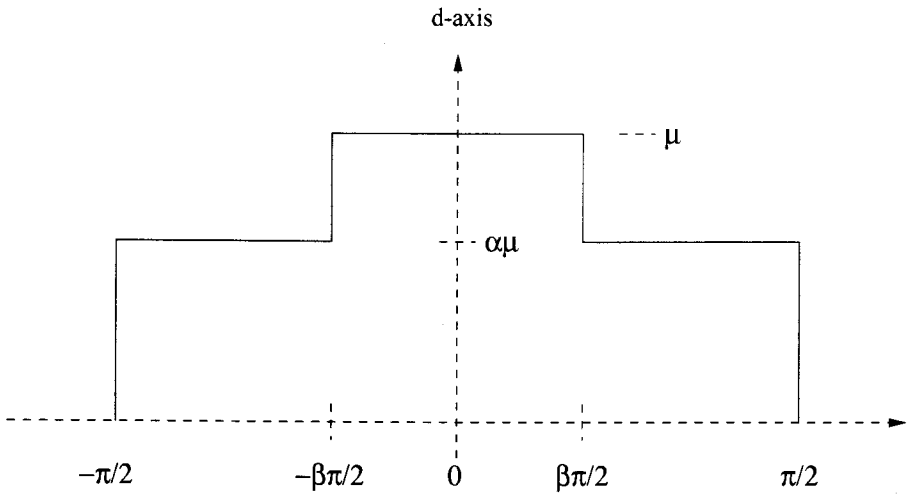

Figure 2.2: Equivalent permeability model of a cylindrical-rotor synchronous machine

2.2 Equations of the components of the air-gap magnetic flux

Using Eqs.(2.1) and (2.3), the air-gap magnetic flux density at any point θ can be calculated from the following equation:

$$B(\theta) = k_B F(\theta) S(\theta) \mu(\theta), \tag{2.4}$$

where k_B is a constant which is dependent on the machine dimensions. In synchronous machine studies, it is customary to assume that only the fundamental components of the involved electro-magnetic values will determine the operating conditions. The fundamental component of the magnetic flux density can be written as:

$$B_1(\theta) = B_d \cos(\theta) + B_q \sin(\theta), \tag{2.5}$$

where B_d and B_q are the amplitudes of the fundamental d- and q-axis components of the air-gap magnetic flux density. These d- and q-axis components can be calculated

by applying the Fourier series analysis to Eq.(2.4) as follows:

$$\begin{aligned} B_d &= \frac{2}{\pi}\int_{-\frac{\pi}{2}}^{\frac{\pi}{2}} B(\theta)\cos(\theta)d\theta \\ &= \frac{2}{\pi}\int_{-\frac{\pi}{2}}^{\frac{\pi}{2}} k_B F(\theta)S(\theta)\mu(\theta)\cos(\theta)d\theta \end{aligned} \tag{2.6}$$

$$\begin{aligned} B_q &= \frac{2}{\pi}\int_{-\frac{\pi}{2}}^{\frac{\pi}{2}} B(\theta)\sin(\theta)d\theta \\ &= \frac{2}{\pi}\int_{-\frac{\pi}{2}}^{\frac{\pi}{2}} k_B F(\theta)S(\theta)\mu(\theta)\sin(\theta)d\theta \end{aligned} \tag{2.7}$$

Assuming also that the ampere-turns distribution over one pole pitch is sinusoidal, $F(\theta)$ can be expressed as follows:

$$F(\theta) = AT \cdot \cos(\theta - \zeta), \tag{2.8}$$

where AT is the amplitude of the ampere-turns distribution function and ζ is the angle between the axis of the ampere-turns distribution function and the direct axis. If the axis of the ampere-turns distribution function is located in the direct axis, i.e. $\zeta = 0$, Eq.(2.8) becomes:

$$F(\theta) = AT \cdot \cos(\theta - 0) = AT \cdot \cos(\theta). \tag{2.9}$$

If the axis of the total ampere-turns distribution function is located in the quadrature axis ($\zeta = \frac{\pi}{2}$), Eq.(2.8) becomes:

$$F(\theta) = AT \cdot \cos(\theta - \frac{\pi}{2}) = AT \cdot \sin(\theta). \tag{2.10}$$

2.2.1 The d-axis component of the air-gap magnetic flux

The d-axis component of the air-gap magnetic flux can be calculated using Eq.(2.6) as follows:

$$\begin{aligned} \Phi_d &= k_\Phi B_d \\ &= \frac{2}{\pi} \int_{-\frac{\pi}{2}}^{\frac{\pi}{2}} k_B k_\Phi F(\theta) S(\theta) \mu(\theta) \cos(\theta) d\theta \end{aligned} \tag{2.11}$$

Substituting Eqs.(2.1) and (2.2) in Eq.(2.11), Φ_d can be subsequently written:

$$\begin{aligned} \Phi_d &= \frac{2}{\pi} \int_{-\frac{\pi}{2}}^{-\beta\frac{\pi}{2}} k_B k_\Phi F(\theta) S_q(\theta) \alpha\mu \cos(\theta) d\theta \\ &+ \frac{2}{\pi} \int_{-\beta\frac{\pi}{2}}^{\beta\frac{\pi}{2}} k_B k_\Phi F(\theta) S_d(\theta) \mu \cos(\theta) d\theta \\ &+ \frac{2}{\pi} \int_{\beta\frac{\pi}{2}}^{\frac{\pi}{2}} k_B k_\Phi F(\theta) S_q(\theta) \alpha\mu \cos(\theta) d\theta \end{aligned} \tag{2.12}$$

Since k_B, k_Φ and μ have constant values for a given machine, they can be grouped as a single constant value:

$$k = k_B k_\Phi \mu. \tag{2.13}$$

With the newly introduced factor k, Φ_d becomes:

$$\begin{aligned}
\Phi_d &= \frac{2}{\pi} k\alpha \int_{-\frac{\pi}{2}}^{-\beta\frac{\pi}{2}} F(\theta) S_q(\theta) \cos(\theta) d\theta \\
&+ \frac{2}{\pi} k \int_{-\beta\frac{\pi}{2}}^{\beta\frac{\pi}{2}} F(\theta) S_d(\theta) \cos(\theta) d\theta \\
&+ \frac{2}{\pi} k\alpha \int_{\beta\frac{\pi}{2}}^{\frac{\pi}{2}} F(\theta) S_q(\theta) \cos(\theta) d\theta
\end{aligned} \tag{2.14}$$

Substituting Eqs.(2.3) and (2.8) in Eq.(2.14), the d-axis component of the air-gap magnetic flux can be written as:

$$\begin{aligned}
\Phi_d &= \frac{2}{\pi} k\alpha \int_{-\frac{\pi}{2}}^{-\beta\frac{\pi}{2}} AT\cos(\theta-\zeta) \left(1.00 - \sum_{i=1}^{n} a_{iq} |AT\cos(\theta-\zeta)|^i\right) \cos(\theta) d\theta \\
&+ \frac{2}{\pi} k \int_{-\beta\frac{\pi}{2}}^{\beta\frac{\pi}{2}} AT\cos(\theta-\zeta) \left(1.00 - \sum_{i=1}^{n} a_{id} |AT\cos(\theta-\zeta)|^i\right) \cos(\theta) d\theta \\
&+ \frac{2}{\pi} k\alpha \int_{\beta\frac{\pi}{2}}^{\frac{\pi}{2}} AT\cos(\theta-\zeta) \left(1.00 - \sum_{i=1}^{n} a_{iq} |AT\cos(\theta-\zeta)|^i\right) \cos(\theta) d\theta
\end{aligned} \tag{2.15}$$

Equation (2.15) can be simplified to:

$$\Phi_d = \left(\alpha I_{0q}^d + I_{0d}^d\right) AT - \sum_{i=1}^{n} AT^{i+1}\left(\alpha a_{iq} I_{iq}^d + a_{id} I_{id}^d\right) \tag{2.16}$$

where:

$$\begin{aligned} I_{0q}^d &= \frac{2}{\pi} k \int_{-\frac{\pi}{2}}^{-\beta\frac{\pi}{2}} \cos(\theta-\zeta)\cos(\theta)d\theta \\ &\quad + \frac{2}{\pi} k \int_{\beta\frac{\pi}{2}}^{\frac{\pi}{2}} \cos(\theta-\zeta)\cos(\theta)d\theta \end{aligned} \tag{2.17}$$

$$I_{0d}^d = \frac{2}{\pi} k \int_{-\beta\frac{\pi}{2}}^{\beta\frac{\pi}{2}} \cos(\theta-\zeta)\cos(\theta)d\theta \tag{2.18}$$

$$\begin{aligned} I_{iq}^d &= \frac{2}{\pi} k \int_{-\frac{\pi}{2}}^{-\beta\frac{\pi}{2}} \cos(\theta-\zeta)|\cos(\theta-\zeta)|^i \cos(\theta)d\theta \\ &\quad + \frac{2}{\pi} k \int_{\beta\frac{\pi}{2}}^{\frac{\pi}{2}} \cos(\theta-\zeta)|\cos(\theta-\zeta)|^i \cos(\theta)d\theta \end{aligned} \tag{2.19}$$

$$I_{id}^d = \frac{2}{\pi} k \int_{-\beta\frac{\pi}{2}}^{\beta\frac{\pi}{2}} \cos(\theta-\zeta)|\cos(\theta-\zeta)|^i \cos(\theta)d\theta \tag{2.20}$$

2.2.2 The q-axis component of the air-gap magnetic flux

Using Eq.(2.7) and applying the same approach as for the d-axis component of the air-gap magnetic flux, the q-axis component of the air-gap magnetic flux can be written

as:

$$\begin{aligned}
\Phi_q &= \frac{2}{\pi}k\alpha\int_{-\frac{\pi}{2}}^{-\beta\frac{\pi}{2}} AT\cos(\theta-\zeta)\left(1-\sum_{i=1}^{n}a_{iq}|AT\cos(\theta-\zeta)|^i\right)\sin(\theta)d\theta \\
&\quad +\frac{2}{\pi}k\int_{-\beta\frac{\pi}{2}}^{\beta\frac{\pi}{2}} AT\cos(\theta-\zeta)\left(1-\sum_{i=1}^{n}a_{id}|AT\cos(\theta-\zeta)|^i\right)\sin(\theta)d\theta \\
&\quad +\frac{2}{\pi}k\alpha\int_{\beta\frac{\pi}{2}}^{\frac{\pi}{2}} AT\cos(\theta-\zeta)\left(1-\sum_{i=1}^{n}a_{iq}|AT\cos(\theta-\zeta)|^i\right)\sin(\theta)d\theta \qquad (2.21) \\
&= \left(\alpha I_{0q}^q + I_{0d}^q\right)AT - \sum_{i=1}^{n}\left(\alpha a_{iq}I_{iq}^q + a_{id}I_{id}^q\right)AT^{i+1}, \qquad (2.22)
\end{aligned}$$

where:

$$\begin{aligned}
I_{0q}^q &= \frac{2}{\pi}k\int_{-\frac{\pi}{2}}^{-\beta\frac{\pi}{2}}\cos(\theta-\zeta)\sin(\theta)d\theta \\
&\quad +\frac{2}{\pi}k\int_{\beta\frac{\pi}{2}}^{\frac{\pi}{2}}\cos(\theta-\zeta)\sin(\theta)d\theta \qquad (2.23) \\
I_{0d}^q &= \frac{2}{\pi}k\int_{-\beta\frac{\pi}{2}}^{\beta\frac{\pi}{2}}\cos(\theta-\zeta)\sin(\theta)d\theta \qquad (2.24) \\
I_{iq}^q &= \frac{2}{\pi}k\int_{-\frac{\pi}{2}}^{-\beta\frac{\pi}{2}}\cos(\theta-\zeta)|\cos(\theta-\zeta)|^i\sin(\theta)d\theta \\
&\quad +\frac{2}{\pi}k\int_{\beta\frac{\pi}{2}}^{\frac{\pi}{2}}\cos(\theta-\zeta)|\cos(\theta-\zeta)|^i\sin(\theta)d\theta \qquad (2.25) \\
I_{id}^q &= \frac{2}{\pi}k\int_{-\beta\frac{\pi}{2}}^{\beta\frac{\pi}{2}}\cos(\theta-\zeta)|\cos(\theta-\zeta)|^i\sin(\theta)d\theta \qquad (2.26)
\end{aligned}$$

In the above depicted equations, two types of unknowns have been introduced. The constants α, k, a_{id} and a_{iq} are not variable for a given machine and can be conveniently calculated once. On the other hand, the coefficients $I_{id}^{d}, I_{iq}^{d}, I_{id}^{q}, I_{iq}^{q}$ $(i = 0 \cdots n)$ are dependent on the location of the axis of the ampere-turns distribution function, expressed by the angle ζ, and they have to be calculated for each operating condition separately.

2.3 Determination of the constants k and α

The parameters α and k can be determined from the values of the unsaturated d- and q-axis mutual reactances. In general, the mutual reactance in per-unit can be represented by the equation:

$$X_m = \frac{\Phi}{AT}. \tag{2.27}$$

Substituting $\zeta = 0$, $a_{id} = 0$ (i.e. $S_d(\theta) = 1.00$), and $a_{iq} = 0$ (i.e. $S_q(\theta) = 1.00$) in Eq.(2.15) and using Eq.(2.27), the unsaturated d-axis mutual reactance in per-unit can be represented by the equation:

$$\begin{aligned} X_{mdu} &= \frac{2}{\pi} k\alpha \int_{-\frac{\pi}{2}}^{-\beta\frac{\pi}{2}} \cos(\theta) \cdot \cos(\theta) d\theta \\ &+ \frac{2}{\pi} k \int_{-\beta\frac{\pi}{2}}^{\beta\frac{\pi}{2}} \cos(\theta) \cdot \cos(\theta) d\theta \\ &+ \frac{2}{\pi} k\alpha \int_{\beta\frac{\pi}{2}}^{\frac{\pi}{2}} \cos(\theta) \cdot \cos(\theta) d\theta \end{aligned}$$

$$= \frac{4}{\pi}k \cdot \left\{ \int_0^{\beta\frac{\pi}{2}} \cos^2(\theta) \cdot d\theta + \alpha \cdot \int_{\beta\frac{\pi}{2}}^{\frac{\pi}{2}} \cos^2(\theta) d\theta \right\}. \tag{2.28}$$

In order to evaluate analytically Eq.(2.28), the following relationship will be used:

$$\int \cos^2(\theta) d\theta = \frac{\sin(2\theta) + 2\theta}{4} + c, \tag{2.29}$$

and Eq.(2.28) will become:

$$X_{mdu} = k \cdot \{(1-\alpha) \cdot \sin(\beta\pi) + (1-\alpha) \cdot \beta\pi + \alpha\pi\}. \tag{2.30}$$

Similarly, the unsaturated q-axis mutual reactance in per-unit can be determined using Eq.(2.27) and substituting $\zeta = \frac{\pi}{2}$, $a_{id} = 0$ (i.e. $S_d(\theta) = 1.00$) and $a_{iq} = 0$ (i.e. $S_q(\theta) = 1.00$) in Eq.(2.21). This reactance can then be expressed as follows:

$$X_{mqu} = \frac{4}{\pi}k \left\{ \int_0^{\beta\frac{\pi}{2}} \sin^2(\theta) d\theta + \alpha \int_{\beta\frac{\pi}{2}}^{\frac{\pi}{2}} \sin^2(\theta) d\theta \right\} \tag{2.31}$$

In order to evaluate Eq.(2.31), the following relationship will be used:

$$\int \sin^2(\theta) d\theta = \frac{2\theta - \sin(2\theta)}{4} + c, \tag{2.32}$$

and Eq.(2.31) will become:

$$X_{mqu} = k \{(\alpha - 1)\sin(\beta\pi) + (1-\alpha)\beta\pi + \alpha\pi\}. \tag{2.33}$$

Knowing the values of the unsaturated d- and q-axis mutual reactances, X_{mdu} and X_{mqu}, and β, the parameters α and k can be obtained by solving Eqs.(2.30) and (2.33) as follows:

$$k = \frac{\pi X_{mqu}}{\{(\alpha-1)\cdot\sin(\beta\pi)+(1-\alpha)\cdot\beta\pi+\alpha\pi\}} \tag{2.34}$$

$$\alpha = \frac{(X_{mqu}+X_{mdu})\cdot\sin(\beta\pi)+(X_{mqu}-X_{mdu})\cdot\beta\pi}{(X_{mqu}+X_{mdu})\cdot\sin(\beta\pi)+(X_{mqu}-X_{mdu})\cdot\beta\pi+(X_{mdu}-X_{mqu})\cdot\pi} \tag{2.35}$$

For cylindrical-rotor synchronous machines, the value of β lies in practice in the range of 0.2 to 0.4 and can be taken as the ratio of the unslotted region width over one pole to the pole pitch. It is worthy to mention here, that it has been found that the accuracy of determining the saturation characteristics in the various axes of cylindrical-rotor synchronous machines is insensitive to any reasonable variation of the value β. Figures (2.3) to (2.6) illustrate how the constants α and k will depend on β and the unsaturated d- and q-axis mutual reactances.

2.4 Determination of the saturation function coefficients

The coefficients a_{id} and a_{iq} $(i = 1\cdots n)$ of the saturation functions are constant for a given machine. They can be obtained from the measured d- and q-axis saturation curves by applying the least square errors fitting technique.

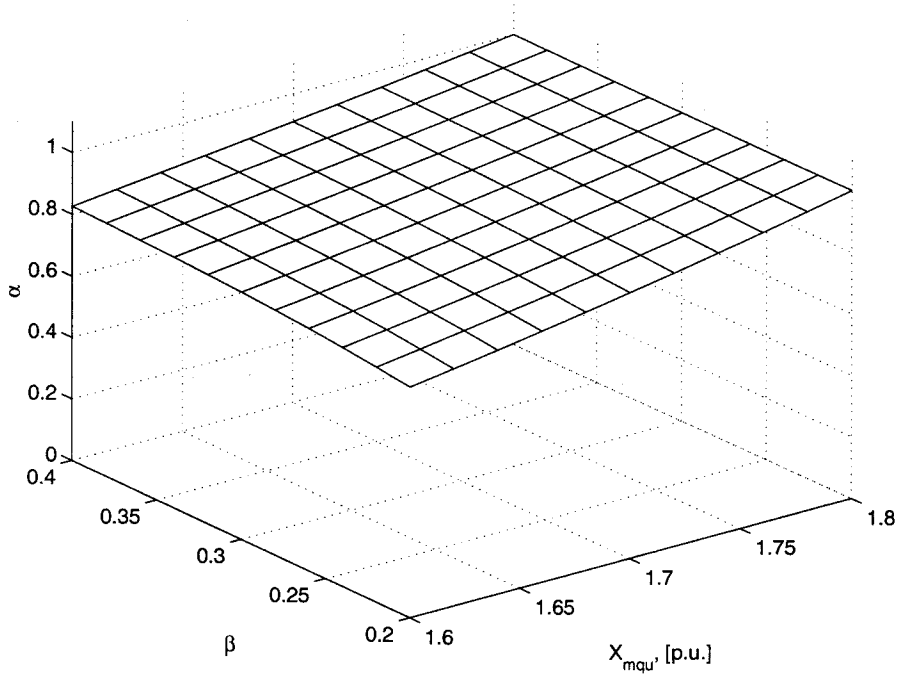

Figure 2.3: The constant α as a function of β and X_{mqu}, $X_{mdu} = 1.8$ p.u.

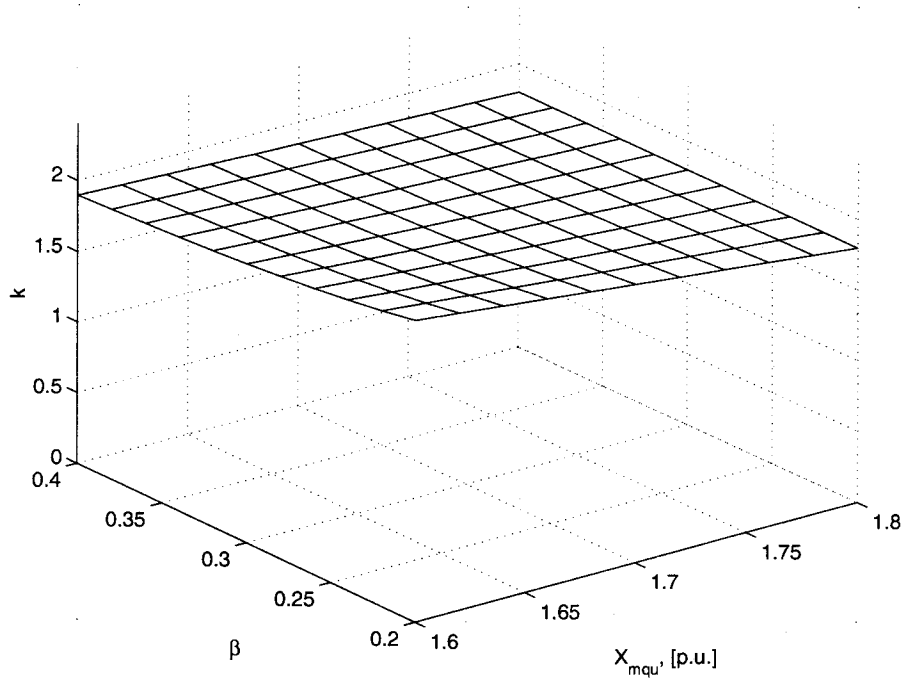

Figure 2.4: The constant k as a function of β and X_{mqu}, $X_{mdu} = 1.8$ p.u.

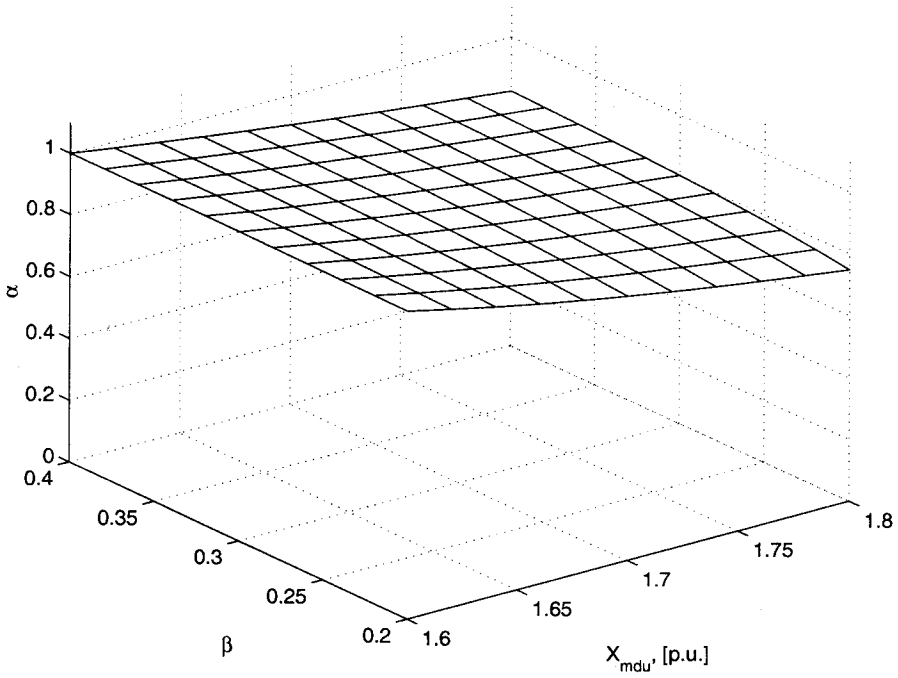

Figure 2.5: The constant α as a function of β and X_{mdu}, $X_{mqu} = 1.6$ p.u.

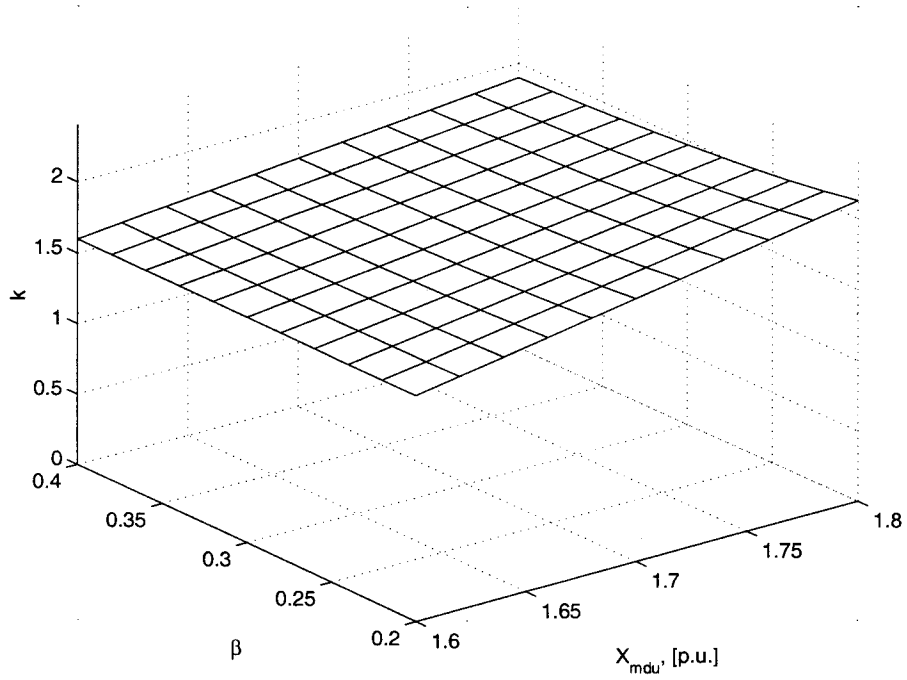

Figure 2.6: The constant k as a function of β and X_{mdu}, $X_{mqu} = 1.6$ p.u.

Substituting $\zeta = 0$ in Eq.(2.15), the equation of the d-axis saturation curve can be written as follows:

$$\begin{aligned}
\Phi_d &= \frac{2}{\pi}\int_{-\frac{\pi}{2}}^{-\beta\frac{\pi}{2}} \alpha k A T \cos^2(\theta) d\theta + \frac{2}{\pi}\int_{-\beta\frac{\pi}{2}}^{\beta\frac{\pi}{2}} k A T \cos^2(\theta) d\theta \\
&+ \frac{2}{\pi}\int_{\beta\frac{\pi}{2}}^{\frac{\pi}{2}} \alpha k A T \cos^2(\theta) d\theta \\
&- \sum_{i=1}^{n} \frac{2}{\pi}\int_{-\frac{\pi}{2}}^{-\beta\frac{\pi}{2}} a_{iq} \alpha k A T^{i+1} \cos^{i+2}(\theta) d\theta \\
&- \sum_{i=1}^{n} \frac{2}{\pi}\int_{-\beta\frac{\pi}{2}}^{\beta\frac{\pi}{2}} a_{id} k A T^{i+1} \cos^{i+2}(\theta) d\theta \\
&- \sum_{i=1}^{n} \frac{2}{\pi}\int_{\beta\frac{\pi}{2}}^{\frac{\pi}{2}} a_{iq} \alpha k A T^{i+1} \cos^{i+2}(\theta) d\theta
\end{aligned} \tag{2.36}$$

The above equation can be rewritten as follows:

$$\Phi_d = c_0^d A T - \sum_{i=1}^{n} (c_{iq}^d a_{iq} \alpha + c_{id}^d a_{id}) A T^{i+1} \tag{2.37}$$

where:

$$c_0^d = \frac{2}{\pi} k \alpha \left(\int_{-\frac{\pi}{2}}^{-\beta\frac{\pi}{2}} \cos^2(\theta) d\theta + \int_{\beta\frac{\pi}{2}}^{\frac{\pi}{2}} \cos^2(\theta) d\theta \right) + \frac{2}{\pi} k \int_{-\beta\frac{\pi}{2}}^{\beta\frac{\pi}{2}} \cos^2(\theta) d\theta \tag{2.38}$$

$$c_{iq}^{d} = \frac{2}{\pi}k\left(\int_{-\frac{\pi}{2}}^{-\beta\frac{\pi}{2}}\cos^{i+2}(\theta)d\theta + \int_{\beta\frac{\pi}{2}}^{\frac{\pi}{2}}\cos^{i+2}(\theta)d\theta\right) \tag{2.39}$$

$$c_{id}^{d} = \frac{2}{\pi}k\int_{-\beta\frac{\pi}{2}}^{\beta\frac{\pi}{2}}\cos^{i+2}(\theta)d\theta \tag{2.40}$$

Substituting $\zeta = \frac{\pi}{2}$ in Eq.(2.21) and taking into consideration that $|F(\theta)| = -F(\theta)$ for $-\frac{\pi}{2} < \theta < 0$ for this case, the equation of the q-axis saturation curve can similarly be written as follows:

$$\begin{aligned}
\Phi_q &= \frac{2}{\pi}\int_{-\frac{\pi}{2}}^{-\beta\frac{\pi}{2}}\alpha kAT\sin^2(\theta)d\theta + \frac{2}{\pi}\int_{-\beta\frac{\pi}{2}}^{\beta\frac{\pi}{2}}kAT\sin^2(\theta)d\theta \\
&\quad + \frac{2}{\pi}\int_{\beta\frac{\pi}{2}}^{\frac{\pi}{2}}\alpha kAT\sin^2(\theta)d\theta \\
&\quad - \sum_{i=1}^{n}(-1)^i\frac{2}{\pi}\int_{-\frac{\pi}{2}}^{-\beta\frac{\pi}{2}}a_{iq}\alpha kAT^{i+1}\sin^{i+2}(\theta)d\theta \\
&\quad - \sum_{i=1}^{n}\frac{2}{\pi}\left[(-1)^i\int_{-\beta\frac{\pi}{2}}^{0}a_{id}kAT^{i+1}\sin^{i+2}(\theta)d\theta + \int_{0}^{\beta\frac{\pi}{2}}a_{id}kAT^{i+1}\sin^{i+2}(\theta)d\theta\right] \\
&\quad - \sum_{i=1}^{n}\frac{2}{\pi}\int_{\beta\frac{\pi}{2}}^{\frac{\pi}{2}}a_{iq}\alpha kAT^{i+1}\sin^{i+2}(\theta)d\theta
\end{aligned} \tag{2.41}$$

The above equation can also be rewritten as:

$$\Phi_q = c_0^q AT - \sum_{i=1}^{n}(c_{iq}^q a_{iq}\alpha + c_{id}^q a_{id})AT^{i+1}, \tag{2.42}$$

where:

$$c_0^q = \frac{2}{\pi}k\alpha\left(\int_{-\frac{\pi}{2}}^{-\beta\frac{\pi}{2}}\sin^2(\theta)d\theta + \int_{\beta\frac{\pi}{2}}^{\frac{\pi}{2}}\sin^2(\theta)d\theta\right) + \frac{2}{\pi}k\int_{-\beta\frac{\pi}{2}}^{\beta\frac{\pi}{2}}\sin^2(\theta)d\theta \tag{2.43}$$

$$c_{iq}^q = (-1)^i\frac{2}{\pi}k\int_{-\frac{\pi}{2}}^{-\beta\frac{\pi}{2}}\sin^{i+2}(\theta)d\theta + \frac{2}{\pi}k\int_{\beta\frac{\pi}{2}}^{\frac{\pi}{2}}\sin^{i+2}(\theta)d\theta \tag{2.44}$$

$$c_{id}^q = (-1)^i\frac{2}{\pi}k\int_{-\beta\frac{\pi}{2}}^{0}\sin^{i+2}(\theta)d\theta + \frac{2}{\pi}k\int_{0}^{\beta\frac{\pi}{2}}\sin^{i+2}(\theta)d\theta. \tag{2.45}$$

Comparing Eqs.(2.28) and (2.31) with Eqs.(2.38) and (2.43), respectively, it is clear that:

$$c_0^d = X_{mdu} \tag{2.46}$$

$$c_0^q = X_{mqu} \tag{2.47}$$

The representation of the d- and q-axis saturation curves of Eqs.(2.37) and (2.42) are polynomials in terms of the ampere-turns AT, and can be rewritten in the following forms:

$$\Phi_d = b_0^d AT - \sum_{i=1}^{n} b_i^d AT^{i+1} \tag{2.48}$$

$$\Phi_q = b_0^q AT - \sum_{i=1}^{n} b_i^q AT^{i+1}, \tag{2.49}$$

where:

$$b_0^d = c_0^d = X_{mdu} \tag{2.50}$$

$$b_0^q = c_0^q = X_{mqu} \tag{2.51}$$

$$b_i^d = c_{iq}^d a_{iq}\alpha + c_{id}^d a_{id} \tag{2.52}$$

$$b_i^q = c_{iq}^q a_{iq}\alpha + c_{id}^q a_{id} \tag{2.53}$$

with $i = 1 \cdots n$.

Using the measured d-axis saturation curve, the coefficients b_0^d and b_i^d of Eqs.(2.48) and (2.49) can be obtained by applying the least square errors fitting technique. If $AT_{d1}, AT_{d2}, \ldots AT_{dm}$ (m =number of measured points) are the ampere-turns of the measured points on the d-axis saturation curve, and Φ_{d1}, Φ_{d2}, ... Φ_{dm} are the corresponding measured magnetic fluxes on the saturation curve, the following matrix equation can be set up:

$$\begin{bmatrix} \Phi_{d1} \\ \Phi_{d2} \\ \vdots \\ \Phi_{dm} \end{bmatrix} = \begin{bmatrix} AT_{d1} & AT_{d1}^2 & \cdots & AT_{d1}^n \\ AT_{d2} & AT_{d2}^2 & \cdots & AT_{d2}^n \\ \vdots & \vdots & \vdots & \vdots \\ AT_{dm} & AT_{dm}^2 & \cdots & AT_{dm}^n \end{bmatrix} \begin{bmatrix} b_0^d \\ -b_1^d \\ \vdots \\ -b_n^d \end{bmatrix} \tag{2.54}$$

Using the notations:

$$A_d = \begin{bmatrix} \Phi_{d1} \\ \Phi_{d2} \\ \vdots \\ \Phi_{dm} \end{bmatrix}, \quad C_d = \begin{bmatrix} AT_{d1} & AT_{d1}^2 & \cdots & AT_{d1}^n \\ AT_{d2} & AT_{d2}^2 & \cdots & AT_{d2}^n \\ \vdots & \vdots & \vdots & \vdots \\ AT_{dm} & AT_{dm}^2 & \cdots & AT_{dm}^n \end{bmatrix}, \quad D_d = \begin{bmatrix} b_0^d \\ -b_1^d \\ \vdots \\ -b_n^d \end{bmatrix} \tag{2.55}$$

Eq.(2.54) becomes:

$$A_d = C_d D_d. \tag{2.56}$$

To obtain the values of the coefficients b_i^d $(i = 0 \cdots n)$, Eq.(2.56) can be solved using the pseudo-inverse of C_d. Multiplying both left sides of Eq.(2.56) with C_d^T, the following relationship is obtained:

$$C_d^T \cdot A_d \;=\; C_d^T \cdot C_d \cdot D_d. \tag{2.57}$$

Then,

$$D_d = [C_d^T \cdot C_d]^{-1} \cdot C_d^T \cdot A_d \tag{2.58}$$

Applying the same procedure of obtaining Eq.(2.58), a similar equation for the quadrature axis can be set up:

$$D_q = [C_q^T \cdot C_q]^{-1} \cdot C_q^T \cdot A_q \tag{2.59}$$

with:

$$A_q = \begin{bmatrix} \Phi_{q1} \\ \Phi_{q2} \\ \vdots \\ \Phi_{qm} \end{bmatrix}, \quad C_q = \begin{bmatrix} AT_{q1} & AT_{q1}^2 & \cdots & AT_{q1}^n \\ AT_{q2} & AT_{q2}^2 & \cdots & AT_{q2}^n \\ \vdots & \vdots & \vdots & \vdots \\ AT_{qm} & AT_{qm}^2 & \cdots & AT_{qm}^n \end{bmatrix}, \quad D_q = \begin{bmatrix} b_0^q \\ -b_1^q \\ \vdots \\ -b_n^q \end{bmatrix} \tag{2.60}$$

where $AT_{q1}, AT_{q2}, \ldots AT_{qm}$ (m =number of measured points) are the ampere-turns of the measured points on the q-axis saturation curve, and Φ_{q1}, Φ_{q2}, ... Φ_{qm} are the corresponding measured magnetic fluxes on the saturation curve.

Knowing the values of b_i^d and b_i^q, a set of linear equations with the saturation functions coefficients, a_{id} and a_{iq}, as unknowns can be set up using Eqs.(2.52) and (2.53) as follows:

$$\begin{cases} b_i^d &= \alpha c_{iq}^d a_{iq} + c_{id}^d a_{id} \\ b_i^q &= \alpha c_{iq}^q a_{iq} + c_{id}^q a_{id} \end{cases} \tag{2.61}$$

Solving Eqs.(2.61), the saturation functions coefficients can be obtained as follows:

$$\begin{bmatrix} a_i^q \\ a_i^d \end{bmatrix} = \begin{bmatrix} \alpha c_{iq}^d & c_{id}^d \\ \alpha c_{iq}^q & c_{id}^q \end{bmatrix}^{-1} \cdot \begin{bmatrix} b_i^d \\ b_i^q \end{bmatrix} \tag{2.62}$$

where $i = 1, \cdots, n$.

2.5 Calculation of the saturation curve in an intermediate axis

As seen from Eq.(2.3), the expressions of the saturation function contains the absolute value of the ampere-turns and it is necessary to substitute $-F(\theta)$ for $|F(\theta)|$

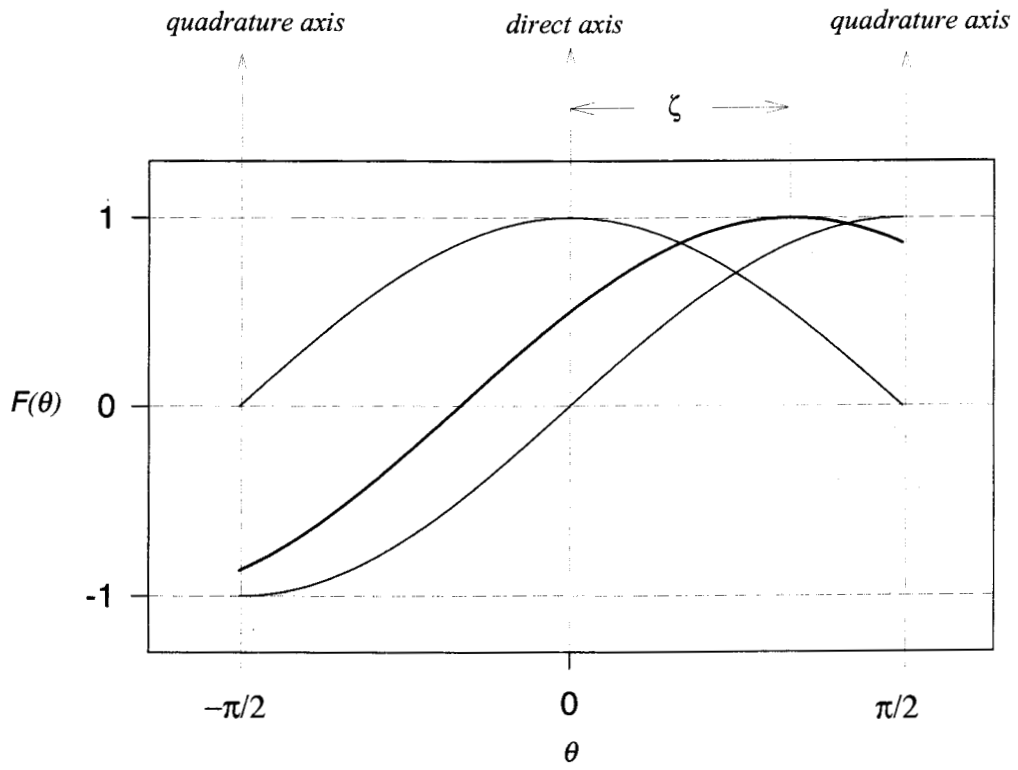

Figure 2.7: Total air-gap ampere-turns in different axes

for the regions where $F(\theta) < 0$ (Fig.(2.7)). In order to obtain analytical solutions for Eqs.(2.19), (2.20), (2.25) and (2.26), different integration intervals have to be identified. These are represented in Fig.(2.8) for the case when $\zeta < \frac{\pi}{2}(1-\beta)$ and in Fig.(2.9) for the case when $\zeta > \frac{\pi}{2}(1-\beta)$. For the case that $\zeta < \frac{\pi}{2}(1-\beta)$, the intervals are also listed in Table (2.1), while for the case $\zeta > \frac{\pi}{2}(1-\beta)$, the intervals are listed in Table (2.2).

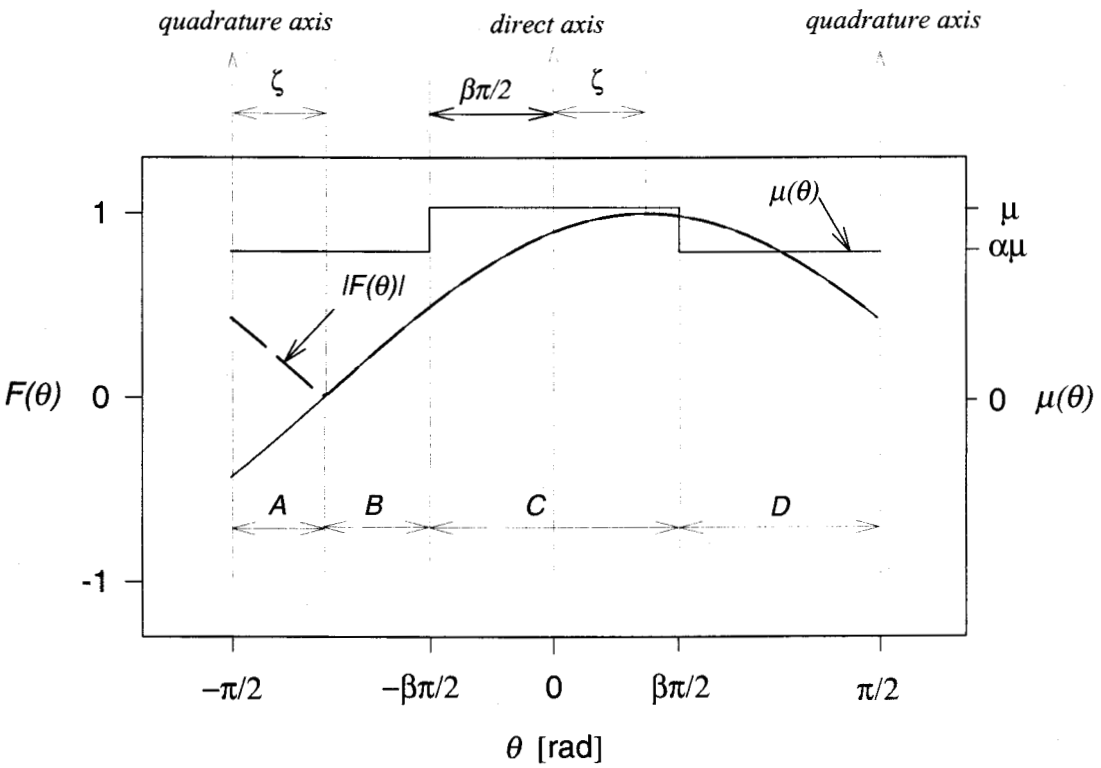

Figure 2.8: Integration intervals for $\zeta < \frac{\pi}{2}(1-\beta)$

Table 2.1: Integration intervals for $\zeta < \frac{\pi}{2}(1-\beta)$

interval	$\lvert F(\theta)\rvert$	$\mu(\theta)$
A	$-F(\theta)$	$\alpha\mu$
B	$F(\theta)$	$\alpha\mu$
C	$F(\theta)$	μ
D	$F(\theta)$	$\alpha\mu$

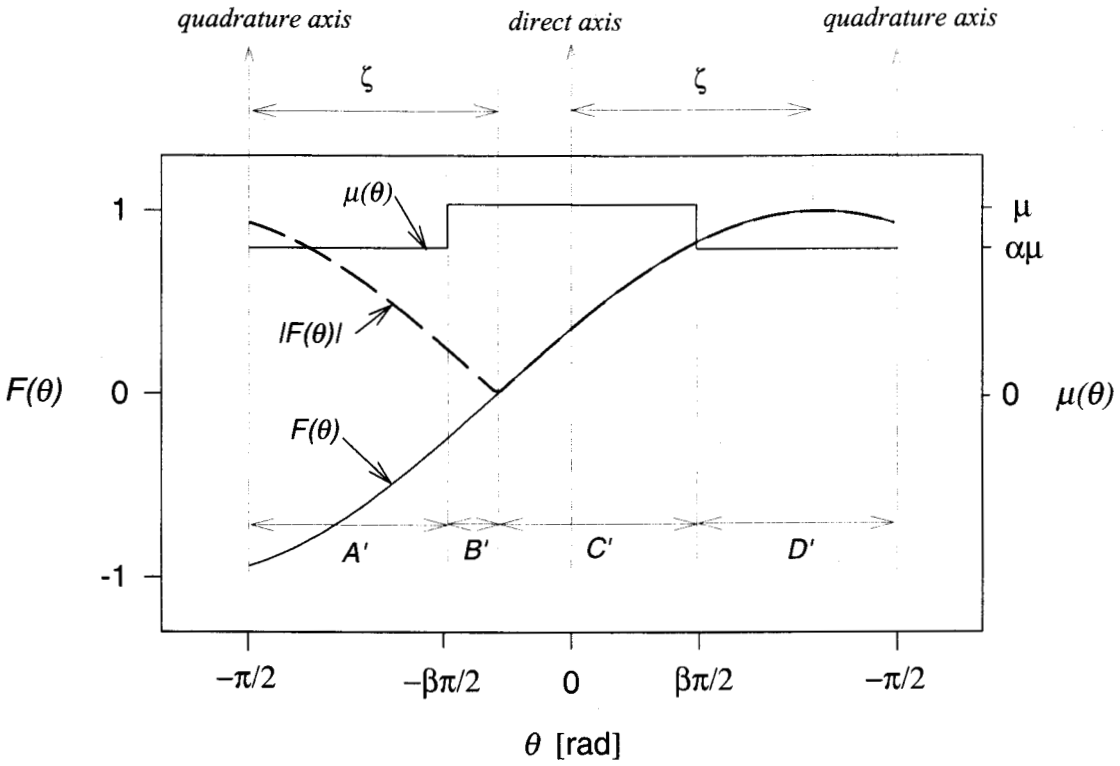

Figure 2.9: Integration intervals for $\zeta > \frac{\pi}{2}(1-\beta)$

Table 2.2: Integration intervals for $\zeta > \frac{\pi}{2}(1-\beta)$

interval	$\lvert F(\theta)\rvert$	$\mu(\theta)$
A'	$-F(\theta)$	$\alpha\mu$
B'	$-F(\theta)$	μ
C'	$F(\theta)$	μ
D'	$F(\theta)$	$\alpha\mu$

2.5.1 Case $\zeta < \frac{\pi}{2}(1-\beta)$

For the case $\zeta < \frac{\pi}{2}(1-\beta)$, the d-axis component of the air-gap magnetic flux can be obtained using Eq.(2.16). In it, the coefficients I^d_{0q} and I^d_{0d} are given by Eqs.(2.17) and (2.18), respectively. Using Table (2.1) and Eqs.(2.19) and (2.20), the other coefficients I^d_{iq} and I^d_{id} $(i = 1 \cdots n)$ can be written as:

$$I^d_{iq} = \frac{2}{\pi}k \left\{ \begin{array}{l} \int_{-\frac{\pi}{2}}^{-\frac{\pi}{2}+\zeta} (-1)^i \cos^{i+1}(\theta-\zeta)\cos(\theta)d\theta + \int_{-\frac{\pi}{2}+\zeta}^{-\beta\frac{\pi}{2}} \cos^{i+1}(\theta-\zeta)\cos(\theta)d\theta \\ + \int_{\beta\frac{\pi}{2}}^{\frac{\pi}{2}} \cos^{i+1}(\theta-\zeta)\cos(\theta)d\theta \end{array} \right\} \tag{2.63}$$

$$I^d_{id} = \frac{2}{\pi}k \int_{-\beta\frac{\pi}{2}}^{\beta\frac{\pi}{2}} \cos^{i+1}(\theta-\zeta)\cos(\theta)d\theta \tag{2.64}$$

For the case when $\zeta < \frac{\pi}{2}(1-\beta)$, the q-axis component of the air-gap magnetic flux can be obtained using Eq.(2.22). In it, the coefficients I^q_{0q} and I^q_{0d} are given by Eqs.(2.23) and (2.24), respectively. Using Table (2.1) and Eqs.(2.25) and (2.26), the other coefficients I^q_{iq} and I^q_{id} $(i = 1 \cdots n)$ can be written as:

$$I^q_{iq} = \frac{2}{\pi}k \left\{ \begin{array}{l} \int_{-\frac{\pi}{2}}^{-\frac{\pi}{2}+\zeta} (-1)^i \cos^{i+1}(\theta-\zeta)\sin(\theta)d\theta + \int_{-\frac{\pi}{2}+\zeta}^{-\beta\frac{\pi}{2}} \cos^{i+1}(\theta-\zeta)\sin(\theta)d\theta \\ + \int_{\beta\frac{\pi}{2}}^{\frac{\pi}{2}} \cos^{i+1}(\theta-\zeta)\sin(\theta)d\theta \end{array} \right\} \tag{2.65}$$

$$I_{id}^{q} = \frac{2}{\pi} k \int_{-\beta\frac{\pi}{2}}^{\beta\frac{\pi}{2}} \cos^{i+1}(\theta - \zeta) \sin(\theta) d\theta \tag{2.66}$$

2.5.2 Case $\zeta > \frac{\pi}{2}(1-\beta)$

For the case $\zeta > \frac{\pi}{2}(1-\beta)$, the d-axis component of the air-gap magnetic flux can be obtained using Eq.(2.16). In it, the coefficients I_{0q}^{d} and I_{0d}^{d} will have the same expression as in Eqs.(2.17) and (2.18). Using Table (2.2) and Eqs.(2.19) and (2.20), the other coefficients can be written as:

$$I_{iq}^{d} = \frac{2}{\pi} k \left\{ \int_{-\frac{\pi}{2}}^{-\beta\frac{\pi}{2}} (-1)^{i} \cos^{i+1}(\theta - \zeta) \cos(\theta) d\theta + \int_{\beta\frac{\pi}{2}}^{\frac{\pi}{2}} \cos^{i+1}(\theta - \zeta) \cos(\theta) d\theta \right\} \tag{2.67}$$

$$I_{id}^{d} = \frac{2}{\pi} k \left\{ \int_{-\beta\frac{\pi}{2}}^{-\frac{\pi}{2}+\zeta} (-1)^{i} \cos^{i+1}(\theta - \zeta) \cos(\theta) d\theta + \int_{-\frac{\pi}{2}+\zeta}^{\beta\frac{\pi}{2}} \cos^{i+1}(\theta - \zeta) \cos(\theta) d\theta \right) \tag{2.68}$$

When $\zeta > \frac{\pi}{2}(1-\beta)$, the q-axis component of the air-gap magnetic flux can be obtained from Eq.(2.22), with the coefficients I_{0q}^{q} and I_{0d}^{q} given by Eqs.(2.23) and (2.24). The other coefficients can be written as:

$$I_{iq}^{q} = \frac{2}{\pi} k \left\{ \int_{-\frac{\pi}{2}}^{-\beta\frac{\pi}{2}} (-1)^{i} \cos^{i+1}(\theta - \zeta) \sin(\theta) d\theta + \int_{\beta\frac{\pi}{2}}^{\frac{\pi}{2}} \cos^{i+1}(\theta - \zeta) \sin(\theta) d\theta \right\} \tag{2.69}$$

$$I_{id}^{q} = \frac{2}{\pi}k\left\{\int_{-\beta\frac{\pi}{2}}^{-\frac{\pi}{2}+\zeta}(-1)^{i}\cos^{i}(\theta-\zeta)\sin(\theta)d\theta + \int_{-\frac{\pi}{2}+\zeta}^{\beta\frac{\pi}{2}}\cos^{i+1}(\theta-\zeta)\sin(\theta)d\theta\right\} \tag{2.70}$$

2.6 The total air-gap magnetic flux

Using the d- and q-axis components of the total air-gap magnetic flux Φ_d and Φ_q expressed in Eqs.(2.16) and (2.22), the magnitude of the total air-gap magnetic flux can be calculated as:

$$\Phi_t = \sqrt{\Phi_d^2 + \Phi_q^2}. \tag{2.71}$$

The angle between the axis of the total air-gap magnetic flux and the direct axis is also obtainable from Eqs.(2.16) and (2.22), and can be calculated as:

$$\delta' = \tan^{-1}\frac{\Phi_q}{\Phi_d}. \tag{2.72}$$

In general, the angles ζ and δ' are not equal (Fig.(2.10)). The difference between them is partly due to the difference in the saturation levels in the direct and quadrature axes and partly due to any existence of saliency when the machine is unsaturated.

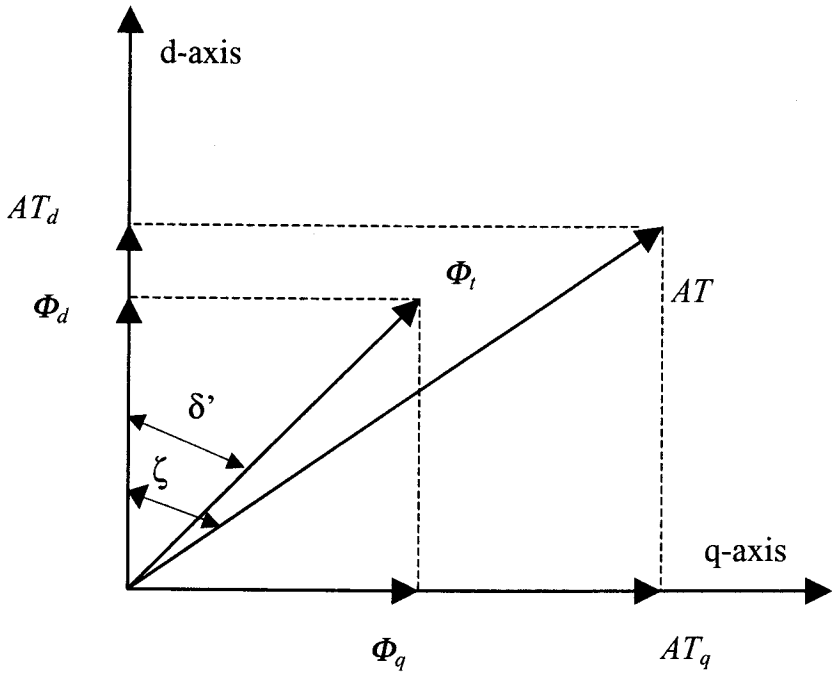

Figure 2.10: Air-gap magnetic flux and ampere-turns

Chapter 3

Experimental verification of the accuracy of the proposed method for determining the intermediate-axis saturation curves

In the previous chapter, a new method for determining the saturation curves in the intermediate axes of cylindrical-rotor synchronous machines has been introduced. The experimental investigations carried out to check the accuracy of this method are presented in this chapter.

3.1 The machine used in the investigation

To verify the accuracy of the proposed method for determining the saturation curves in the intermediate axes of cylindrical-rotor synchronous machines, experimental investigations were carried out on a 3-kVA, 220-V, three-phase, 4-pole, 60-Hz, cylindrical-rotor synchronous machine (Mawdsley's Machine, S.N. EA41875). The stator of this machine has a three-phase, four-wire, star-connected winding. The rotor is fitted with two field windings, one in the direct axis and the other in the quadrature axis and, thus, the machine can be excited from both axes. This will allow for its excitation in any intermediate axis.

3.2 The electrical parameters of the cylindrical-rotor synchronous machine used in the investigations

The values of the unsaturated d- and q-axis synchronous reactances and the armature leakage reactance of the machine used in the investigation were obtained experimentally. These values are needed to determine the k and α constants of the previously proposed method. They will also be used to find a suitable per unit system for the machine.

3.2.1 The unsaturated synchronous reactances

In order to obtain the unsaturated values of the d- and q-axis synchronous reactances, the conventional open-circuit and short-circuit tests were used [25, 27]. The unsaturated d-axis synchronous reactance X_{du} was obtained from the open-circuit and short-circuit tests when the machine was excited by the d-axis field winding, while the unsaturated q-axis synchronous reactance X_{qu} was obtained from the open-circuit and short-circuit tests when the machine was excited by the q-axis field winding.

If α_{do} [V/A] is the slope of the d-axis open-circuit characteristic (o.c.c.) air-gap line and α_{dsc} [A/A] is the slope of the d-axis short-circuit characteristic (s.c.c.) (Fig. (3.1)), then X_{du} can be written as:

$$X_{du} = \frac{\alpha_{do}}{\sqrt{3}\alpha_{dsc}} = 30.14 \ \Omega \tag{3.1}$$

If the open-circuit characteristic is represented using the phase voltages, the $\sqrt{3}$ has to be omitted from Eq.(3.1).

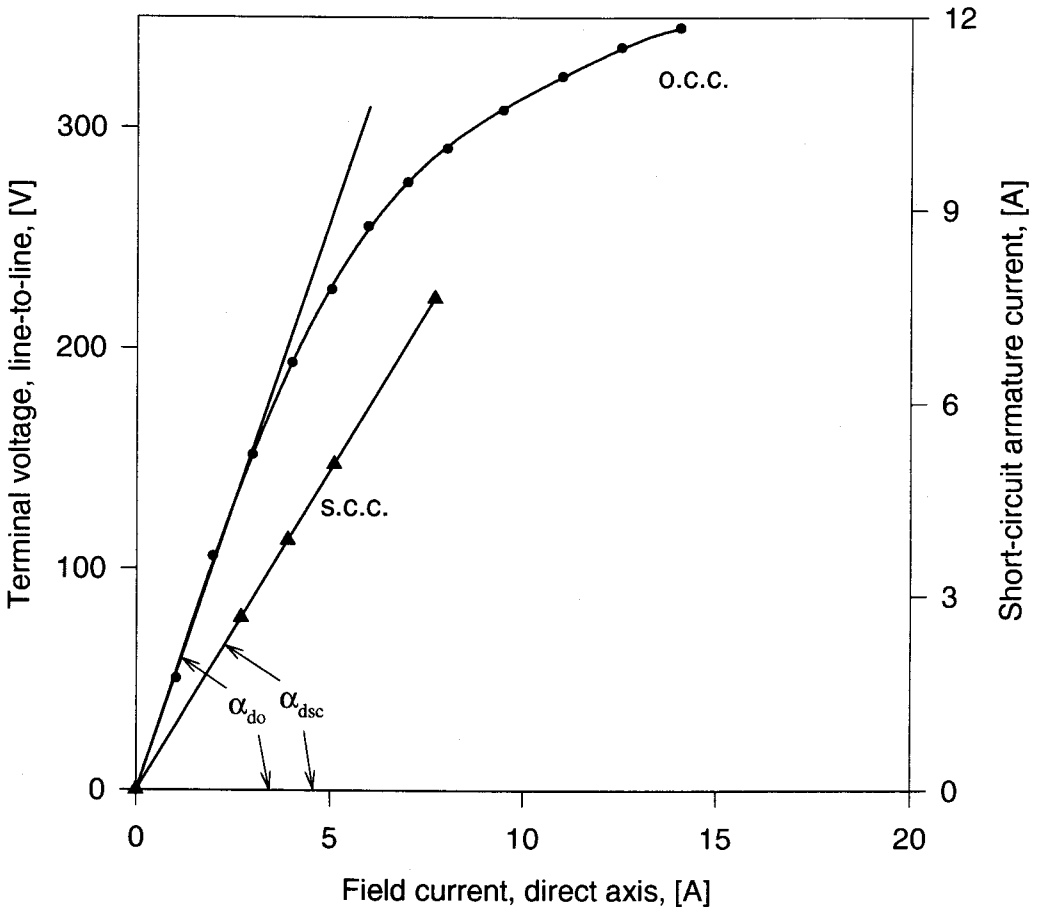

Figure 3.1: Direct-axis open-circuit and short-circuit characteristics

Similarly, if α_{qo} [V/A] is the slope of the q-axis open-circuit characteristic air-gap line and α_{qsc} [A/A] is the slope of the q-axis short-circuit characteristic (Fig.(3.2)), then X_{qu} can be written as:

$$X_{qu} = \frac{\alpha_{qo}}{\sqrt{3}\alpha_{qsc}} = 28.93 \ \Omega. \tag{3.2}$$

3.2.2 The armature leakage reactance

It is a common procedure to approximate the leakage reactance by the Potier reactance measured at rated terminal voltage [18]. However, investigators have found

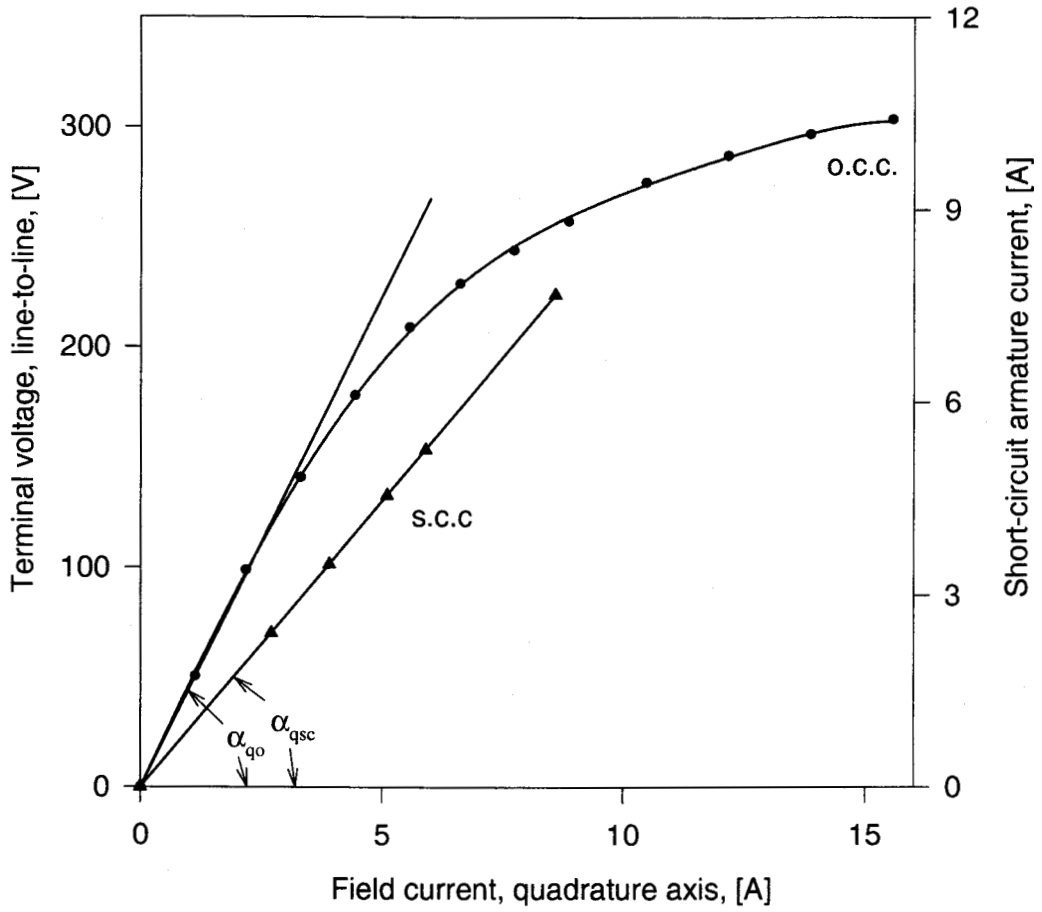

Figure 3.2: Quadrature-axis open-circuit and short-circuit characteristics

that the value of the Potier reactance determined by this method is larger than the value of the leakage reactance [28]. Several authors have reported that the value of the leakage reactance approaches the value of the Potier reactance only if the latter is measured under highly saturated conditions [29]. In Fig.(3.3) the Potier reactance has been obtained [25] for the highly saturated conditions using the open-circuit, short-circuit and zero-power-factor (z.p.f.) characteristics and, thus, its value can be considered equal to the value of the leakage reactance.

$$X_l = X_p = 2.58\ \Omega \tag{3.3}$$

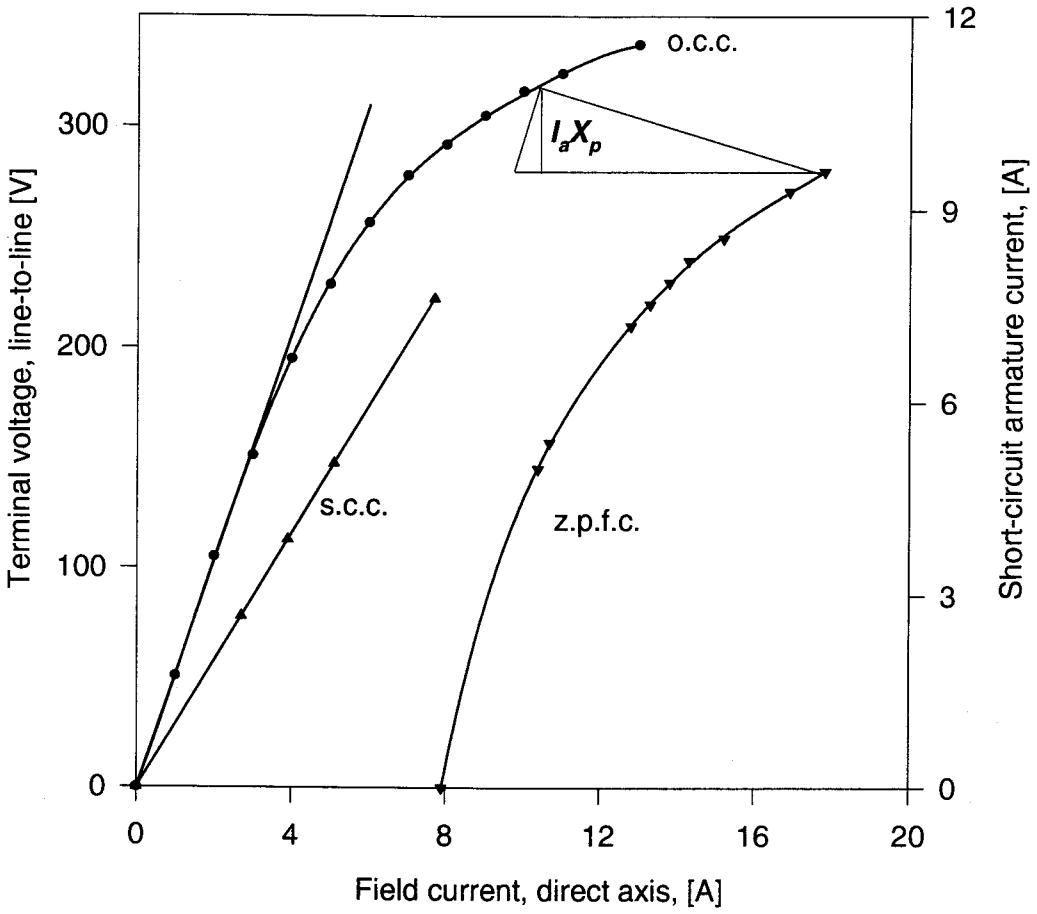

Figure 3.3: Determination of the Potier reactance

3.3 The per-unit system

Per-unit systems have been extensively used in the analysis of electrical machines. In such an approach, all machine parameters and electrical quantities are used in per-unit values, obtained using corresponding base values. In an adequately chosen per-unit system, the per-unit values of the open-circuit terminal voltage and the corresponding air-gap magnetic flux of a synchronous machine will be equal. Also, the per-unit values of the field current and the corresponding ampere-turns will be

equal. Thus, the open-circuit characteristics will represent the saturation curves.

3.3.1 Stator base values

It is a common practice to choose the rated armature current and the rated terminal voltage of synchronous machines to be the stator current and voltage base values, respectively:

$$I_a^b[\text{A}] = I_a^n[\text{A}] = 7.87 \text{ A} \tag{3.4}$$

$$V_t^b[\text{V}] = V_t^n[\text{V}] = 220 \text{ V} \tag{3.5}$$

where V_t^b and I_a^b are the voltage and armature current base values, and V_t^n and I_a^n are the rated terminal voltage and armature current, respectively. Thus, the per-unit values of the terminal voltage and armature current can be introduced as:

$$V_t[\text{p.u.}] = \frac{V_t[\text{V}]}{V_t^b[\text{V}]} = \frac{V_t[\text{V}]}{V_t^n[\text{V}]} \tag{3.6}$$

$$I_a[\text{p.u.}] = \frac{I_a[\text{A}]}{I_a^b[\text{A}]} = \frac{I_a[\text{A}]}{I_a^n[\text{A}]}, \tag{3.7}$$

Also, the power base value is taken equal to the rated VA, i.e.:

$$S_b = S_n \text{ [VA]} = 3000 \text{ VA}, \tag{3.8}$$

and thus, the per-unit representation of the powers can be introduced as:

$$S[\text{p.u.}] = \frac{S[\text{VA}]}{S_b[\text{VA}]} = \frac{S[\text{VA}]}{S_n[\text{VA}]} \tag{3.9}$$

$$P[\text{p.u.}] = \frac{P[\text{W}]}{S_b[\text{VA}]} = \frac{P[\text{W}]}{S_n[\text{VA}]} \tag{3.10}$$

$$Q[\text{p.u.}] = \frac{Q[\text{VAr}]}{S_b[\text{VA}]} = \frac{Q[\text{VAr}]}{S_n[\text{VA}]} \tag{3.11}$$

Using Eqs.(3.6) and (3.7) the impedance base value is obtained as follows [30]:

$$Z_b\ [\Omega] = \frac{V_{tb}\ [\text{V}]}{\sqrt{3} I_a^b\ [\text{A}]} = 16.13\ \Omega \tag{3.12}$$

3.3.2 Rotor base values

The base values for the d- and q-axis field currents are chosen according to the "X_{md}"-base per-unit system [31]. In this case, the base value of the d-axis field current is expressed as follows:

$$I_{fd}^b = \frac{I_a^b \cdot X_{mdu}}{\alpha_{0d}} = \frac{I_a^b \cdot (X_{du} - X_l)}{\alpha_{0d}} = 7.28\ \text{A}. \tag{3.13}$$

It should be noticed that α_{0d} has to be calculated here using the phase value of the terminal voltage. Similarly, the q-axis field current base value can be expressed as follows:

$$I_{fq}^b = \frac{I_a^b \cdot (X_{qu} - X_l)}{\alpha_{0q}} = 8.06\ \text{A} \tag{3.14}$$

Using Eqs.(3.13) and (3.14), the base values of the -d and q-axis field winding ampere-turns can be expressed as follows:

$$AT_d^b = I_{fd}^b N_d \tag{3.15}$$

$$AT_q^b = I_{fq}^b N_q, \tag{3.16}$$

where N_d and N_q are the effective number of turns of the d- and q-axis field windings, respectively. For the cylindrical-rotor synchronous machine used for the investigations of this thesis, N_d and N_q are 103 and 93, respectivelly.

From the definitions of the adopted per-unit system, the d- and q-axis base values of the field windings ampere-turns should be equal, i.e.:

$$AT_d^b = AT_q^b. \tag{3.17}$$

Using Eqs.(3.13) to (3.16), Eq.(3.17) can be rewritten as follows:

$$\frac{I_a^b \cdot (X_{du} - X_l)}{\alpha_{0d}} N_d = \frac{I_a^b \cdot (X_{qu} - X_l)}{\alpha_{0q}} N_q. \tag{3.18}$$

Knowing the values of the effective number of turns of the d- and q-axis field windings, N_d and N_q, Eqs.(3.18) suggests another approach to find experimentally the value of X_l, which can be expressed as follows:

$$X_l = \frac{X_{du}\frac{N_d}{\alpha_{0d}} - X_{qu}\frac{N_q}{\alpha_{0q}}}{\frac{N_d}{\alpha_{0d}} - \frac{N_q}{\alpha_{0q}}} = 2.55 \ \Omega. \tag{3.19}$$

This value is very close to the value obtained in section 3.2.2.

3.3.3 Per-unit values of the electrical parameters of the cylindrical-rotor synchronous machine used in the investigations

Using the base impedance value given in Eq.(3.12), the per-unit values of the resistance and reactances of the cylindrical-rotor synchronous machine used in the investigation are calculated, and they are listed in Table (3.1).

Table 3.1: Data of the cylindrical-rotor synchronous machine

Unit	X_{mdu}	X_{mqu}	X_l	R_a
[Ω]	30.14	28.93	2.58	0.371
[p.u.]	1.708	1.633	0.160	0.023

3.4 Calculation of the α and k constants

Using Eqs.(2.34) and (2.35), and the data of Table (3.1), the constants k and α, which are needed to determine the intermediate-axis saturation curves, were calculated for the cylindrical-rotor synchronous machine. In this calculation, β was taken as the ratio of the unslotted region width over one pole to the pole pitch of the machine. Table (3.2) lists the values of all these constants.

Table 3.2: Constants β, α and k of the cylindrical-rotor synchronous machine

β	α	k
0.2	0.891	1.83

3.5 The open-circuit characteristic curves

To verify the accuracy of the method proposed in Chapter 2 for calculating the saturation curves of the cylindrical-rotor synchronous machine under investigation, its open-circuit characteristic curves were obtained experimentally by exciting it from both its direct and quadrature axes simultaneously, and were compared with the saturation curves calculated using the proposed technique. As mentioned in section 3.3, the open-circuit characteristics and the saturation curves, represented using the adopted per-unit system, should be similar.

In the calculation of the saturation curves, different orders for the polynomials representing the saturation functions S_d and S_q have been used to check the minimal order of the polynomials which would give acceptable results.

3.5.1 Using second-order polynomials to represent the saturation functions

The first set of calculations are done using second-order polynomials to represent the saturation functions. In this case, n is equal 2, and the saturation functions can be expressed as follows:

$$S_d(\theta) = 1.00 - a_{1d}|F(\theta)| - a_{2d}|F(\theta)|^2 \tag{3.20}$$

$$S_q(\theta) = 1.00 - a_{1q}|F(\theta)| - a_{2q}|F(\theta)|^2 \tag{3.21}$$

Applying the method presented in section 2.4 for obtaining the saturation function

coefficients, the values of a_{id} and a_{iq} can be calculated (Table (3.3)). Using Eqs.(2.16) and (2.22), the d- and q-axis saturation curves are calculated and depicted in Fig.(3.4) together with the corresponding measured open-circuit characteristics. Intermediate-axis saturation curves for $\zeta = 30^o, 45^o, 60^o$ and 75^o are also obtained using Eq.(2.71), and are depicted in Figs.(3.5) to (3.8) together with the corresponding measured open-circuit characteristics. It can be observed from these figures that a second order polynomial representation for S_d and S_q is not accurate enough, and a higher order than $n = 2$ should be considered.

Table 3.3: Second-order saturation function coefficients

i	a_{id}	a_{iq}
1	0.214	0.397
2	0.042	-0.027

3.5.2 Using third-order polynomials to represent the saturation functions

Since the second-order polynomial representation of the saturation functions has not produced acceptable results, the case of third-order polynomials has been applied. The saturation function coefficients for the case when $n = 3$ are listed in Table (3.4). Figure (3.9) depicts the measured d- and q-axis open-circuit characteristics together with the calculated saturation curves. Figures (3.10) to (3.13) are representing the measured intermediate-axis open-circuit characteristics and the calculated saturation curves for $\zeta = 30^o, 45^o, 60^o$ and 75^o, respectively. As seen from these figures, the calculated saturation curves are still not adequately close to the measured values,

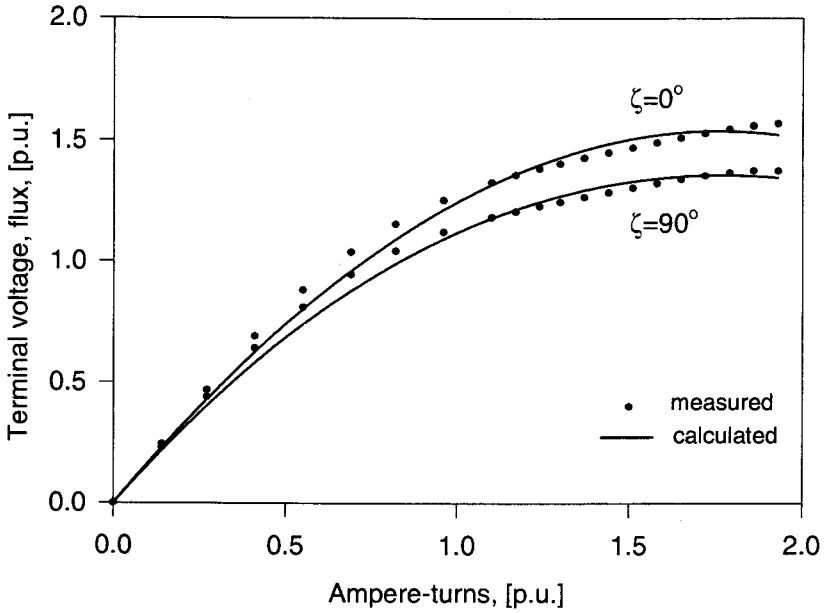

Figure 3.4: Direct- and quadrature-axis saturation curves of the cylindrical-rotor synchronous machine using second-order saturation functions

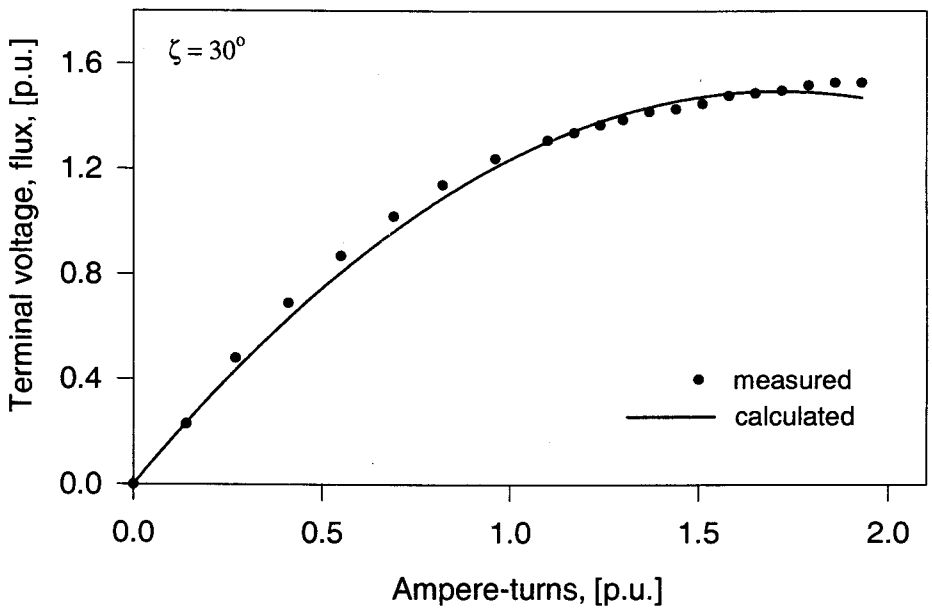

Figure 3.5: Intermediate-axis ($\zeta = 30^o$) saturation curve of the cylindrical-rotor synchronous machine using second-order saturation functions

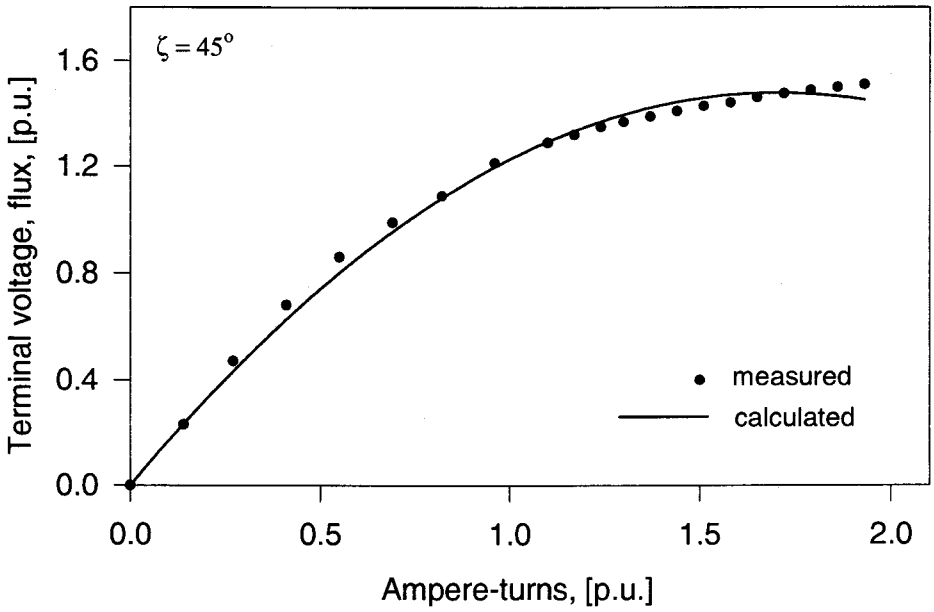

Figure 3.6: Intermediate-axis ($\zeta = 45^o$) saturation curve of the cylindrical-rotor synchronous machine using second-order saturation functions

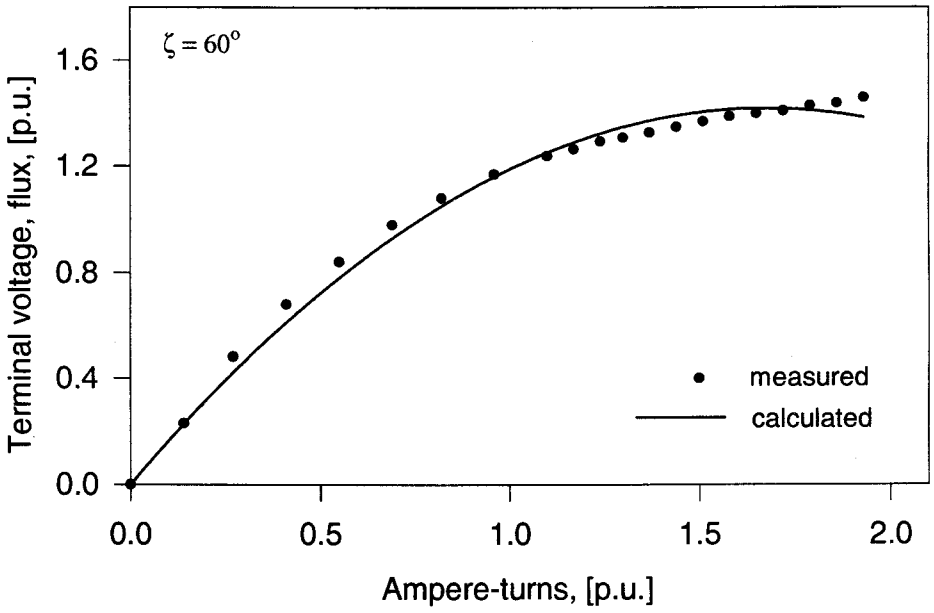

Figure 3.7: Intermediate-axis ($\zeta = 60^o$) saturation curve of the cylindrical-rotor synchronous machine using second-order saturation functions

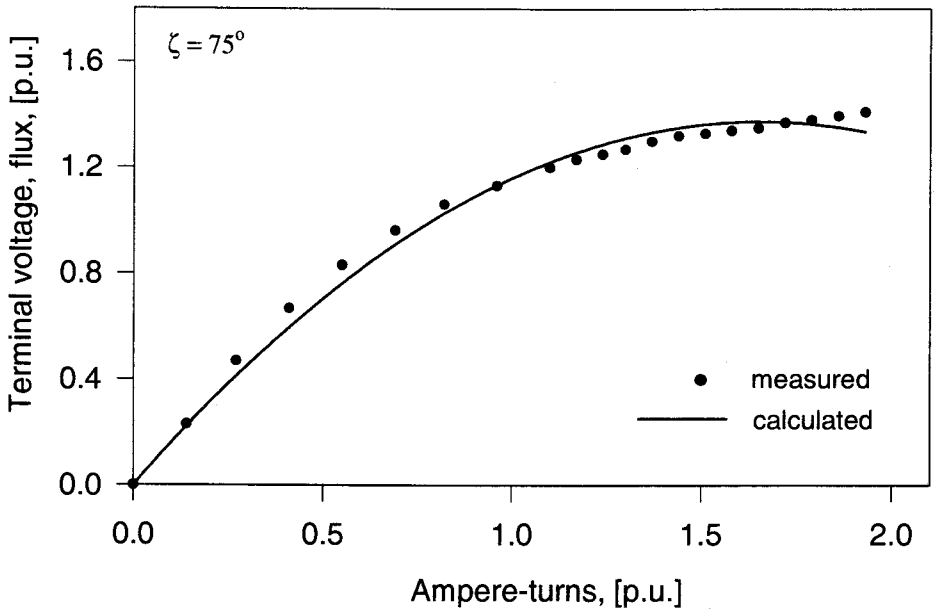

Figure 3.8: Intermediate-axis ($\zeta = 75^o$) saturation curve of the cylindrical-rotor synchronous machine using second-order saturation functions

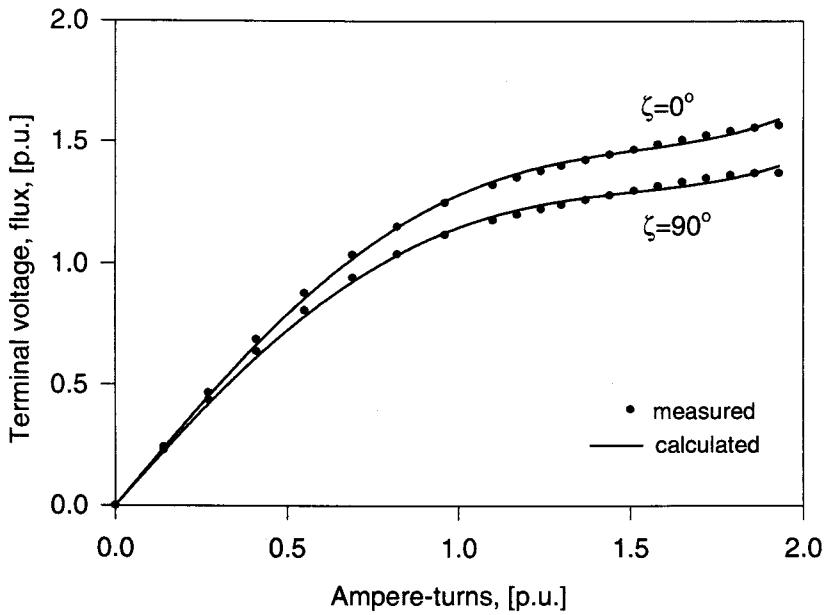

Figure 3.9: Direct- and quadrature-axis saturation curves of the cylindrical-rotor synchronous machine using third-order saturation functions

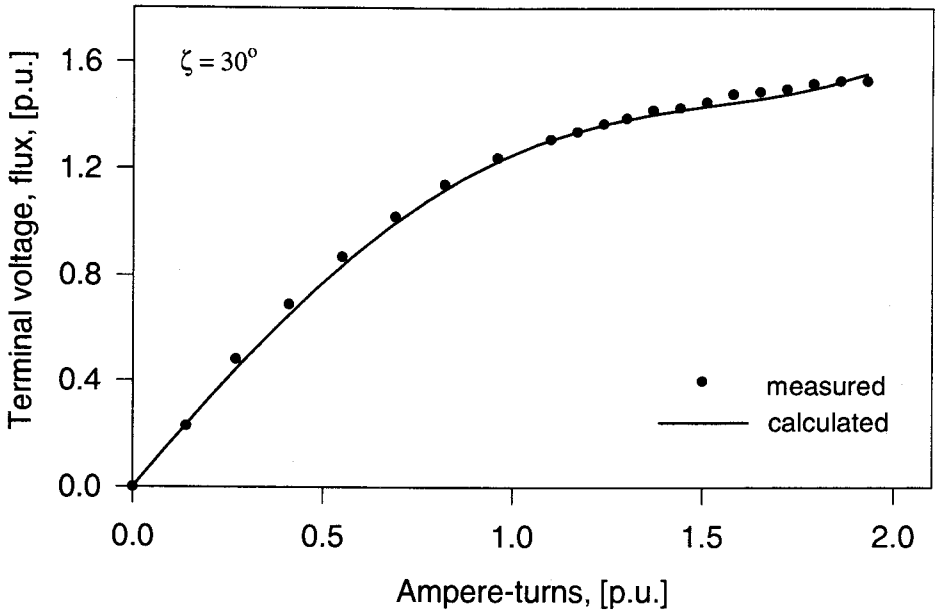

Figure 3.10: Intermediate-axis ($\zeta = 30^o$) saturation curve of the cylindrical-rotor synchronous machine using third-order saturation functions

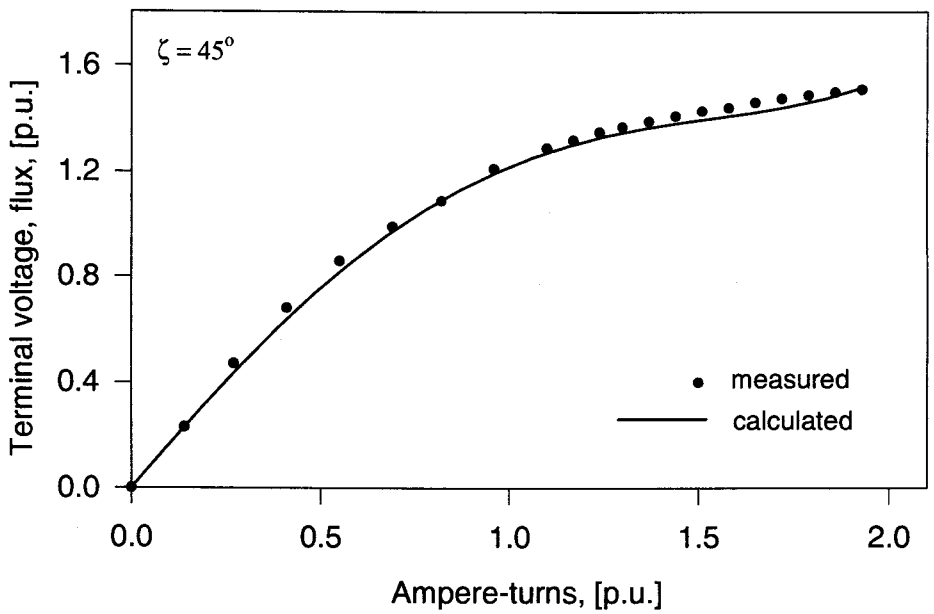

Figure 3.11: Intermediate-axis ($\zeta = 45^o$) saturation curve of the cylindrical-rotor synchronous machine using third-order saturation functions

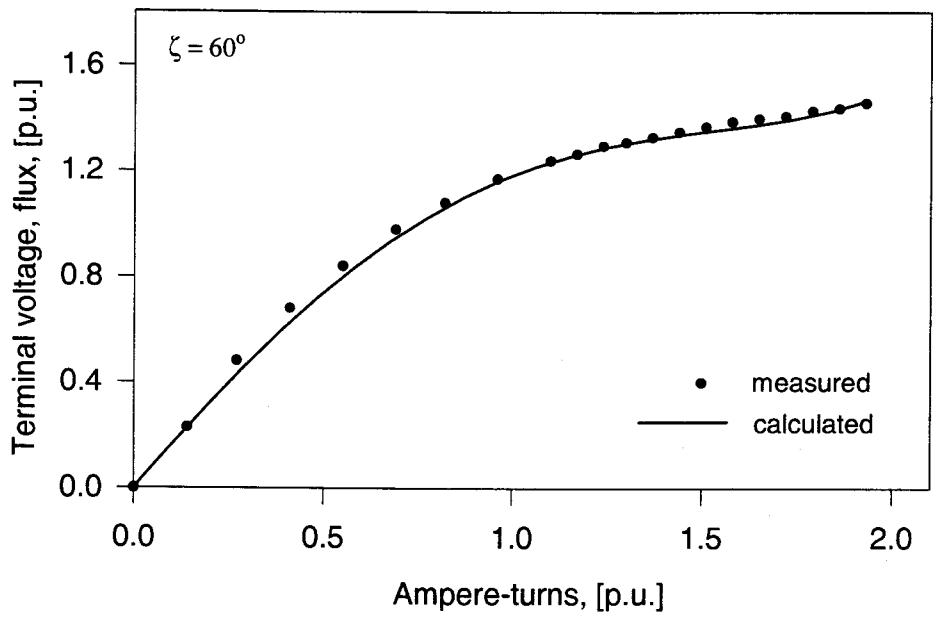

Figure 3.12: Intermediate-axis ($\zeta = 60^o$) saturation curve of the cylindrical-rotor synchronous machine using third-order saturation functions

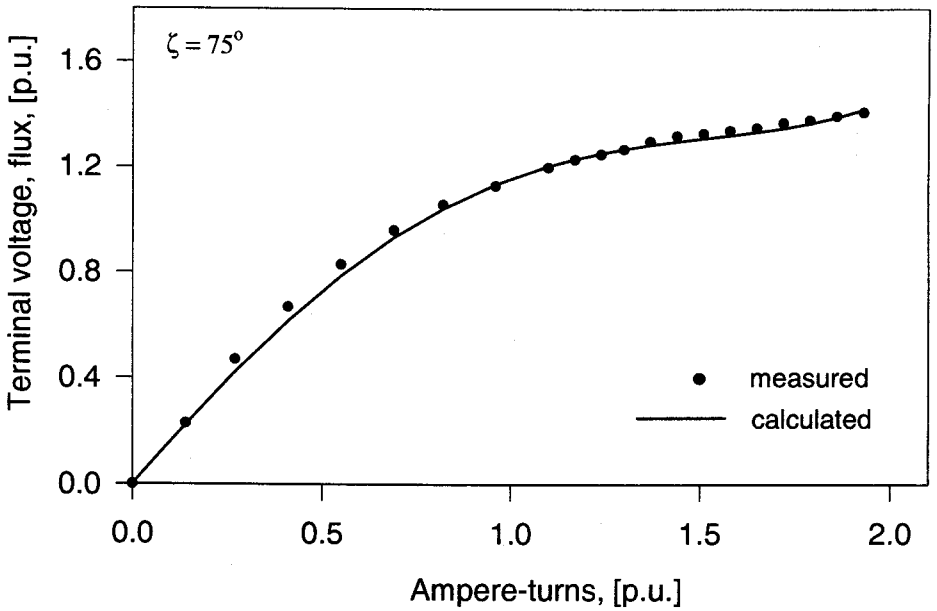

Figure 3.13: Intermediate-axis ($\zeta = 75^o$) saturation curve of the cylindrical-rotor synchronous machine using third-order saturation functions

Table 3.4: Third-order saturation function coefficients

i	a_{id}	a_{iq}
1	-0.174	0.121
2	0.620	0.401
3	-0.205	-0.156

and still higher order polynomials should be considered.

3.5.3 Using fourth-order polynomials to represent the saturation functions

As it can be seen from Figs.(3.14) to (3.18), the use of the fourth-order polynomials to represent the saturation functions result in calculated saturation curves which are adequatly close to the measured open-circuit characteristics. The coefficients of these saturation function polynomials are listed in Table (3.5).

Table 3.5: Fourth-order saturation function coefficients

i	a_{id}	a_{iq}
1	-0.425	-0.261
2	1.315	1.420
3	-0.791	-0.994
4	0.154	0.216

3.5.4 Comparison between the measured and calculated results

The discrepancies between the measured open-circuit characteristics and the calculated saturation curves can be represented in the sense of the average error per measurement, and can be found using the following equation:

$$\epsilon = \frac{\sum_{j=1}^{m} |\Phi_j - \Phi_j^c|}{m}. \tag{3.22}$$

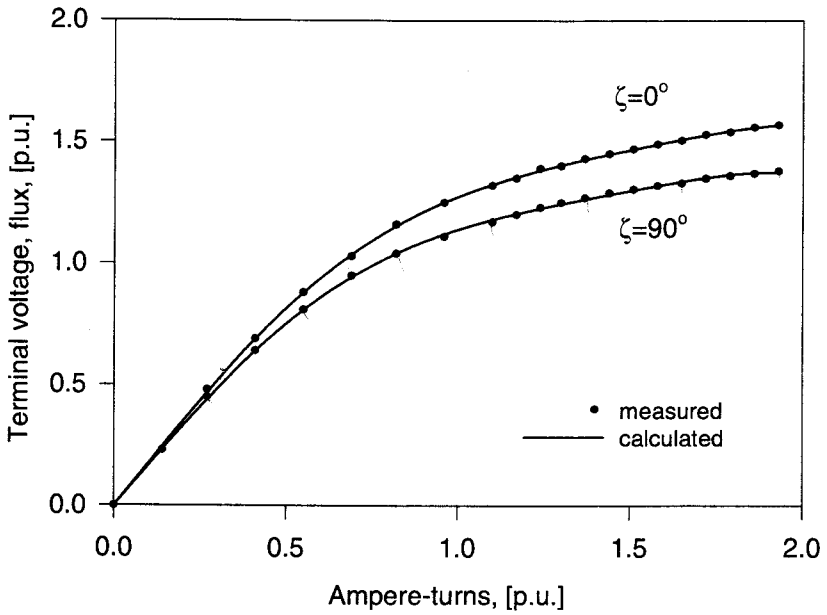

Figure 3.14: Direct- and quadrature-axis saturation curves of the cylindrical-rotor synchronous machine using fourth-order saturation functions

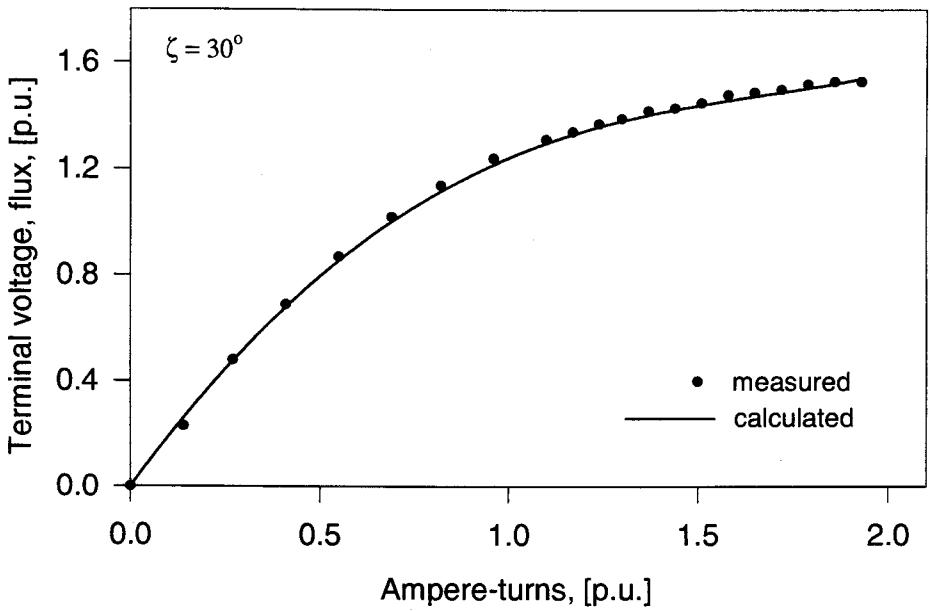

Figure 3.15: Intermediate-axis ($\zeta = 30^o$) saturation curve of the cylindrical-rotor synchronous machine using fourth-order saturation functions

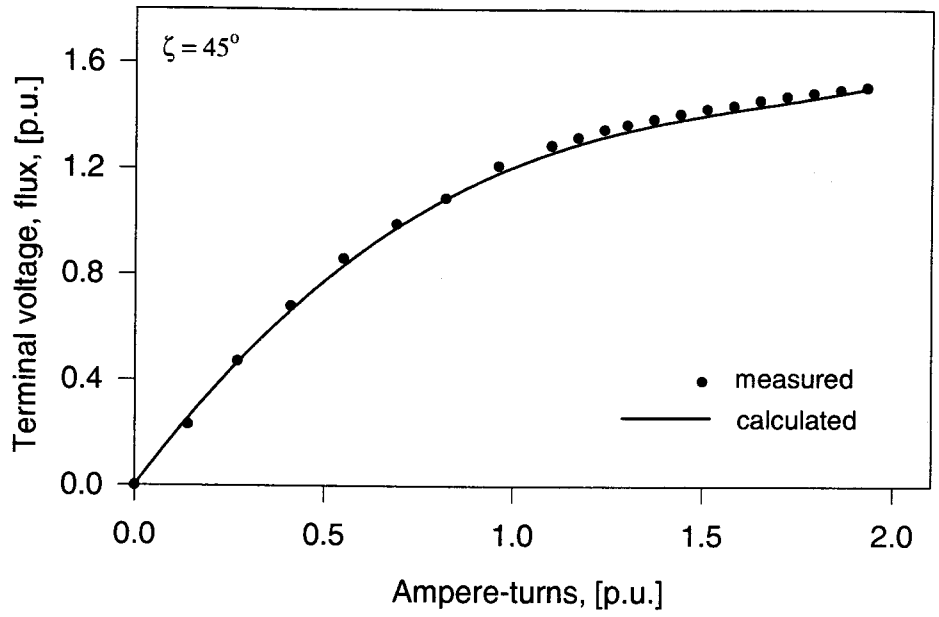

Figure 3.16: Intermediate-axis ($\zeta = 45^o$) saturation curve of the cylindrical-rotor synchronous machine using fourth-order saturation functions

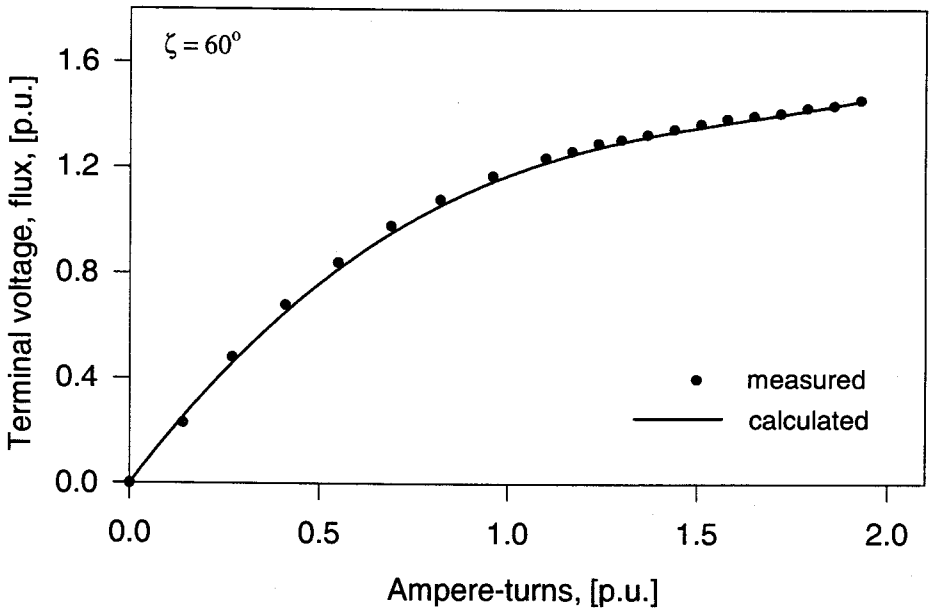

Figure 3.17: Intermediate-axis ($\zeta = 60^o$) saturation curve of the cylindrical-rotor synchronous machine using fourth-order saturation functions

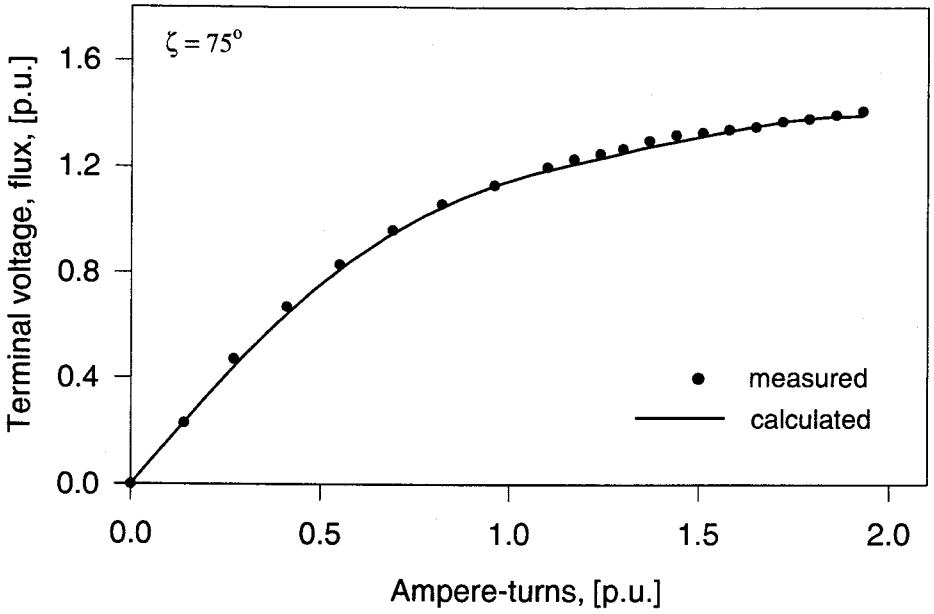

Figure 3.18: Intermediate-axis ($\zeta = 75^o$) saturation curve of the cylindrical-rotor synchronous machine using fourth-order saturation functions

In Eq.(3.22), m is the number of the measured points on an open-circuit characteristic curve, Φ_j are the measured values, and Φ_j^c are the calculated values at the measured points. Table (3.6) depicts the values obtained for ϵ for the axes $\zeta = 0^o, 30^o, 45^o, 60^o, 75^o, 90^o$. As these results show, the discrepancy between the measured open-circuit characteristics and the calculated saturation curves decreases as the order of the polynomials representing the saturation functions increases. It is clear that the fourth-order representation is sufficient to give an adequate result for the calculated saturation curves for the cylindrical-rotor synchronous machine used in the investigations of this thesis.

Table 3.6: Errors obtained using different order polynomials for the saturation functions

ζ	2^{nd} order	3^{rd} order	4^{th} order
0	0.031	0.012	0.004
30	0.029	0.016	0.012
45	0.032	0.022	0.019
60	0.030	0.016	0.014
75	0.028	0.016	0.011
90	0.026	0.014	0.004

3.6 The air-gap magnetic flux angles

During the experimental investigations, the air-gap magnetic flux angles δ' were also measured using a digital load-angle instrument which has an accuracy within one degree, and are given in Fig.(3.19). The values of this angle were also calculated using the method presented in Chapter 2, and are depicted in the same figure. It can be seen from this figure that there is a good agreement between the calculated ($n = 4$) and the measured values. It has also been observed that the order of the polynomials representing the saturation functions has no major influence on the accuracy of the calculated values of the air-gap magnetic flux angles.

3.7 Application to the cases of salient-pole synchronous machines

Although the method proposed in Chapter 2 is mainly developed to calculate the intermediate-axis saturation curves for cylindrical-rotor synchronous machines, it is general in nature and can be applied to the cases of salient-pole synchronous ma-

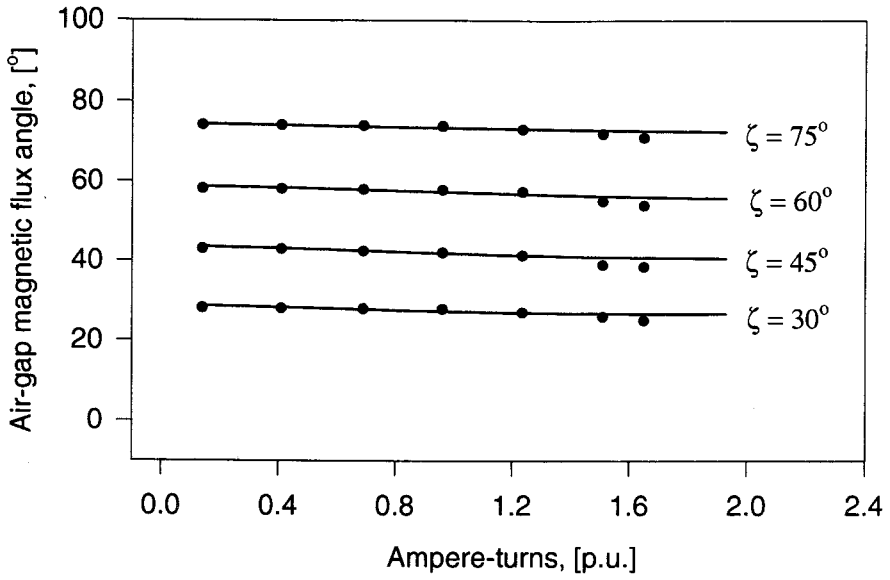

Figure 3.19: Air-gap magnetic flux angles δ' of the cylindrical-rotor synchronous machine

chines. In order to verify this, the method was applied to obtain the intermediate-axis saturation curves of a salient-pole synchronous machine.

The tested salient-pole synchronous machine has two wound damper windings, one in the direct axis and the other in the quadrature axis, in addition to the d-axis field winding. Exciting the machine from the direct axis using the field winding, and from the quadrature axis using the wound q-axis damper winding, the d-, q- and intermediate-axis open-circuit characteristics were obtained. Moreover, the corresponding saturation curves were calculated using the proposed method. Tables (3.7) and (3.8) give the data of this machine which are needed to apply the proposed

method and the measured open-circuit characteristics and the calculated saturation curves of this salient-pole synchronous machine are presented in Fig.(3.20). The air-gap magnetic flux angles were also obtained for this machine, and their measured and calculated values are depicted in Fig.(3.21). The presented calculated results are for the case using fourth-order polynomials for representing the saturation function and Table (3.9) gives the coefficients of these polynomials. As it can be seen from Figs.(3.20) and (3.21), there is a good agreement between the measured and calculated results.

Table 3.7: Data of the salient-pole synchronous machine

	X_{du}	X_{qu}	X_l	R_a
$[\Omega]$	16.15	9.84	2.58	0.371
$[p.u.]$	1.001	0.610	0.230	0.023

Table 3.8: Constants β, α and k of the salient-pole synchronous machine

β	α	k
0.75	0.175	1.004

Table 3.9: Fourth-order saturation function coefficients for the salient-pole synchronous machine

i	a_{id}	a_{iq}
1	0.037	-0.149
2	-0.111	-0.330
3	0.180	0.365
4	-0.045	-0.086

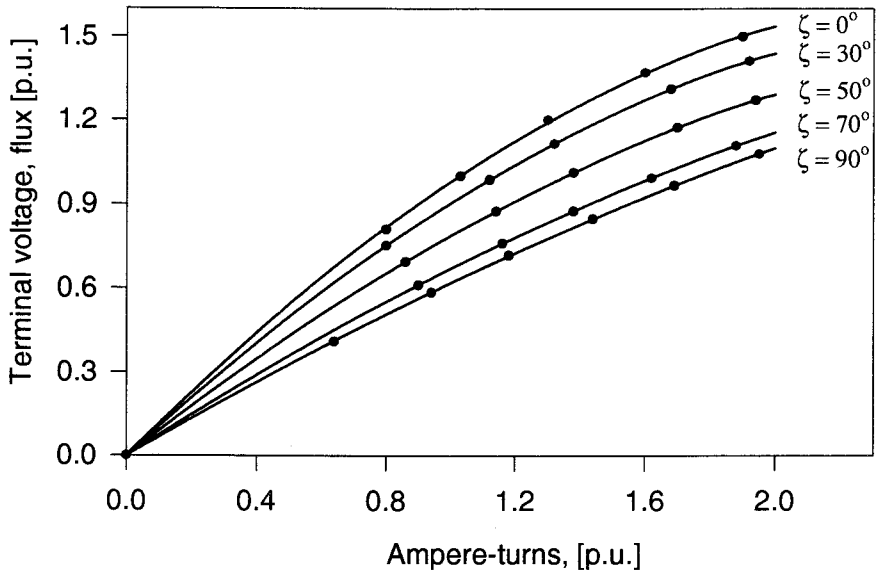

Figure 3.20: Saturation curves of the salient-pole synchronous machine

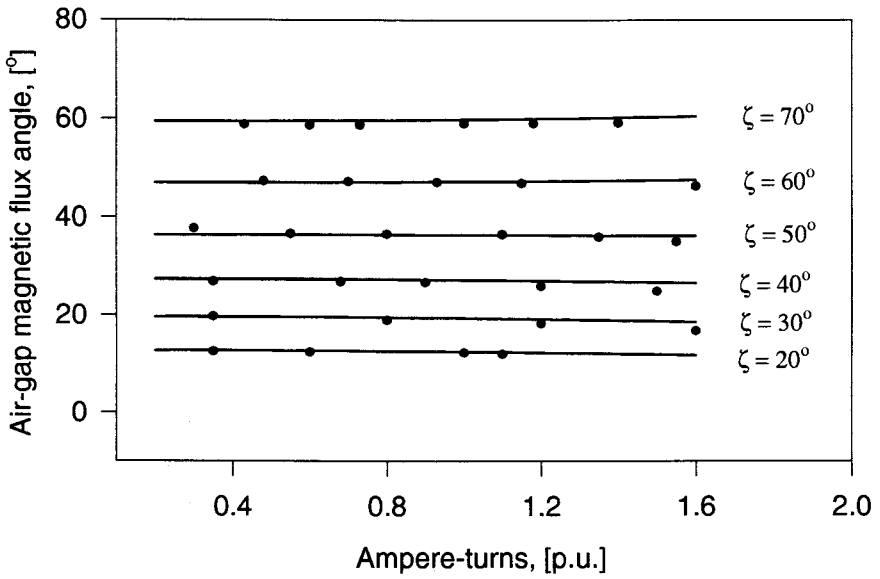

Figure 3.21: Air-gap magnetic flux angles δ' of the salient-pole synchronous machine

Chapter 4

Inclusion of the cross-magnetizing effect in the two-axis frame model of a saturated synchronous generator

As mentioned in Chapter 1, the assumption that there is no magnetic coupling between the direct and quadrature axes in the two-axis frame model of saturated synchronous machines is one of the main sources of errors when these models are used in power systems analysis. Such a magnetic coupling is usually, as mentioned in Chapter 1, referred to in the literature as the cross-magnetizing phenomenon. In this chapter, a physical interpretation of this phenomenon is presented and the inclusion of its effect in the two-axis frame model is discussed. To verify the accuracy of this modified two-axis frame model, experimental investigations were carried out on the synchronous machines described in Chapter 3.

4.1 Mathematical representation of the cross-magnetizing phenomenon

As shown in Chapters 2 and 3, the total ampere-turns in a saturated synchronous machine will result in a total air-gap magnetic flux, whose magnitude, Φ_t, and location depend on the total ampere-turns, AT_t, and the angle between the axis of the ampere-

turns and the direct axis, ζ. In general, the angle between the axis of the resulted air-gap magnetic flux and the direct axis, δ', is smaller than the angle ζ. Figure (4.1) shows these relationships represented in a phasor diagram form. In this case, the total ampere-turns, AT_t, could be represented by two components: one in the direct axis, AT_d, and one in the quadrature axis, AT_q. These two components can be expressed mathematically as follows:

$$AT_d = AT_t \cos(\zeta) \tag{4.1}$$

$$AT_q = AT_t \sin(\zeta) \tag{4.2}$$

Similarly, the resulted air-gap magnetic flux could be represented by two components: one in the direct-axis, Φ_{td}, and the other in the quadrature axis, Φ_{tq}. These two components can also be expressed mathematically as follows:

$$\Phi_{td} = \Phi_t \cos(\delta') \tag{4.3}$$

$$\Phi_{tq} = \Phi_t \sin(\delta') \tag{4.4}$$

If the d- and q-axis components of the total ampere-turns, AT_d and AT_q, are applied separately to the d- and q-axis saturation curves respectively, as it is the case in the conventional two-axis frame model, i.e. if the magnetic coupling between the two axes (cross-magnetizing phenomenon) is neglected, the corresponding air-gap

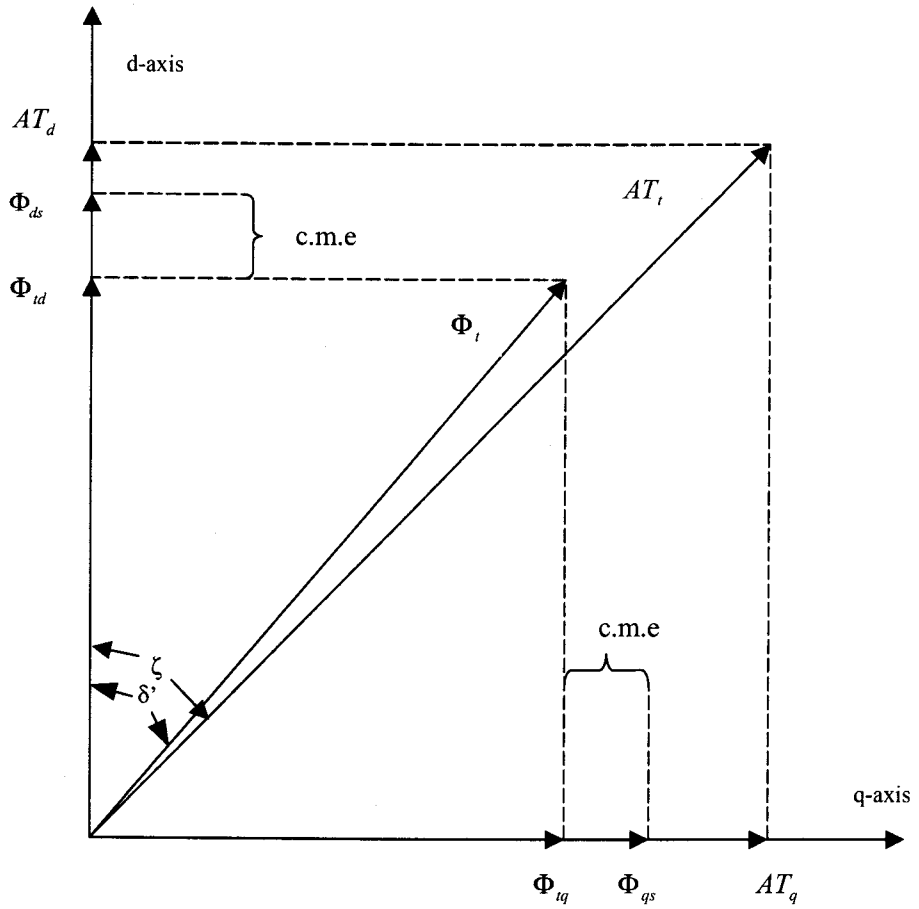

Figure 4.1: Air-gap flux and ampere-turns phasor diagram

magnetic flux, Φ_{ds} and Φ_{qs}, will be larger than Φ_{td} and Φ_{tq}, respectively. Thus, the effect of the cross-magnetizing phenomena is to reduce the components of the air-gap magnetic flux of the conventional two-axis frame model and can be represented by the differences between Φ_{ds} and Φ_{td}, and between Φ_{qs} and Φ_{tq}. Mathematically, the cross-magnetizing effect (c.m.e.) can be expressed as follows:

$$\Phi_{dq} = \Phi_{ds} - \Phi_{td} \tag{4.5}$$

$$= K_d\Phi_{du} - \Phi_t \cos(\delta') \tag{4.6}$$

$$\Phi_{qd} = \Phi_{qs} - \Phi_{tq} \tag{4.7}$$

$$= K_q\Phi_{qu} - \Phi_t \sin(\delta'), \tag{4.8}$$

where Φ_{dq} and Φ_{qd} are the parameters representing the cross-magnetizing effects in the direct and quadrature axes, respectively.

Analytically, the values of Φ_{dq} and Φ_{qd} can be determined using Eqs.(4.6) and (4.8). In these equations, the values of the total air-gap magnetic flux Φ_t and the angle δ' can be calculated using Eqs.(2.71) and (2.72), respectively. The values of Φ_{ds} and Φ_{qs} can be obtained from the measured d- and q-axis saturation curves, or can be calculated using Eqs.(2.37) and (2.42), respectively. To check the accuracy of this analytical approach, the two synchronous machines described in Chapter 3 were used. From their measured open-circuit characteristics and air-gap magnetic flux angle curves for the various axes, the values of Φ_{dq} and Φ_{qd} can also be calculated using the above described procedure. It is worthy to mention here again, that the per-unit values of the open-circuit terminal voltage and the corresponding air-gap magnetic flux of a synchronous machine are equal. Figures (4.2) to (4.9) show the analytically determined values of Φ_{dq} and Φ_{qd} for both the cylindrical-rotor and salient-pole synchronous machines described in Chapter 3. In Figs.(4.2), (4.3), (4.5) and (4.6), the measured values of Φ_{dq} and Φ_{qd} are also depicted.

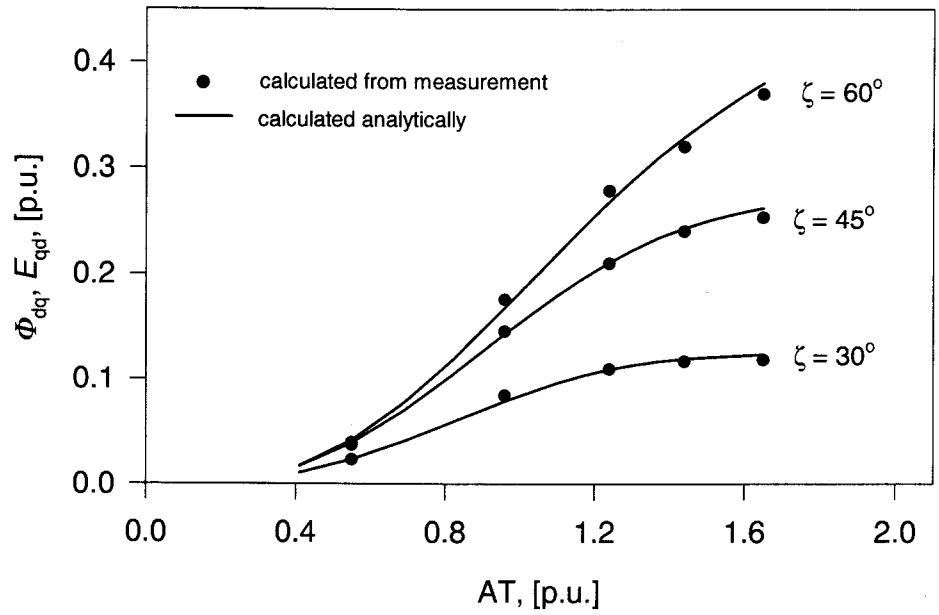

Figure 4.2: The cross-magnetization effect Φ_{dq} of the cylindrical-rotor synchronous machine in various intermediate axes

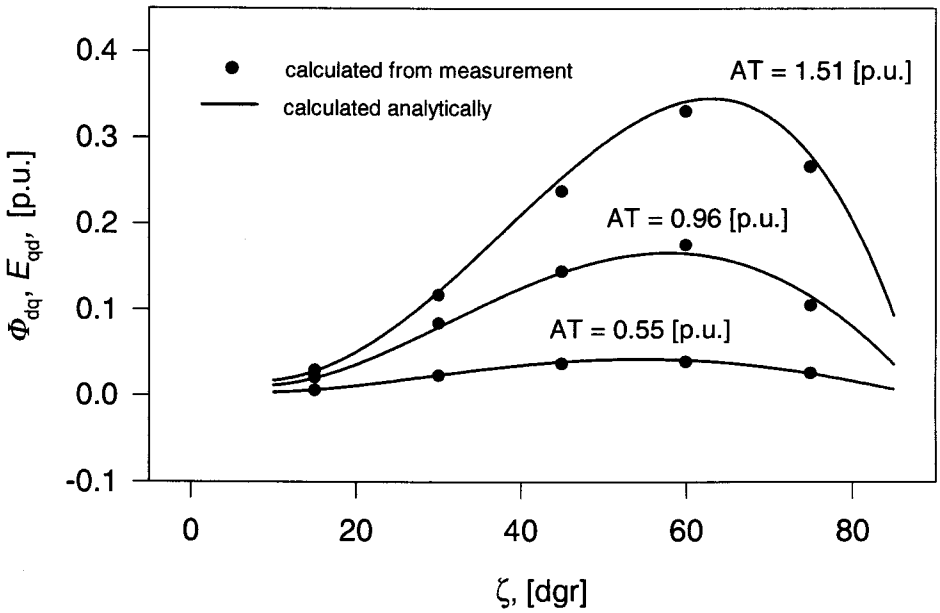

Figure 4.3: The cross-magnetization effect Φ_{dq} of the cylindrical-rotor synchronous machine, at constant ampere-turns

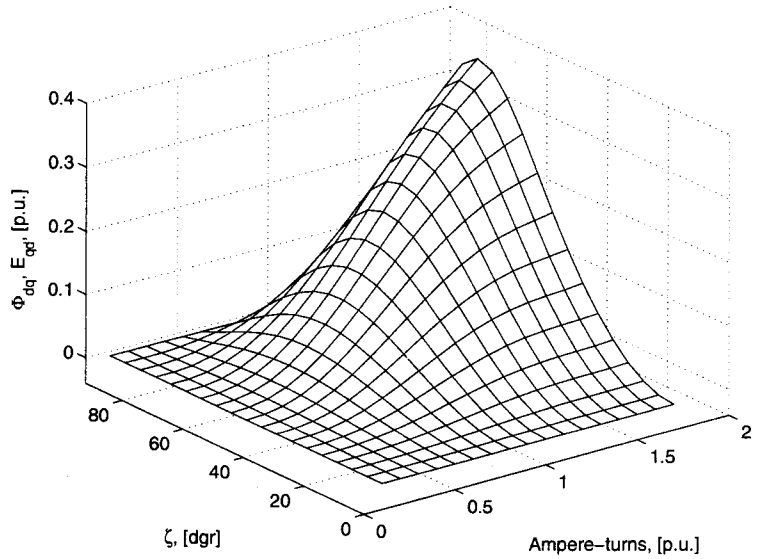

Figure 4.4: The cross-magnetization effect Φ_{dq} of the cylindrical-rotor synchronous machine in 3D representation

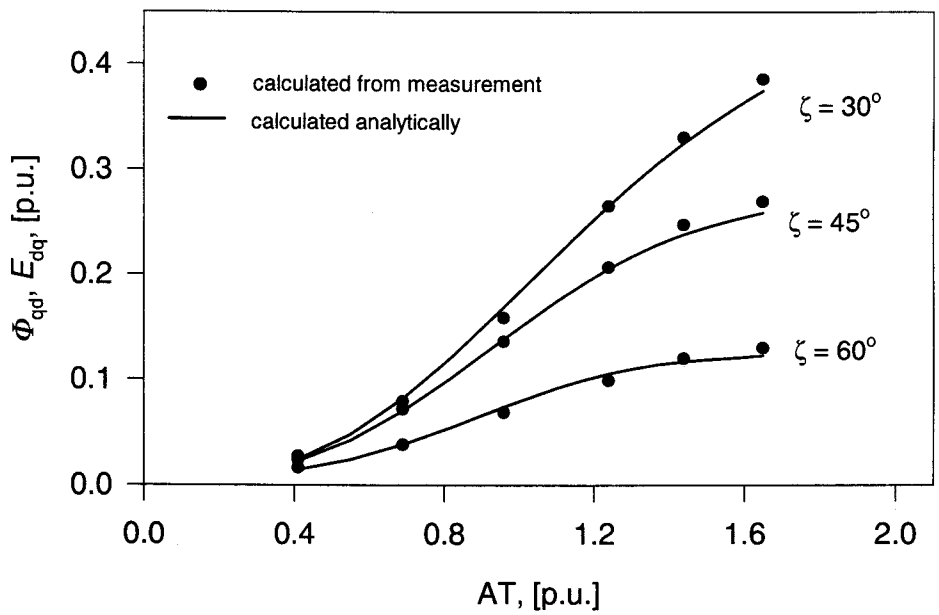

Figure 4.5: The cross-magnetization effect Φ_{qd} of the cylindrical-rotor synchronous machine in various intermediate axes

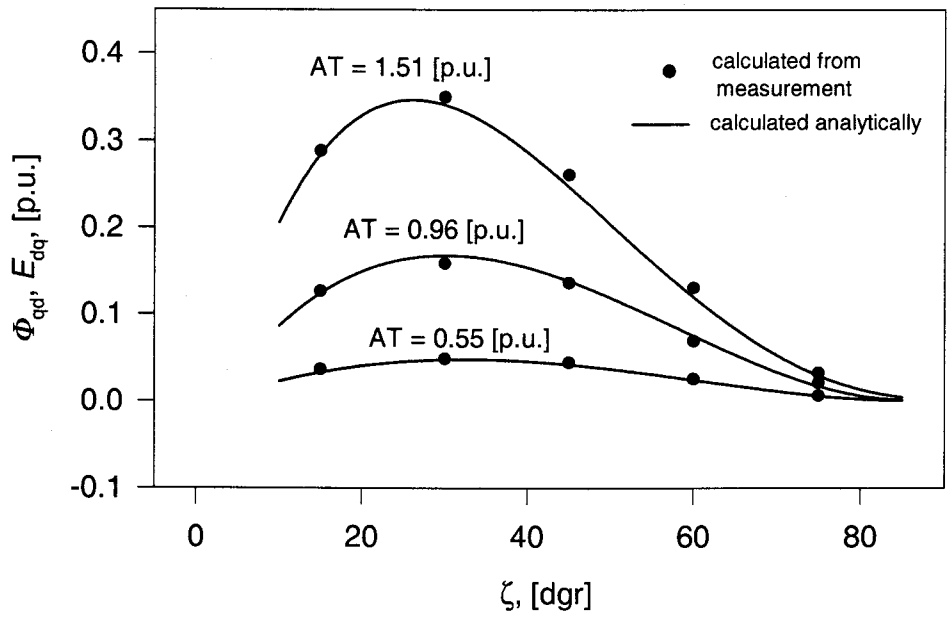

Figure 4.6: The cross-magnetization effect Φ_{qd} of the cylindrical-rotor synchronous machine, at constant ampere-turns

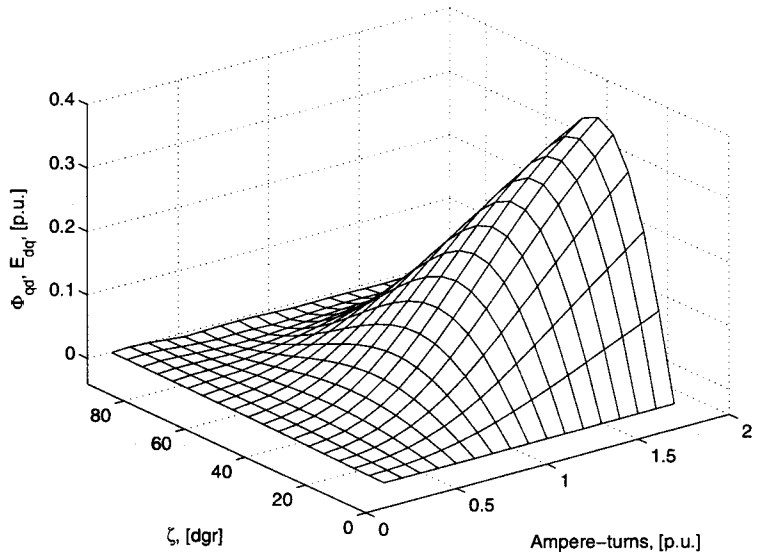

Figure 4.7: The cross-magnetization effect Φ_{qd} of the cylindrical-rotor synchronous machine in 3D representation

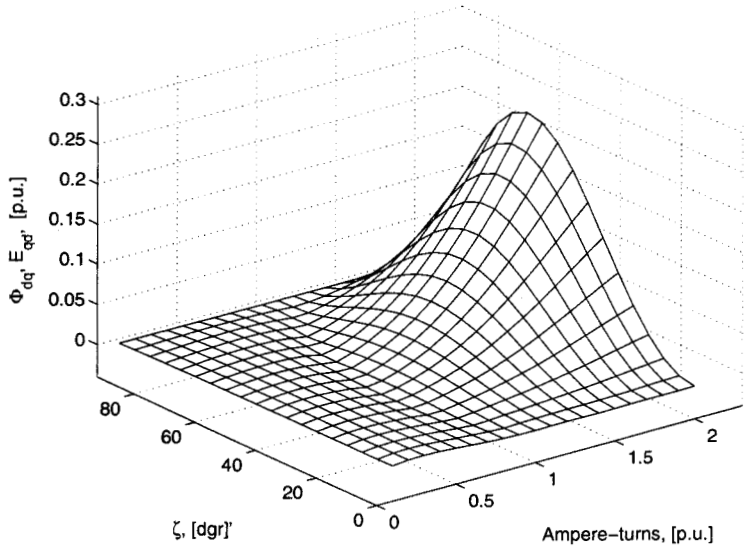

Figure 4.8: The cross-magnetization effect Φ_{dq} of the salient-pole synchronous machine in 3D representation

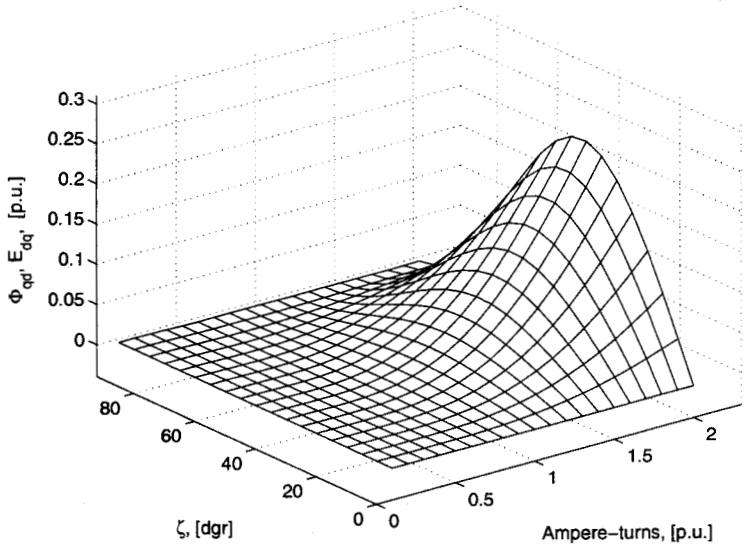

Figure 4.9: The cross-magnetization effect Φ_{qd} of the salient-pole synchronous machine in 3D representation

4.2 The phasor diagram of a synchronous generator with the cross-magnetizing effect included

The reductions in the d- and q-axis components of the air-gap magnetic flux of the two-axis frame model of saturated synchronous machines due to the cross-magnetizing effect, Φ_{dq} and Φ_{qd}, could be considered as reductions in the corresponding induced e.m.fs., E'_{qd} and E'_{dq}, respectively. In the adopted per-unit system, these reductions in the induced e.m.fs. are equal to the corresponding reductions in the magnetic fluxes components, i.e. $E'_{qd} = \Phi_{dq}$ and $E'_{dq} = \Phi_{qd}$, and should lag the corresponding reductions of the magnetic flux components by $\frac{\pi}{2}$, as shown in the phasor diagram of Fig.(4.10).

Since the effect of armature reaction is traditionally represented in the voltage phasor diagrams of synchronous machines by voltage drops, $I_d X_{ds}$ and $I_q X_{qs}$, the same practice is also applied here in representing the effect of the cross-magnetization. As shown in the voltage phasor diagram of Fig.(4.10), the inclusion of the cross-magnetizing effect is represented by two voltage drops, E_{qd} and E_{dq}, which are equal to, and in a direction opposing the corresponding reduction in the induced e.m.fs., E'_{qd} and E'_{dq}, respectively.

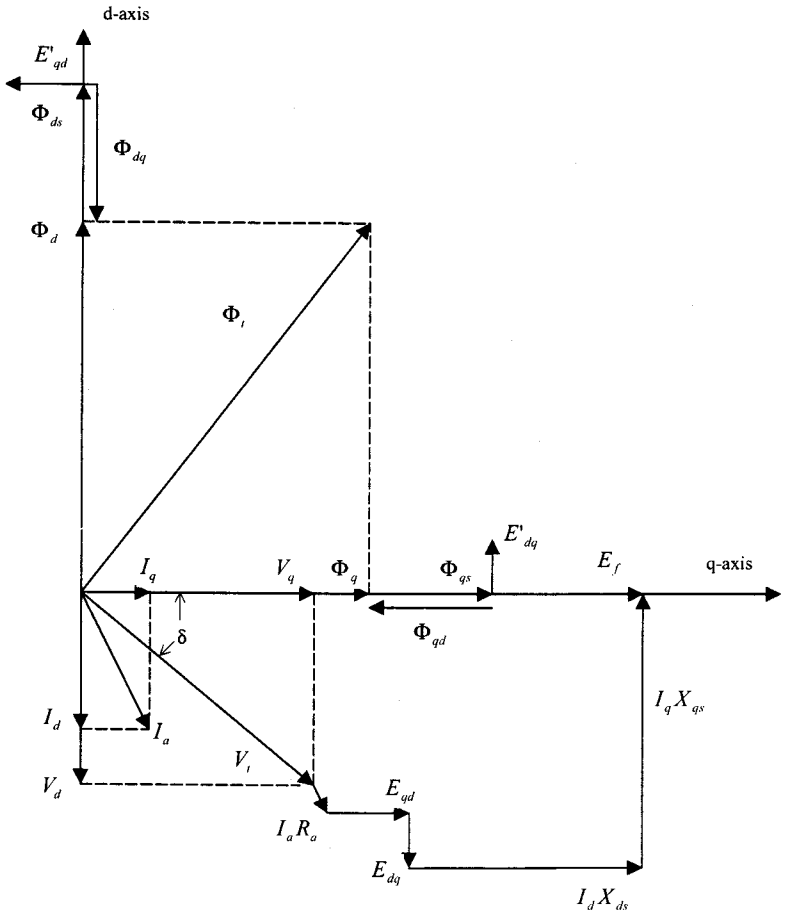

Figure 4.10: Phasor diagram of a saturated synchronous generator with the cross-magnetizing effect included

4.3 Power/load angle curves with the cross-magnetizing effect included

From the phasor diagram of Fig.(4.10), the following equations can be written for the direct and quadrature axes:

$$0 = I_d R_a + V_t \sin(\delta) + E_{dq} - I_q X_{qs} \tag{4.9}$$

$$E_f = I_d X_{ds} + V_t \cos(\delta) + I_q R_a + E_{qd} \tag{4.10}$$

Using Eqs.(4.9) and (4.10), the d- and q-axis components of the armature current can be expressed as:

$$I_d = \frac{E_f}{X_{ds}} - \frac{V_t}{X_{ds}}\cos(\delta) - \frac{R_a}{X_{ds}}I_q - \frac{E_{qd}}{X_{ds}} \tag{4.11}$$

$$I_q = \frac{V_t}{X_{qs}}\sin(\delta) + \frac{R_a}{X_{qs}}I_d + \frac{E_{dq}}{X_{qs}}. \tag{4.12}$$

Also, the active and reactive powers at the terminal of the machine can be obtained as:

$$\begin{aligned} P &= I_d V_{td} + I_q V_{tq} \\ &= I_d V_t \sin(\delta) + I_q V_t \cos(\delta) \end{aligned} \tag{4.13}$$

$$\begin{aligned} Q &= I_d V_{tq} - I_q V_{td} \\ &= I_d V_t \cos(\delta) - I_q V_t \sin(\delta) \end{aligned} \tag{4.14}$$

Substituting Eqs.(4.11) and (4.12) in Eqs.(4.13) and (4.14) the expressions of the steady-state power/load-angle characteristics of synchronous machines including the cross-magnetizing effect can be written as follows:

$$P = \frac{V_t E_f}{X_{ds}}\sin(\delta) + \frac{V_t^2}{2}\left(\frac{1}{X_{qs}} - \frac{1}{X_{ds}}\right)\sin(2\delta) + V_t R_a\left(\frac{I_d\cos(\delta)}{X_{qs}} - \frac{I_q\sin(\delta)}{X_{ds}}\right)$$

$$+V_t\left(\frac{E_{dq}}{X_{qs}}\cos(\delta)-\frac{E_{qd}}{X_{ds}}\sin(\delta)\right) \tag{4.15}$$

$$\begin{aligned} Q &= \frac{V_tE_f}{X_{ds}}\cos(\delta)-\frac{V_t^2}{2}\left(\frac{1}{X_{ds}}+\frac{1}{X_{qs}}\right)-\frac{V_t^2}{2}\left(\frac{1}{X_{ds}}-\frac{1}{X_{qs}}\right)\cos(2\delta) \\ &\quad -R_aV_t\left(\frac{I_q}{X_{ds}}\cos(\delta)+\frac{I_d}{X_{qs}}\sin(\delta)\right)-V_t\left(\frac{E_{qd}}{X_{ds}}\cos(\delta)+\frac{E_{dq}}{X_{qs}}\sin(\delta)\right) \end{aligned} \tag{4.16}$$

If the effect of the cross-magnetization is neglected (i.e. $E_{dq}=0$, $E_{qd}=0$), the expressions of the power/load angle characteristics could be obtained using Eqs.(4.15) and (4.16), and expressed as follows:

$$P = \frac{V_tE_f}{X_{ds}}\sin(\delta)+\frac{V_t^2}{2}\left(\frac{1}{X_{qs}}-\frac{1}{X_{ds}}\right)\sin(2\delta)+V_tR_a\left(\frac{I_d\cos(\delta)}{X_{qs}}-\frac{I_q\sin(\delta)}{X_{ds}}\right) \tag{4.17}$$

$$\begin{aligned} Q &= \frac{V_tE_f}{X_{ds}}\cos(\delta)-\frac{V_t^2}{2}\left(\frac{1}{X_{ds}}+\frac{1}{X_{qs}}\right)-\frac{V_t^2}{2}\left(\frac{1}{X_{ds}}-\frac{1}{X_{qs}}\right)\cos(2\delta) \\ &\quad -R_aV_t\left(\frac{I_q}{X_{ds}}\cos(\delta)+\frac{I_d}{X_{qs}}\sin(\delta)\right). \end{aligned} \tag{4.18}$$

Since the values of the saturated reactances X_{ds} and X_{qs} and the components representing the cross-magnetizing effect depend on the saturation level determined

by the loading conditions of the machine, the active and reactive powers as functions of the load angle have to be calculated using iterative techniques. The flow chart of the program used for such calculations is presented in Fig.(4.11).

4.4 Experimental verification of the accuracy of the modified two-axis frame model

To check the accuracy of the modified two-axis frame model with the cross-magnetizing effect included, the active and reactive powers under various levels of saturation have been measured at different load angles for the cylindrical-rotor and salient-pole synchronous generators described in Chapter 3. The measured values have been compared with the analytically determined results using the modified two-axis frame model, the same model without including the cross-magnetizing effect, and a two-axis frame model with the saturation effect neglected. The values obtained by measurement together with the calculated curves are depicted in Figs.(4.12) to (4.21) for both these machines.

As can be seen from Figs.(4.12), (4.13), (4.18) and (4.19), when the machine is operating in the unsaturated region, the effect of saturation is negligible. Under saturated operating conditions, the effect of the cross-magnetization on the calculated active and reactive powers is evident as shown in Figs.(4.14)-(4.17), (4.20) and (4.21). For the calculations using the two-axis frame model with saturation neglected or without the proper representation of the cross-magnetizing effect, discrepancies arise between the measured and calculated active and reactive power/load angle curves as

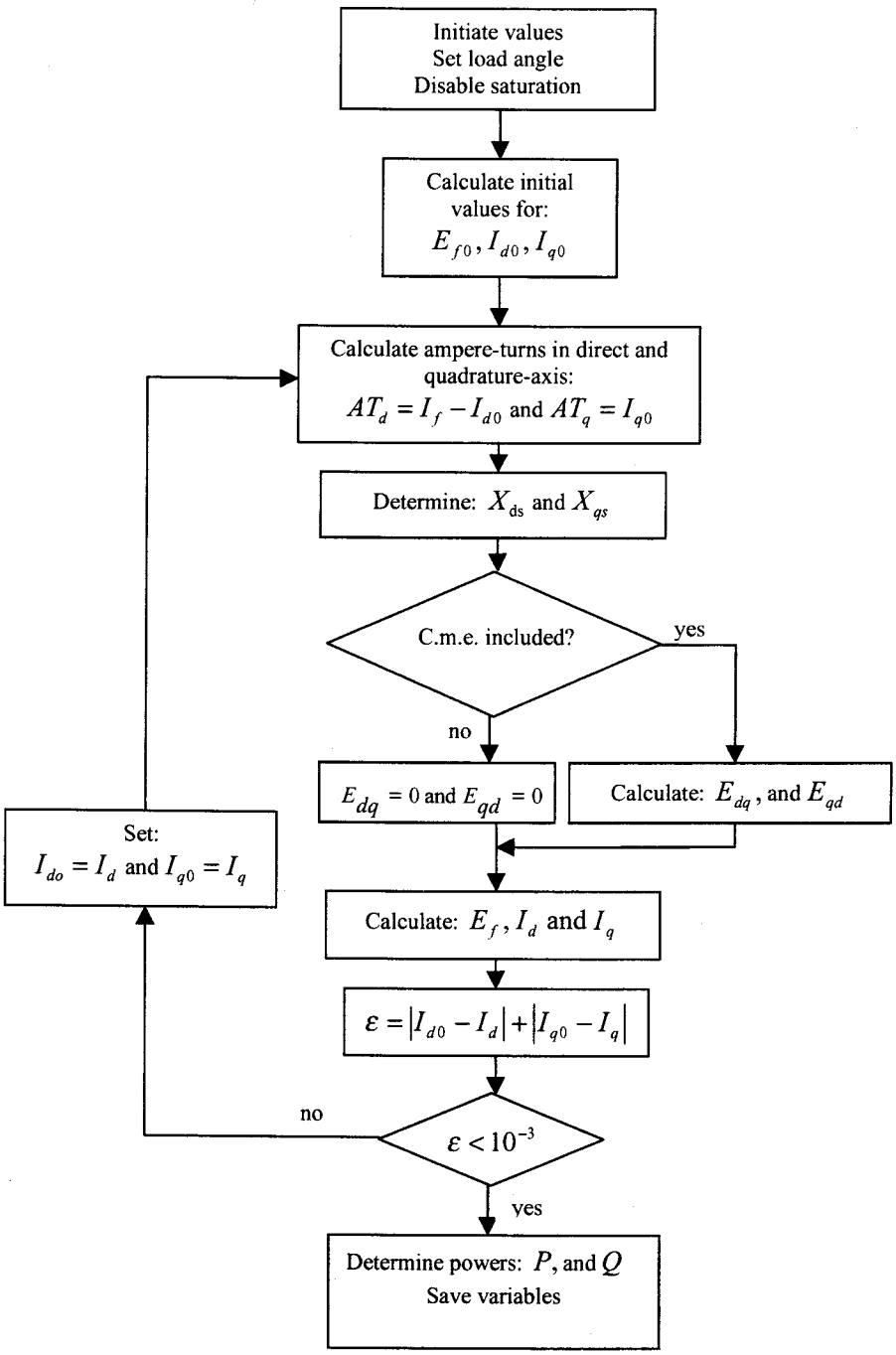

Figure 4.11: Flow chart of the program used for calculating the active and reactive powers for a saturated synchronous machine

seen from these figures. From these figures, it can be seen also that the accuracy of the calculated reactive powers are more influenced by the neglection of the cross-magnetizing effect.

In general, it is clear from all these figures, that there is a good agreement between the measured and calculated results when the effect of the cross-magnetization is included in the two-axis frame model of saturated synchronous machines.

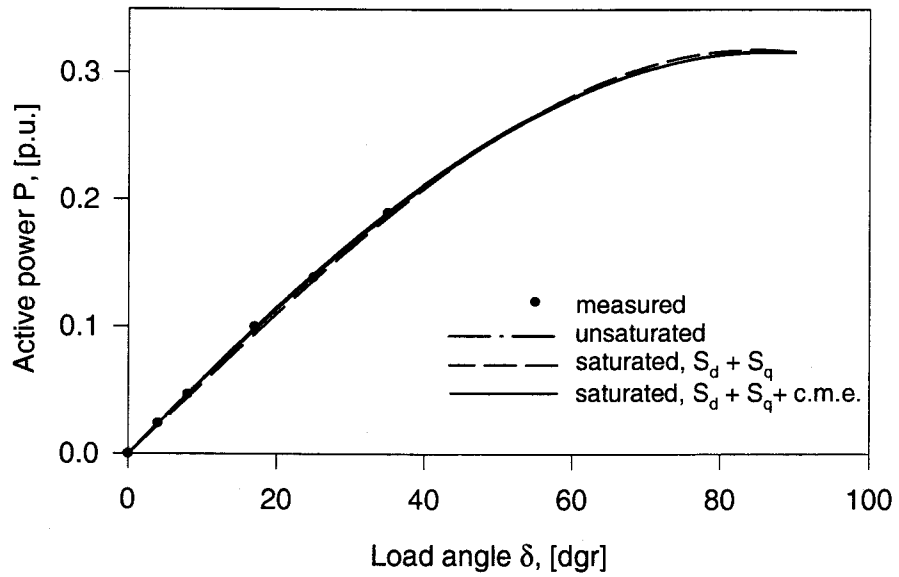

Figure 4.12: Active power/load angle curve of the cylindrical-rotor synchronous machine; $V_t = 0.63$ p.u., $I_f = 0.54$ p.u.

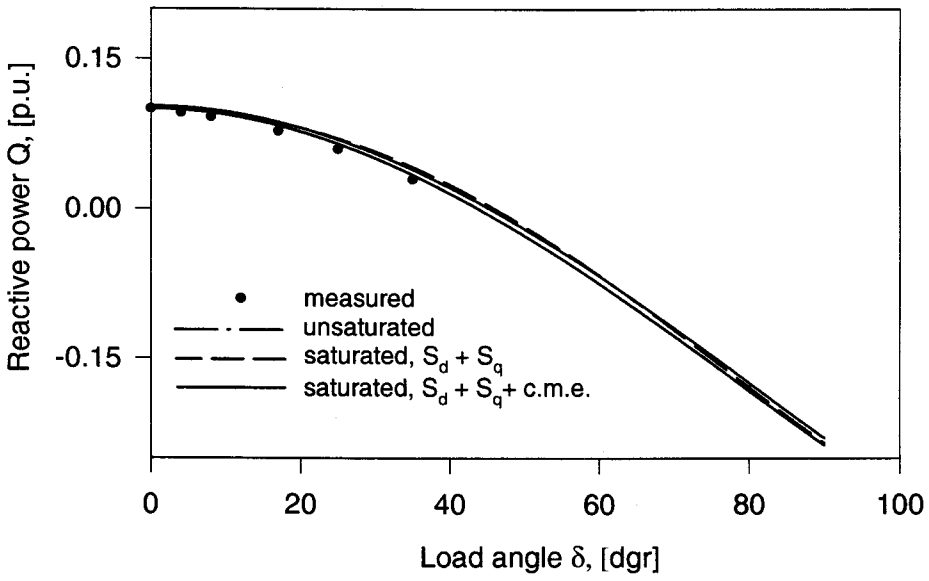

Figure 4.13: Reactive power/load angle curve of the cylindrical-rotor synchronous machine; $V_t = 0.63$ p.u., $I_f = 0.54$ p.u.

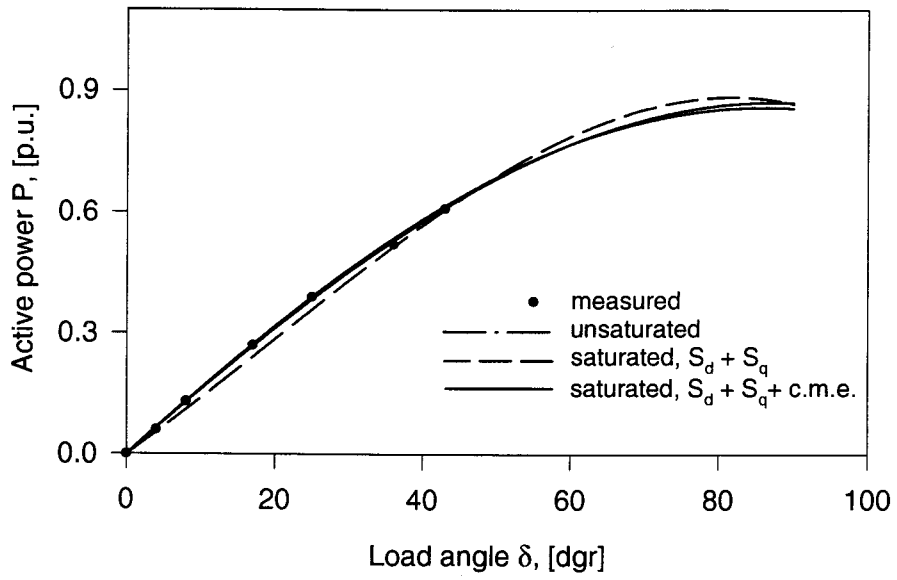

Figure 4.14: Active power/load angle curve of the cylindrical-rotor synchronous machine; $V_t = 1$ p.u., $I_f = 0.96$ p.u.

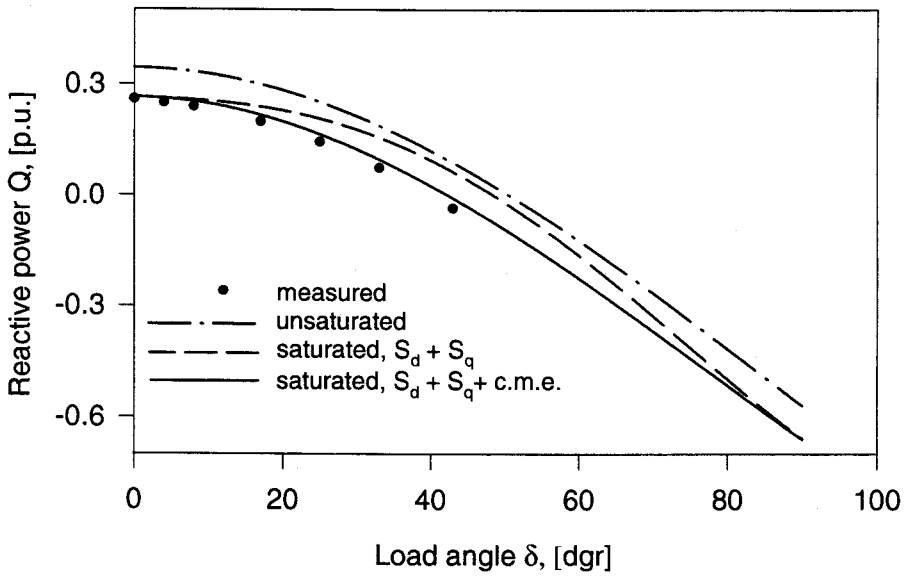

Figure 4.15: Reactive power/load angle curve of the cylindrical-rotor synchronous machine; $V_t = 1$ p.u., $I_f = 0.96$ p.u.

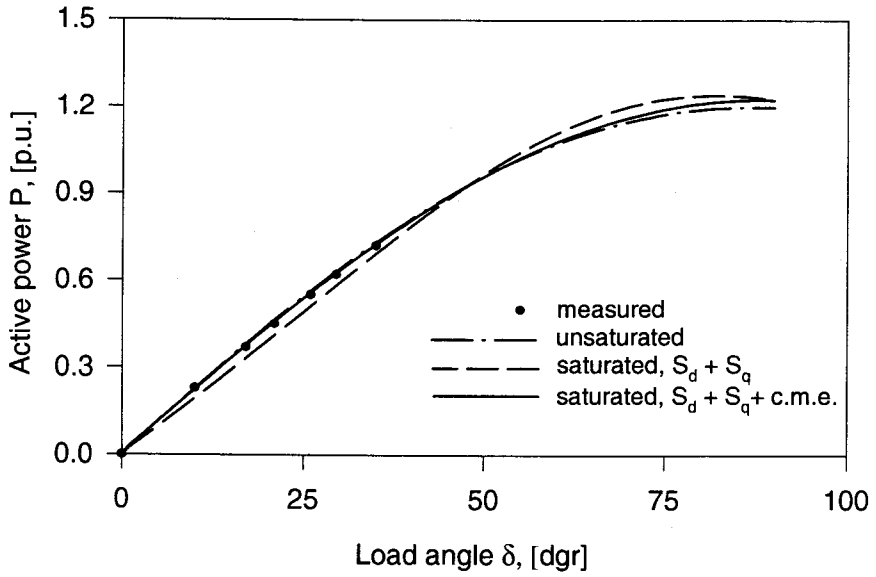

Figure 4.16: Active power/load angle curve of the cylindrical-rotor synchronous machine; $V_t = 1.09$ p.u., $I_f = 1.23$ p.u.

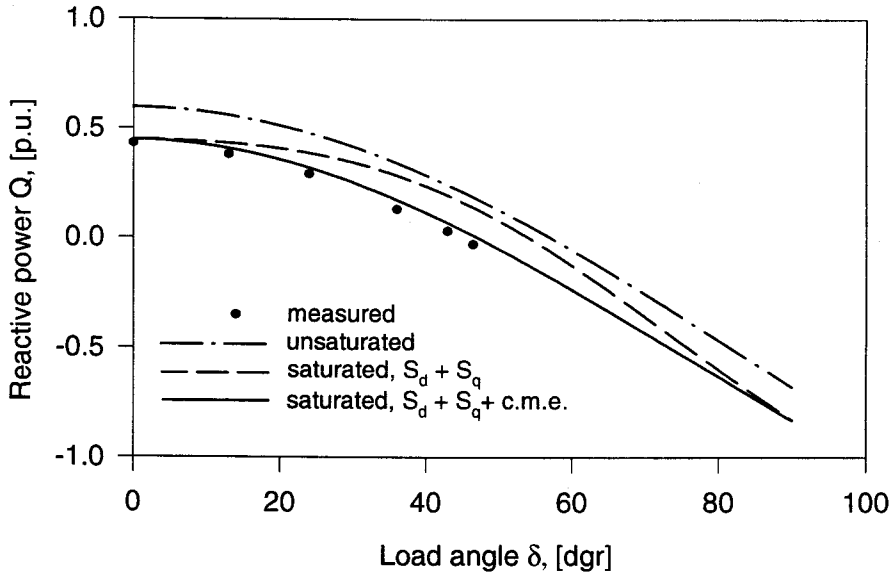

Figure 4.17: Reactive power/load angle curve of the cylindrical-rotor synchronous machine; $V_t = 1.09$ p.u., $I_f = 1.23$ p.u.

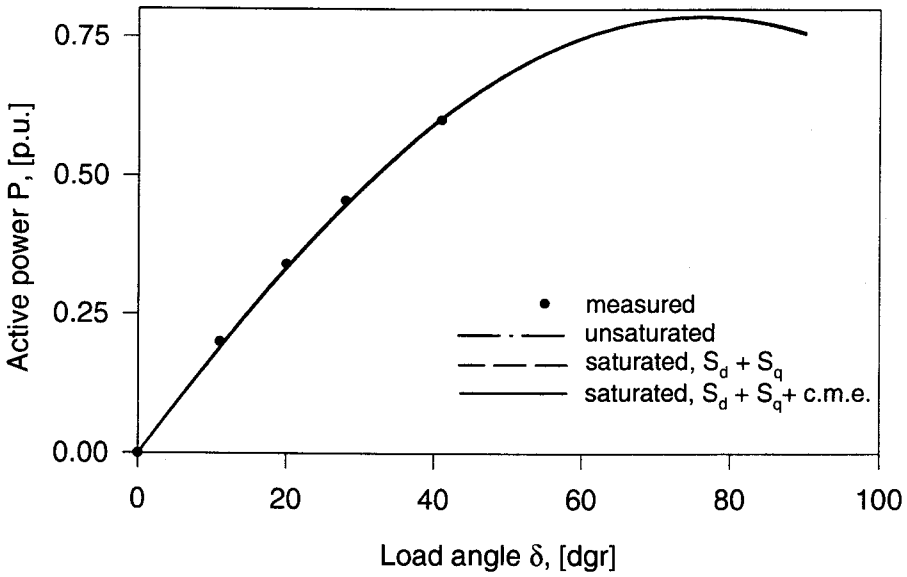

Figure 4.18: Active power/load angle curve of the salient-pole synchronous machine; $V_t = 0.727$ p.u., $I_f = 1.35$ p.u.

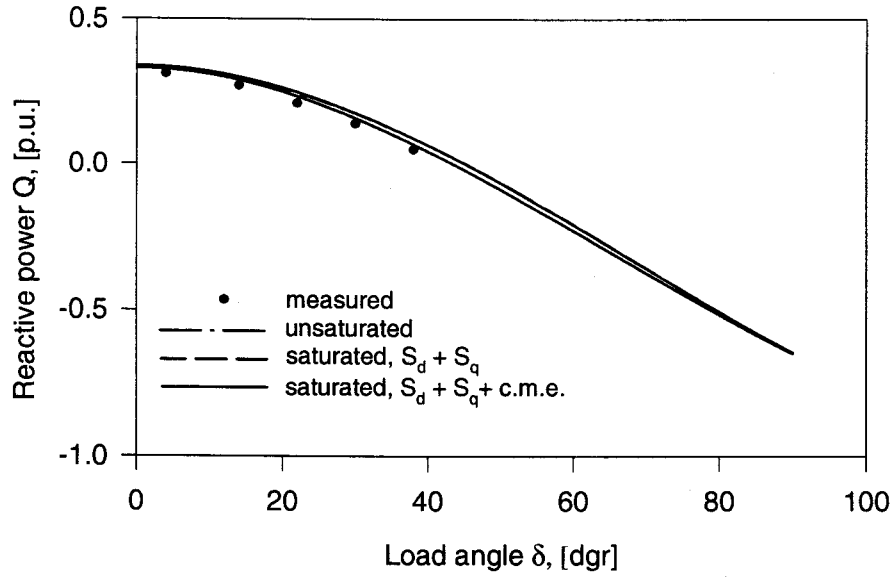

Figure 4.19: Reactive power/load angle curve of the salient-pole synchronous machine; $V_t = 0.727$ p.u., $I_f = 1.35$ p.u.

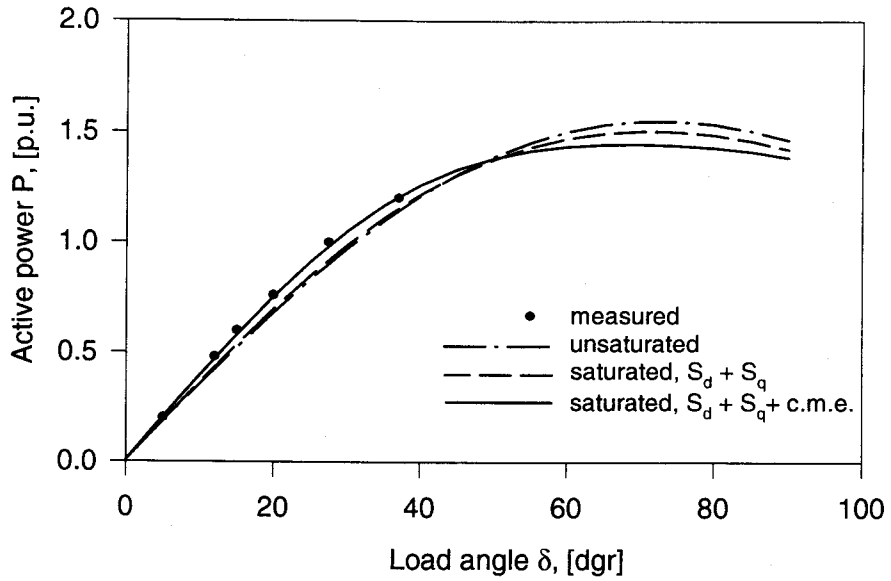

Figure 4.20: Active power/load angle curve of the salient-pole synchronous machine; $V_t = 1.182$ p.u., $I_f = 1.57$ p.u.

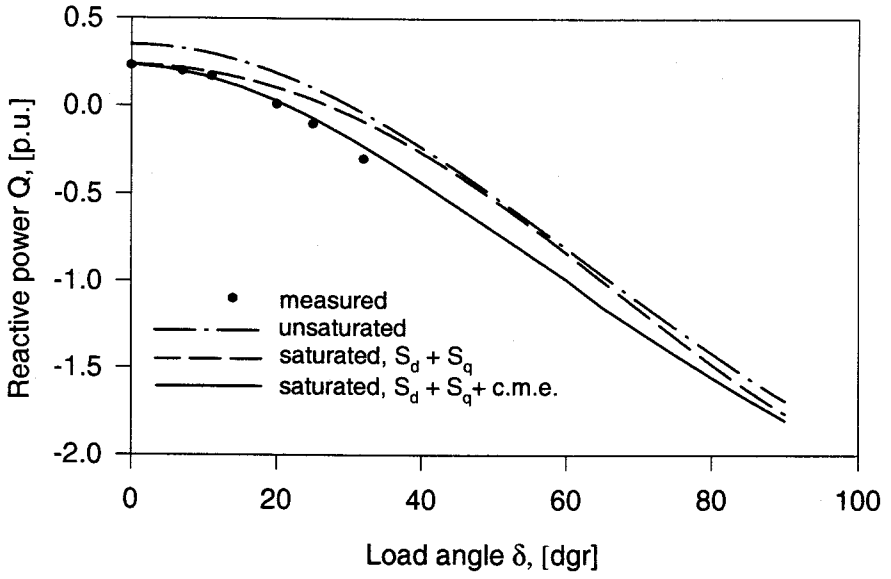

Figure 4.21: Reactive power/load angle curve of the salient-pole synchronous machine; $V_t = 1.182$ p.u., $I_f = 1.57$ p.u.

Chapter 5

Summary and conclusions

5.1 Summary

This thesis presents some aspects of the effect of saturation on the modeling and steady-state performance of cylindrical-rotor synchronous machines. The main aspects of the thesis can be summarized as follows:

- Chapter 1 is an introduction to the saturation phenomena in synchronous machines, and a presentation of the conventional approaches to saturated synchronous machines modeling.

- Chapter 2 presents an analytical method for determining the saturation curves in the intermediate axes of cylindrical-rotor synchronous machines from their measured d- and q-axis open-circuit characteristics. In the proposed method, an equivalent permeability is assumed for the magnetic paths of the synchronous machine. Saturation of these magnetic paths is represented by modifying the values of the equivalent permeability using polynomial saturation functions.

The coefficients of these polynomial functions are determined by applying fitting techniques to the measured d- and q-axis open-circuit characteristics of the machine. Using the proposed method, the intermediate-axis saturation curves and the angles between the air-gap magnetic flux and the direct axis have been obtained analytically.

- In Chapter 3, the accuracy of this proposed method has been verified by comparing the measured open-circuit characteristics and the calculated saturation curves for various axes for a cylindrical-rotor and a salient-pole synchronous machines that can be excited from both their direct and quadrature axes.

- The concept of the magnetic coupling between the direct and quadrature axes (cross-magnetizing phenomenon) of saturated synchronous machines is presented in Chapter 4. The inclusion of this cross-magnetizing phenomenon in the two-axis frame model of synchronous machines is introduced. The cross-magnetization has been represented as voltage drops caused by the cross-magnetizing effect, therefore, allowing the inclusion of the cross-magnetizing effect in the phasor diagram of the machine. Power/load angle relationships have been developed with the cross-magnetizing effect included. The accuracy of this modified two-axis frame model has been verified for both the cylindrical-rotor and salient-pole machines by comparing the measured values of the active and reactive powers with the calculated values for different load angles and saturation levels.

- In the Appendices, analytical derivations for the saturation function coefficients have been included up to the fourth-order polynomial representation. The proof of the simplified equations applied in the thesis for the calculation of the unsaturated synchronous reactances is also included.

5.2 Conclusions

The investigations conducted in this thesis yield the following conclusions:

- Accurate modeling of saturated synchronous machines in power systems studies cannot be done without the knowledge of the intermediate-axis saturation curves.

- The method proposed in this thesis for determining the intermediate-axis saturation curves of cylindrical-rotor synchronous machines provides an accurate approach for achieving this. The accuracy of this proposed method can be improved significantly by using higher order polynomial functions to represent the saturation function used to modify the equivalent permeability of the magnetic machine model. The order of the polynomials which gives an acceptable accuracy is machine dependent.

- Regarding the air-gap magnetic flux angles of cylindrical-rotor synchronous machines, the experimental investigations have found that the proposed method gives also a good approximation for the calculation of the angles between the

axis of the air-gap magnetic flux and the direct axis. Moreover, it has been found in the investigations of this thesis, that the calculated values of the angle are not sensitive to the order of the polynomials representing the saturation functions.

- The proposed method for determining the intermediate-axis saturation curves of cylindrical-rotor synchronous machines is general in nature and can be applied also to the cases of salient-pole synchronous machines.

- It has been found that magnetic coupling (cross-magnetizing phenomenon) exists between the direct and quadrature axes of both cylindrical-rotor and salient-pole saturated synchronous machines. This cross-magnetizing phenomenon is machine dependent, and it is caused by both the nonlinearity of the saturation curves and the saliency of the synchronous machines.

- The inclusion of the cross-magnetizing effect in the two-axis frame model of synchronous machines improves its accuracy. Neglecting this phenomenon results in noticeable inaccuracies in the calculated results using these models.

References

[1] B. Adkins and R. Harley, *The General Theory of Alternating Current Machines: Application to Practical Problems.* London: Chapman and Hall, Ltd., 1978.

[2] M. Kamous and M. Poloujadoff, "Experimental study of the effect of saturation on the steady state operation of a salient pole microalternator," *Electrical Machines and Power Systems*, vol. 10, pp. 325–334, 1985.

[3] R. Slemon, "Analytic models for saturated synchronous machines," *IEEE Transactions on Power Apparatus and Systems*, vol. PAS-90, pp. 409–417, 1971.

[4] G. Shackshaft, "Generator parameters for stability studies," Tech. Rep. 32-15, CIGRE, 1976.

[5] J. Lemay and T. Barton, "Small perturbation linearization of the saturated synchronous machine equations," *IEEE Transactions on Power Apparatus and Systems*, vol. PAS-91, pp. 233–240, 1972.

[6] N. Demerdash and H. Hamilton, "A simplified approach to determination of saturated synchronous machine reactances of large turbogenerators under load," *IEEE Transactions on Power Apparatus and Systems*, vol. PAS-95, pp. 560–569, 1976.

[7] A.M. El-Serafi and J. Wu, "A new method for determining the saturation curves in the intermediate axes of salient-pole synchronous machines," *Electric Machines and Power Systems*, vol. 21, pp. 199–215, 1993.

[8] A.M. El-Serafi and J. Wu, "Determination of the parameters representing the cross-magnetizatizing effect in saturated synchronous machines," *IEEE Transactions on Energy Conversion*, vol. 8, pp. 333–342, 1993.

[9] K. Binns, "Prediction of the no-load magnetization characteristics of large turbogenerators," *Proceedings IEE*, vol. 112, no. 4, pp. 720–730, 1965.

[10] G. Shackshaft, "General purpose turbo-alternator model," *Proceedings IEE*, vol. 110, no. 4, pp. 703–713, 1963.

[11] T. Hammons and D. Winning, "Comparisons of synchronous machine models in the study of the transient behaviors of electrical power systems," *Proceedings IEE*, vol. 118, no. 10, pp. 1442–1458, 1971.

[12] G. Shackshaft and P. Hanser, "Model of generator saturation for use in power systems studies," *Proceedings IEE*, vol. 126, no. 8, pp. 759–763, 1979.

[13] D. Harley, R.G. Limebeer and E. Chirricoeei, "Comparative study of saturation methods in synchronous machines models," *Proceedings IEE*, vol. 127, Part B, pp. 1–7, 1980.

[14] E. De Mello and L. Hannett, "Representation of saturation in synchronous machines," *IEEE Transactions on Power Apparatus and Systems*, vol. PWRS-1, pp. 8–18, 1986.

[15] E. Fuchs and E. Erdelyi, "Nonlinear theory of turboalternator, part ii: Load dependent synchronous reactances," *IEEE Transactions on Power Apparatus and Systems*, vol. PAS-92, pp. 592–599, 1973.

[16] M. Stiebler and C. Ritter, "Synchronous machine model including d/q flux coupling due to saturation," *IEE Second International Conference on Electrical Machines - Design and Applications, IEE Publication No. 254*, pp. 108–112, London, Sept. 1985.

[17] V. Brandwajn, "Representation of magnetic saturation in the synchronous machine model in an electro-magnetic transient program," *IEEE Transactions on Power Apparatus and Systems*, vol. PAS-99, pp. 1996–2001, 1980.

[18] J. Wu, "Theoretical and experimental investigations of the cross-magnetizing phenomenon in saturated synchronous machines," Master's thesis, University of Saskatchewan, 1989.

[19] A.M. El-Serafi, A.S. Abdallah, M.K. El-Sherbiny and E. Badawy, "Experimental study of the saturation and the cross magnetizing phenomenon in saturated synchronous machines," *IEEE Transactions on Energy Conversion*, vol. EC-3, pp. 815–823, 1988.

[20] G. Shackshaft and R. Neilson, "Results of stability tests on an under-excited 120MW generator," *Proceedings IEE*, vol. 119, pp. 175–188, 1972.

[21] F. Birch, "In discussions on G. Shackshaft and R. Neilson: Results of stability tests on an under-excited 120MW generator," *Proceedings IEE*, vol. 119, pp. 1487–1494, 1972.

[22] T. Hammons and D. Winning, "Comparison of synchronous-machine models in the study of the transient behavior of electrical power systems," *Proceedings IEE*, vol. 118, pp. 1442–1458, 1971.

[23] M. Liwschitz-Garic, *Electric Machinery.* New York: D. van Nostrand Company, Inc., 1946.

[24] J. Dougherty and S. Minnich, "Finite element modeling of large turbine generators: Calculations vs. load test data," *IEEE Transactions on Power Apparatus and Systems*, vol. PAS-100, pp. 3921–3928, 1981.

[25] K. Kovacs, "Cross magnetization in electrical machines with windings in quadrature," *IEE International Conference on Electrical Machines - Design and Applications, IEE Publications No. 254*, pp. 91–94, 17-19 September, 1985, London.

[26] A. Makky, "Representation of saturated salient-pole synchronous machines by a single magnetization curve," *Electrical Machines and Electromechanics*, vol. 7, no. 5, pp. 369–379, 1982.

[27] IEEE Standard, *Test Procedures for Synchronous Machines*, 1995.

[28] L. March and S. Crary, "Armature leakage reactance of synchronous machines," *AIEE Transactions*, vol. 54, pp. 378–381, 1935.

[29] C.J. Flores, G.W. Buckley and G. McPerson Jr., "The effects of saturation on the armature leakage reactance of large synchronous machines," *IEEE Transactions on Power Apparatus and Systems*, vol. PAS-103, pp. 593–600, 1984.

[30] W. Stevenson, *Elements of Power System Analysis.* McGraw Hill, 1982.

[31] A. Rankin, "Per unit impedances of synchronous machines," *AIEE Transactions*, vol. 64, pp. 839–841, 1945.

Appendix A

Analytical derivations

This appendix contains the analythical expressions for the coefficients c_{id}^{d}, c_{iq}^{d}, c_{id}^{q}, c_{iq}^{q}, I_{id}^{d}, I_{iq}^{d}, I_{id}^{q} and I_{iq}^{q}, introduced in Chapter 2.

A.1 The coefficients c_{iq}^{d} and c_{id}^{d} of Eqs.(2.39) and (2.40)

$$
\begin{aligned}
c_{1q}^{d} &= \frac{2}{\pi}k\left(\int_{-\frac{\pi}{2}}^{-\beta\frac{\pi}{2}}\cos^3(\theta)d\theta+\int_{\beta\frac{\pi}{2}}^{\frac{\pi}{2}}\cos^3(\theta)d\theta\right)\\
&= \frac{2}{\pi}k\frac{2\,\sin^3\frac{\pi\beta}{2}-6\,\sin\left(\frac{\pi\beta}{2}\right)+4}{3}\\
c_{2q}^{d} &= \frac{2}{\pi}k\left(\int_{-\frac{\pi}{2}}^{-\beta\frac{\pi}{2}}\cos^4(\theta)d\theta+\int_{\beta\frac{\pi}{2}}^{\frac{\pi}{2}}\cos^4(\theta)d\theta\right)\\
&= -\frac{2}{\pi}k\frac{\sin(2\,\pi\,\beta)+8\,\sin(\pi\,\beta)+6\,\pi\,\beta-6\,\pi}{16}\\
c_{3q}^{d} &= \frac{2}{\pi}k\left(\int_{-\frac{\pi}{2}}^{-\beta\frac{\pi}{2}}\cos^5(\theta)d\theta+\int_{\beta\frac{\pi}{2}}^{\frac{\pi}{2}}\cos^5(\theta)d\theta\right)\\
&= -\frac{2}{\pi}k\frac{6\,\sin^5\frac{\pi\beta}{2}-20\,\sin^3\frac{\pi\beta}{2}+30\,\sin\left(\frac{\pi\beta}{2}\right)-16}{15}
\end{aligned}
$$

$$c_{4q}^{d} = \frac{2}{\pi} k \left(\int_{-\frac{\pi}{2}}^{-\beta\frac{\pi}{2}} \cos^6(\theta) d\theta + \int_{\beta\frac{\pi}{2}}^{\frac{\pi}{2}} \cos^6(\theta) d\theta \right)$$

$$= -\frac{2}{\pi} k \frac{9 \sin(2\pi\beta) - 4 \sin^3(\pi\beta) + 48 \sin(\pi\beta) + 30\pi\beta - 30\pi}{96}$$

$$c_{1d}^{d} = \frac{2}{\pi} k \int_{-\beta\frac{\pi}{2}}^{\beta\frac{\pi}{2}} \cos^3(\theta) d\theta$$

$$= -\frac{2}{\pi} k \frac{2 \sin^3 \frac{\pi\beta}{2} - 6 \sin\left(\frac{\pi\beta}{2}\right)}{3}$$

$$c_{2d}^{d} = \frac{2}{\pi} k \int_{-\beta\frac{\pi}{2}}^{\beta\frac{\pi}{2}} \cos^4(\theta) d\theta$$

$$= \frac{2}{\pi} k \frac{\sin(2\pi\beta) + 8 \sin(\pi\beta) + 6\pi\beta}{16}$$

$$c_{3d}^{d} = \frac{2}{\pi} k \int_{-\beta\frac{\pi}{2}}^{\beta\frac{\pi}{2}} \cos^5(\theta) d\theta$$

$$= \frac{2}{\pi} k \frac{6 \sin^5 \frac{\pi\beta}{2} - 20 \sin^3 \frac{\pi\beta}{2} + 30 \sin\left(\frac{\pi\beta}{2}\right)}{15}$$

$$c_{4d}^{d} = \frac{2}{\pi} k \int_{-\beta\frac{\pi}{2}}^{\beta\frac{\pi}{2}} \cos^6(\theta) d\theta$$

$$= \frac{2}{\pi} k \frac{9 \sin(2\pi\beta) - 4 \sin^3(\pi\beta) + 48 \sin(\pi\beta) + 30\pi\beta}{96}$$

A.2 The coefficients c_{iq}^q and c_{id}^q of Eqs.(2.44) and (2.45)

$$
\begin{aligned}
c_{1q}^q &= \frac{2}{\pi}k\left(\int_{-\frac{\pi}{2}}^{-\beta\frac{\pi}{2}}\sin^3(\theta)d\theta+\int_{\beta\frac{\pi}{2}}^{\frac{\pi}{2}}\sin^3(\theta)d\theta\right)\\
&= -\frac{2}{\pi}k\frac{2\cos^3\frac{\pi\beta}{2}-6\cos\left(\frac{\pi\beta}{2}\right)}{3}\\
c_{2q}^q &= \frac{2}{\pi}k\left(\int_{-\frac{\pi}{2}}^{-\beta\frac{\pi}{2}}\sin^4(\theta)d\theta+\int_{\beta\frac{\pi}{2}}^{\frac{\pi}{2}}\sin^4(\theta)d\theta\right)\\
&= -\frac{2}{\pi}k\frac{\sin(2\pi\beta)-8\sin(\pi\beta)+6\pi\beta-6\pi}{16}\\
c_{3q}^q &= \frac{2}{\pi}k\left(\int_{-\frac{\pi}{2}}^{-\beta\frac{\pi}{2}}\sin^5(\theta)d\theta+\int_{\beta\frac{\pi}{2}}^{\frac{\pi}{2}}\sin^5(\theta)d\theta\right)\\
&= \frac{2}{\pi}k\frac{6\cos^5\frac{\pi\beta}{2}-20\cos^3\frac{\pi\beta}{2}+30\cos\left(\frac{\pi\beta}{2}\right)}{15}\\
c_{4q}^q &= \frac{2}{\pi}k\left(\int_{-\frac{\pi}{2}}^{-\beta\frac{\pi}{2}}\sin^6(\theta)d\theta+\int_{\beta\frac{\pi}{2}}^{\frac{\pi}{2}}\sin^6(\theta)d\theta\right)\\
&= -\frac{2}{\pi}k\frac{9\sin(2\pi\beta)+4\sin^3(\pi\beta)-48\sin(\pi\beta)+30\pi\beta-30\pi}{96}
\end{aligned}
$$

$$
\begin{aligned}
c_{1d}^q &= \frac{2}{\pi}k\int_{-\beta\frac{\pi}{2}}^{\beta\frac{\pi}{2}}\sin^3(\theta)d\theta\\
&= \frac{2}{\pi}k\frac{2\cos^3\frac{\pi\beta}{2}-6\cos\left(\frac{\pi\beta}{2}\right)+4}{3}
\end{aligned}
$$

$$c_{2d}^{q} = \frac{2}{\pi}k\int_{-\beta\frac{\pi}{2}}^{\beta\frac{\pi}{2}} \sin^4(\theta)d\theta$$

$$= \frac{2}{\pi}k\frac{\sin(2\,\pi\,\beta) - 8\,\sin(\pi\,\beta) + 6\,\pi\,\beta}{16}$$

$$c_{3d}^{q} = \frac{2}{\pi}k\int_{-\beta\frac{\pi}{2}}^{\beta\frac{\pi}{2}} \sin^5(\theta)d\theta$$

$$= -\frac{2}{\pi}k\frac{6\,\cos^5\frac{\pi\,\beta}{2} - 20\,\cos^3\frac{\pi\,\beta}{2} + 30\,\cos\left(\frac{\pi\,\beta}{2}\right) - 16}{15}$$

$$c_{4q}^{q} = \frac{2}{\pi}k\int_{-\beta\frac{\pi}{2}}^{\beta\frac{\pi}{2}} \sin^6(\theta)d\theta$$

$$= \frac{2}{\pi}k\frac{9\,\sin(2\,\pi\,\beta) + 4\,\sin^3(\pi\,\beta) - 48\,\sin(\pi\,\beta) + 30\,\pi\,\beta}{96}$$

A.3 The coefficients I_{iq}^{d} and I_{id}^{d} of Eqs.(2.17) to (2.20) for the case $\zeta < \frac{\pi}{2}(1-\beta)$

$$I_{0q}^{d} = \frac{2}{\pi}k\left(\int_{-\frac{\pi}{2}}^{-\beta\frac{\pi}{2}} \cos(\theta-\zeta)\cos(\theta)d\theta + \int_{\beta\frac{\pi}{2}}^{\frac{\pi}{2}} \cos(\theta-\zeta)\cos(\theta)d\theta\right)$$

$$= -\frac{2}{\pi}k\frac{\sin(\zeta+\pi\,\beta) - \sin(\zeta-\pi\,\beta) + (2\,\pi\,\beta - 2\,\pi)\,\cos\zeta}{4}$$

$$I_{1q}^{d} = \frac{2}{\pi}k\left(\begin{array}{l}\int_{-\frac{\pi}{2}}^{-\frac{\pi}{2}+\zeta}[-\cos^2(\theta-\zeta)]\cos(\theta)d\theta + \int_{-\frac{\pi}{2}+\zeta}^{-\beta\frac{\pi}{2}}\cos^2(\theta-\zeta)\cos(\theta)d\theta \\ + \int_{\beta\frac{\pi}{2}}^{\frac{\pi}{2}}\cos^2(\theta-\zeta)\cos(\theta)d\theta\end{array}\right)$$

$$= -\frac{2}{\pi}k\frac{\sin\left(\frac{4\,\zeta+3\,\pi\,\beta}{2}\right) + 3\,\sin\left(\frac{4\,\zeta+\pi\,\beta}{2}\right) - 3\,\sin\left(\frac{4\,\zeta-\pi\,\beta}{2}\right)}{12}$$

$$-\frac{2}{\pi}\frac{-\sin\left(\frac{4\zeta-3\pi\beta}{2}\right)-16\cos\zeta+12\sin\left(\frac{\pi\beta}{2}\right)}{12}$$

$$I_{2q}^{d} = \frac{2}{\pi}k\left(\begin{array}{l}\int_{-\frac{\pi}{2}}^{-\frac{\pi}{2}+\zeta}\cos^3(\theta-\zeta)\cos(\theta)d\theta+\int_{-\frac{\pi}{2}+\zeta}^{-\beta\frac{\pi}{2}}\cos^3(\theta-\zeta)\cos(\theta)d\theta\\+\int_{\beta\frac{\pi}{2}}^{\frac{\pi}{2}}\cos^2(\theta-\zeta)\cos(\theta)d\theta\end{array}\right)$$

$$= -\frac{2}{\pi}k\frac{\sin(3\zeta+2\pi\beta)+2\sin(3\zeta+\pi\beta)-2\sin(3\zeta-\pi\beta)}{32}$$

$$-\frac{2}{\pi}k\frac{-\sin(3\zeta-2\pi\beta)+6\sin(\zeta+\pi\beta)-6\sin(\zeta-\pi\beta)+(12\pi\beta-12\pi)\cos\zeta}{32}$$

$$I_{3q}^{d} = \frac{2}{\pi}k\left(\begin{array}{l}\int_{-\frac{\pi}{2}}^{-\frac{\pi}{2}+\zeta}\left[-\cos^4(\theta-\zeta)\right]\cos(\theta)d\theta+\int_{-\frac{\pi}{2}+\zeta}^{-\beta\frac{\pi}{2}}\cos^4(\theta-\zeta)\cos(\theta)d\theta\\+\int_{\beta\frac{\pi}{2}}^{\frac{\pi}{2}}\cos^2(\theta-\zeta)\cos(\theta)d\theta\end{array}\right)$$

$$= -\frac{2}{\pi}\frac{3\sin\left(\frac{8\zeta+5\pi\beta}{2}\right)+5\sin\left(\frac{8\zeta+3\pi\beta}{2}\right)-5\sin\left(\frac{8\zeta-3\pi\beta}{2}\right)-3\sin\left(\frac{8\zeta-5\pi\beta}{2}\right)}{240}$$

$$-\frac{2}{\pi}k\frac{20\sin\left(\frac{4\zeta+3\pi\beta}{2}\right)+60\sin\left(\frac{4\zeta+\pi\beta}{2}\right)-60\sin\left(\frac{4\zeta-\pi\beta}{2}\right)}{240}$$

$$-\frac{2}{\pi}k\frac{-20\sin\left(\frac{4\zeta-3\pi\beta}{2}\right)-256\cos\zeta+180\sin\left(\frac{\pi\beta}{2}\right)}{240}$$

$$I_{4q}^{d} = \frac{2}{\pi}k\left(\begin{array}{l}\int_{-\frac{\pi}{2}}^{-\frac{\pi}{2}+\zeta}\cos^5(\theta-\zeta)\cos(\theta)d\theta+\int_{-\frac{\pi}{2}+\zeta}^{-\beta\frac{\pi}{2}}\cos^5(\theta-\zeta)\cos(\theta)d\theta\\+\int_{\beta\frac{\pi}{2}}^{\frac{\pi}{2}}\cos^5(\theta-\zeta)\cos(\theta)d\theta\end{array}\right)$$

$$= -\frac{2}{\pi}k\frac{2\sin(5\zeta+3\pi\beta)+3\sin(5\zeta+2\pi\beta)-3\sin(5\zeta-2\pi\beta)}{384}$$

$$-\frac{2}{\pi}k\frac{-2\sin(5\zeta-3\pi\beta)+15\sin(3\zeta+2\pi\beta)+30\sin(3\zeta+\pi\beta)}{384}$$

$$-\frac{2}{\pi}k\frac{-30\sin(3\zeta-\pi\beta)-15\sin(3\zeta-2\pi\beta)+60\sin(\zeta+\pi\beta)}{384}$$

$$-\frac{2}{\pi}k\frac{-60\sin(\zeta-\pi\beta)+(120\pi\beta-120\pi)\cos\zeta}{384}$$

$$I_{0d}^{d} = \frac{2}{\pi}k\int_{-\beta\frac{\pi}{2}}^{\beta\frac{\pi}{2}}\cos(\theta-\zeta)\cos(\theta)d\theta$$

$$= \frac{2}{\pi}k\frac{\sin(\zeta+\pi\beta)-\sin(\zeta-\pi\beta)+2\pi\beta\cos\zeta}{4}$$

$$I_{1d}^{d} = \frac{2}{\pi}k\int_{-\beta\frac{\pi}{2}}^{\beta\frac{\pi}{2}}\cos^2(\theta-\zeta)\cos(\theta)d\theta$$

$$= \frac{2}{\pi}k\frac{\sin\left(\frac{4\zeta+3\pi\beta}{2}\right)+3\sin\left(\frac{4\zeta+\pi\beta}{2}\right)-3\sin\left(\frac{4\zeta-\pi\beta}{2}\right)-\sin\left(\frac{4\zeta-3\pi\beta}{2}\right)+12\sin\left(\frac{\pi\beta}{2}\right)}{12}$$

$$I_{2d}^{d} = \frac{2}{\pi}k\int_{-\beta\frac{\pi}{2}}^{\beta\frac{\pi}{2}}\cos^3(\theta-\zeta)\cos(\theta)d\theta$$

$$= \frac{2}{\pi}k\frac{\sin(3\zeta+2\pi\beta)+2\sin(3\zeta+\pi\beta)-2\sin(3\zeta-\pi\beta)-\sin(3\zeta-2\pi\beta)}{32}$$

$$+\frac{2}{\pi}k\frac{6\sin(\zeta+\pi\beta)-6\sin(\zeta-\pi\beta)+12\pi\beta\cos\zeta}{32}$$

$$I_{3d}^{d} = \frac{2}{\pi}k\int_{-\beta\frac{\pi}{2}}^{\beta\frac{\pi}{2}}\cos^4(\theta-\zeta)\cos(\theta)d\theta$$

$$= \frac{2}{\pi}k\frac{3\sin\left(\frac{8\zeta+5\pi\beta}{2}\right)+5\sin\left(\frac{8\zeta+3\pi\beta}{2}\right)-5\sin\left(\frac{8\zeta-3\pi\beta}{2}\right)-3\sin\left(\frac{8\zeta-5\pi\beta}{2}\right)}{240}$$

$$+\frac{2}{\pi}k\frac{20\sin\left(\frac{4\zeta+3\pi\beta}{2}\right)+60\sin\left(\frac{4\zeta+\pi\beta}{2}\right)-60\sin\left(\frac{4\zeta-\pi\beta}{2}\right)}{240}$$

$$+\frac{2}{\pi}k\frac{-20\sin\left(\frac{4\zeta-3\pi\beta}{2}\right)+180\sin\left(\frac{\pi\beta}{2}\right)}{240}$$

$$I_{4d}^{d} = \frac{2}{\pi}k\int_{-\beta\frac{\pi}{2}}^{\beta\frac{\pi}{2}}\cos^5(\theta-\zeta)\cos(\theta)d\theta$$

$$= \frac{2}{\pi}k\frac{2\sin(5\zeta+3\pi\beta)+3\sin(5\zeta+2\pi\beta)-3\sin(5\zeta-2\pi\beta)}{384}$$

$$+\frac{2}{\pi}k\frac{-2\sin(5\zeta-3\pi\beta)+15\sin(3\zeta+2\pi\beta)+30\sin(3\zeta+\pi\beta)}{384}$$

$$+\frac{2}{\pi}k\frac{-30\sin(3\zeta-\pi\beta)-15\sin(3\zeta-2\pi\beta)+60\sin(\zeta+\pi\beta)}{384}$$

$$+\frac{2}{\pi}k\frac{-60\sin(\zeta-\pi\beta)+120\pi\beta\cos\zeta}{384}$$

A.4 The coefficients I_{iq}^{q} and I_{id}^{q} of Eqs.(2.23) to (2.26) for the case $\zeta < \frac{\pi}{2}(1-\beta)$

$$I_{0q}^{q} = \frac{2}{\pi}k\left(\int_{-\frac{\pi}{2}}^{-\beta\frac{\pi}{2}}\cos(\theta-\zeta)\sin(\theta)d\theta+\int_{\beta\frac{\pi}{2}}^{\frac{\pi}{2}}\cos(\theta-\zeta)\sin(\theta)d\theta\right)$$

$$= -\frac{2}{\pi}k\frac{\cos(\zeta+\beta\pi)-\cos(\zeta-\beta\pi)+(2\beta\pi-2\pi)\sin\zeta}{4}$$

$$I_{1q}^{q} = \frac{2}{\pi}k\left(\begin{array}{l}\int_{-\frac{\pi}{2}}^{-\frac{\pi}{2}+\zeta}[-\cos^2(\theta-\zeta)]\sin(\theta)d\theta + \int_{-\frac{\pi}{2}+\zeta}^{-\beta\frac{\pi}{2}}\cos^2(\theta-\zeta)\sin(\theta)d\theta \\ +\int_{\beta\frac{\pi}{2}}^{\frac{\pi}{2}}\cos^2(\theta-\zeta)\sin(\theta)d\theta\end{array}\right)$$

$$= -\frac{2}{\pi}k\frac{\cos\left(\frac{4\zeta+3\pi\beta}{2}\right) - 3\cos\left(\frac{4\zeta+\pi\beta}{2}\right) + 3\cos\left(\frac{4\zeta-\pi\beta}{2}\right)}{12}$$

$$-\frac{2}{\pi}k\frac{-\cos\left(\frac{4\zeta-3\pi\beta}{2}\right) - 16\sin\zeta}{12}$$

$$I_{2q}^{q} = \frac{2}{\pi}k\left(\begin{array}{l}\int_{-\frac{\pi}{2}}^{-\frac{\pi}{2}+\zeta}\cos^3(\theta-\zeta)\sin(\theta)d\theta + \int_{-\frac{\pi}{2}+\zeta}^{-\beta\frac{\pi}{2}}\cos^3(\theta-\zeta)\sin(\theta)d\theta \\ +\int_{\beta\frac{\pi}{2}}^{\frac{\pi}{2}}\cos^3(\theta-\zeta)\sin(\theta)d\theta\end{array}\right)$$

$$= -\frac{2}{\pi}k\frac{\cos(3\zeta+2\pi\beta) - 2\cos(3\zeta+\pi\beta) + 2\cos(3\zeta-\pi\beta)}{32}$$

$$-\frac{2}{\pi}k\frac{-\cos(3\zeta-2\pi\beta) + 6\cos(\zeta+\pi\beta) - 6\cos(\zeta-\pi\beta) + (12\pi\beta-12\pi)\sin\zeta}{32}$$

$$I_{3q}^{q} = \frac{2}{\pi}k\left(\begin{array}{l}\int_{-\frac{\pi}{2}}^{-\frac{\pi}{2}+\zeta}[-\cos^4(\theta-\zeta)]\sin(\theta)d\theta + \int_{-\frac{\pi}{2}+\zeta}^{-\beta\frac{\pi}{2}}\cos^4(\theta-\zeta)\sin(\theta)d\theta \\ +\int_{\beta\frac{\pi}{2}}^{\frac{\pi}{2}}\cos^4(\theta-\zeta)\sin(\theta)d\theta\end{array}\right)$$

$$= -\frac{2}{\pi}k\frac{3\cos\left(\frac{8\zeta+5\pi\beta}{2}\right) - 5\cos\left(\frac{8\zeta+3\pi\beta}{2}\right) + 5\cos\left(\frac{8\zeta-3\pi\beta}{2}\right)}{240}$$

$$-\frac{2}{\pi}k\frac{-3\cos\left(\frac{8\zeta-5\pi\beta}{2}\right) + 20\cos\left(\frac{4\zeta+3\pi\beta}{2}\right) - 60\cos\left(\frac{4\zeta+\pi\beta}{2}\right)}{240}$$

$$-\frac{2}{\pi}k\frac{60\cos\left(\frac{4\zeta-\pi\beta}{2}\right) - 20\cos\left(\frac{4\zeta-3\pi\beta}{2}\right) - 256\sin\zeta}{240}$$

$$I_{4q}^{q} = \frac{2}{\pi}k \left(\begin{array}{l} \int_{-\frac{\pi}{2}}^{-\frac{\pi}{2}+\zeta} \cos^5(\theta-\zeta)\sin(\theta)d\theta + \int_{-\frac{\pi}{2}+\zeta}^{-\beta\frac{\pi}{2}} \cos^5(\theta-\zeta)\sin(\theta)d\theta \\ + \int_{\beta\frac{\pi}{2}}^{\frac{\pi}{2}} \cos^5(\theta-\zeta)\sin(\theta)d\theta \end{array} \right)$$

$$= -\frac{2}{\pi}k\frac{2\cos(5\zeta+3\pi\beta) - 3\cos(5\zeta+2\pi\beta) + 3\cos(5\zeta-2\pi\beta)}{32}$$

$$-\frac{2}{\pi}k\frac{-2\cos(5\zeta-3\pi\beta) + 15\cos(3\zeta+2\pi\beta) - 30\cos(3\zeta+\pi\beta)}{32}$$

$$-\frac{2}{\pi}k\frac{30\cos(3\zeta-\pi\beta) - 15\cos(3\zeta-2\pi\beta) + 60\cos(\zeta+\pi\beta)}{32}$$

$$-\frac{2}{\pi}k\frac{-60\cos(\zeta-\pi\beta) + (120\pi\beta - 120\pi)\sin\zeta}{384}$$

$$I_{0d}^{q} = \frac{2}{\pi}k\int_{-\beta\frac{\pi}{2}}^{\beta\frac{\pi}{2}} \cos(\theta-\zeta)\sin(\theta)d\theta$$

$$= \frac{\cos(\zeta+\pi\beta) - \cos(\zeta-\pi\beta) + 2\pi\beta\sin\zeta}{4}$$

$$I_{1d}^{q} = \frac{2}{\pi}k\int_{-\beta\frac{\pi}{2}}^{\beta\frac{\pi}{2}} \cos^2(\theta-\zeta)\sin(\theta)d\theta$$

$$= \frac{\cos\left(\frac{4\zeta+3\pi\beta}{2}\right) - 3\cos\left(\frac{4\zeta+\pi\beta}{2}\right) + 3\cos\left(\frac{4\zeta-\pi\beta}{2}\right) - \cos\left(\frac{4\zeta-3\pi\beta}{2}\right)}{12}$$

$$I_{2d}^{q} = \frac{2}{\pi}k\int_{-\beta\frac{\pi}{2}}^{\beta\frac{\pi}{2}} \cos^3(\theta-\zeta)\sin(\theta)d\theta$$

$$= \frac{2}{\pi}k\frac{\cos(3\zeta+2\pi\beta) - 2\cos(3\zeta+\pi\beta) + 2\cos(3\zeta-\pi\beta)}{32}$$

$$+\frac{2}{\pi}k\frac{-\cos(3\zeta-2\pi\beta)+6\cos(\zeta+\pi\beta)-6\cos(\zeta-\pi\beta)+12\pi\beta\sin\zeta}{32}$$

$$I_{3d}^{q} = \frac{2}{\pi}k\int_{-\beta\frac{\pi}{2}}^{\beta\frac{\pi}{2}}\cos^4(\theta-\zeta)\sin(\theta)d\theta$$

$$= \frac{2}{\pi}k\frac{3\cos\left(\frac{8\zeta+5\pi\beta}{2}\right)-5\cos\left(\frac{8\zeta+3\pi\beta}{2}\right)+5\cos\left(\frac{8\zeta-3\pi\beta}{2}\right)}{240}$$

$$+\frac{2}{\pi}k\frac{-3\cos\left(\frac{8\zeta-5\pi\beta}{2}\right)+20\cos\left(\frac{4\zeta+3\pi\beta}{2}\right)-60\cos\left(\frac{4\zeta+\pi\beta}{2}\right)}{240}$$

$$+\frac{2}{\pi}k\frac{60\cos\left(\frac{4\zeta-\pi\beta}{2}\right)-20\cos\left(\frac{4\zeta-3\pi\beta}{2}\right)}{240}$$

$$I_{4d}^{q} = \frac{2}{\pi}k\int_{-\beta\frac{\pi}{2}}^{\beta\frac{\pi}{2}}\cos^5(\theta-\zeta)\sin(\theta)d\theta$$

$$= \frac{2}{\pi}k\frac{2\cos(5\zeta+3\pi\beta)-3\cos(5\zeta+2\pi\beta)+3\cos(5\zeta-2\pi\beta)}{384}$$

$$+\frac{2}{\pi}k\frac{-2\cos(5\zeta-3\pi\beta)+15\cos(3\zeta+2\pi\beta)-30\cos(3\zeta+\pi\beta)}{384}$$

$$+\frac{2}{\pi}k\frac{30\cos(3\zeta-\pi\beta)-15\cos(3\zeta-2\pi\beta)+60\cos(\zeta+\pi\beta)}{384}$$

$$+\frac{2}{\pi}k\frac{-60\cos(\zeta-\pi\beta)+120\pi\beta\sin\zeta}{384}$$

A.5 The coefficients I_{iq}^d and I_{id}^d of Eqs.(2.17) to (2.20) for the case $\zeta > \frac{\pi}{2}(1-\beta)$

$$I_{0q}^d = \frac{2}{\pi}k\left(\int_{-\frac{\pi}{2}}^{-\beta\frac{\pi}{2}}\cos(\theta-\zeta)\cos(\theta)d\theta + \int_{\beta\frac{\pi}{2}}^{\frac{\pi}{2}}\cos(\theta-\zeta)\cos(\theta)d\theta\right)$$

$$= -\frac{2}{\pi}k\frac{\sin(\zeta+\pi\beta) - \sin(\zeta-\pi\beta) + (2\pi\beta - 2\pi)\cos\zeta}{4}$$

$$I_{1q}^d = \frac{2}{\pi}k\left(\int_{-\frac{\pi}{2}}^{-\beta\frac{\pi}{2}}\left[-\cos^2(\theta-\zeta)\right]\cos(\theta)d\theta + \int_{\beta\frac{\pi}{2}}^{\frac{\pi}{2}}\cos^2(\theta-\zeta)\cos(\theta)d\theta\right)$$

$$= \frac{2}{\pi}k\frac{\sin\left(\frac{4\zeta+3\pi\beta}{2}\right) + 3\sin\left(\frac{4\zeta+\pi\beta}{2}\right) + 3\sin\left(\frac{4\zeta-\pi\beta}{2}\right) + \sin\left(\frac{4\zeta-3\pi\beta}{2}\right)}{12}$$

$$I_{2q}^d = \frac{2}{\pi}k\left(\int_{-\frac{\pi}{2}}^{-\beta\frac{\pi}{2}}\cos^3(\theta-\zeta)\cos(\theta)d\theta + \int_{\beta\frac{\pi}{2}}^{\frac{\pi}{2}}\cos^3(\theta-\zeta)\cos(\theta)d\theta\right)$$

$$= -\frac{2}{\pi}k\frac{\sin(3\zeta+2\pi\beta) + 2\sin(3\zeta+\pi\beta) - 2\sin(3\zeta-\pi\beta)}{32}$$

$$-\frac{2}{\pi}k\frac{-\sin(3\zeta-2\pi\beta) + 6\sin(\zeta+\pi\beta) - 6\sin(\zeta-\pi\beta) - (12\pi\beta - 12\pi)\cos\zeta}{32}$$

$$I_{3q}^d = \frac{2}{\pi}k\left(\int_{-\frac{\pi}{2}}^{-\beta\frac{\pi}{2}}\left[-\cos^4(\theta-\zeta)\right]\cos(\theta)d\theta + \int_{\beta\frac{\pi}{2}}^{\frac{\pi}{2}}\cos^4(\theta-\zeta)\cos(\theta)d\theta\right)$$

$$= \frac{2}{\pi}k\frac{3\sin\left(\frac{8\zeta+5\pi\beta}{2}\right) + 5\sin\left(\frac{8\zeta+3\pi\beta}{2}\right) + 5\sin\left(\frac{8\zeta-3\pi\beta}{2}\right) + 3\sin\left(\frac{8\zeta-5\pi\beta}{2}\right)}{240}$$

$$+\frac{2}{\pi}k\frac{20\sin\left(\frac{4\zeta+3\pi\beta}{2}\right) + 60\sin\left(\frac{4\zeta+\pi\beta}{2}\right) + 60\sin\left(\frac{4\zeta-\pi\beta}{2}\right) + 20\sin\left(\frac{4\zeta-3\pi\beta}{2}\right)}{240}$$

$$I_{4q}^{d} = \frac{2}{\pi}k\left(\int_{-\frac{\pi}{2}}^{-\beta\frac{\pi}{2}}\cos^5(\theta-\zeta)\cos(\theta)d\theta + \int_{\beta\frac{\pi}{2}}^{\frac{\pi}{2}}\cos^5(\theta-\zeta)\cos(\theta)d\theta\right)$$

$$= -\frac{2}{\pi}k\frac{2\sin(5\zeta+3\pi\beta)+3\sin(5\zeta+2\pi\beta)-3\sin(5\zeta-2\pi\beta)}{384}$$

$$-\frac{2}{\pi}k\frac{-2\sin(5\zeta-3\pi\beta)+15\sin(3\zeta+2\pi\beta)+30\sin(3\zeta+\pi\beta)}{384}$$

$$-\frac{2}{\pi}k\frac{-30\sin(3\zeta-\pi\beta)-15\sin(3\zeta-2\pi\beta)+60\sin(\zeta+\pi\beta)}{384}$$

$$-\frac{2}{\pi}k\frac{-60\sin(\zeta-\pi\beta)+(120\pi\beta-120\pi)\cos\zeta}{384}$$

$$I_{0d}^{d} = \frac{2}{\pi}k\int_{-\beta\frac{\pi}{2}}^{\beta\frac{\pi}{2}}\cos(\theta-\zeta)\cos(\theta)d\theta$$

$$= \frac{\sin(\zeta+\pi\beta)-\sin(\zeta-\pi\beta)+2\pi\beta\cos\zeta}{4}$$

$$I_{1d}^{d} = \frac{2}{\pi}k\left(\int_{-\beta\frac{\pi}{2}}^{-\frac{\pi}{2}+\zeta}\left[-\cos^2(\theta-\zeta)\right]\cos(\theta)d\theta + \int_{-\frac{\pi}{2}+\zeta}^{\beta\frac{\pi}{2}}\cos^2(\theta-\zeta)\cos(\theta)d\theta\right)$$

$$= -\frac{2}{\pi}k\frac{\sin\left(\frac{4\zeta+3\pi\beta}{2}\right)+3\sin\left(\frac{4\zeta+\pi\beta}{2}\right)+3\sin\left(\frac{4\zeta-\pi\beta}{2}\right)+\sin\left(\frac{4\zeta-3\pi\beta}{2}\right)-16\cos\zeta}{12}$$

$$I_{2d}^{d} = \frac{2}{\pi}k\left(\int_{-\beta\frac{\pi}{2}}^{-\frac{\pi}{2}+\zeta}\cos^3(\theta-\zeta)\cos(\theta)d\theta + \int_{-\frac{\pi}{2}+\zeta}^{\beta\frac{\pi}{2}}\cos^3(\theta-\zeta)\cos(\theta)d\theta\right)$$

$$= \frac{2}{\pi}k\frac{\sin(3\zeta+2\pi\beta)+2\sin(3\zeta+\pi\beta)-2\sin(3\zeta-\pi\beta)}{32}$$

$$+\frac{2}{\pi}k\frac{-\sin(3\zeta-2\pi\beta)+6\sin(\zeta+\pi\beta)-6\sin(\zeta-\pi\beta)+12\pi\beta\cos\zeta}{32}$$

$$I_{3d}^{d} = \frac{2}{\pi}k\left(\int_{-\beta\frac{\pi}{2}}^{-\frac{\pi}{2}+\zeta}\left[-\cos^4(\theta-\zeta)\right]\cos(\theta)d\theta+\int_{-\frac{\pi}{2}+\zeta}^{\beta\frac{\pi}{2}}\cos^4(\theta-\zeta)\cos(\theta)d\theta\right)$$

$$= -\frac{2}{\pi}k\frac{3\sin\left(\frac{8\zeta+5\pi\beta}{2}\right)+5\sin\left(\frac{8\zeta+3\pi\beta}{2}\right)+5\sin\left(\frac{8\zeta-3\pi\beta}{2}\right)}{240}$$

$$-\frac{2}{\pi}k\frac{3\sin\left(\frac{8\zeta-5\pi\beta}{2}\right)+20\sin\left(\frac{4\zeta+3\pi\beta}{2}\right)+60\sin\left(\frac{4\zeta+\pi\beta}{2}\right)}{240}$$

$$-\frac{2}{\pi}k\frac{60\sin\left(\frac{4\zeta-\pi\beta}{2}\right)+20\sin\left(\frac{4\zeta-3\pi\beta}{2}\right)-256\cos\zeta}{240}$$

$$I_{4d}^{d} = \frac{2}{\pi}k\left(\int_{-\beta\frac{\pi}{2}}^{-\frac{\pi}{2}+\zeta}\cos^5(\theta-\zeta)\cos(\theta)d\theta+\int_{-\frac{\pi}{2}+\zeta}^{\beta\frac{\pi}{2}}\cos^5(\theta-\zeta)\cos(\theta)d\theta\right)$$

$$= \frac{2}{\pi}k\frac{2\sin(5\zeta+3\pi\beta)+3\sin(5\zeta+2\pi\beta)-3\sin(5\zeta-2\pi\beta)}{384}$$

$$+\frac{2}{\pi}k\frac{-2\sin(5\zeta-3\pi\beta)+15\sin(3\zeta+2\pi\beta)+30\sin(3\zeta+\pi\beta)}{384}$$

$$+\frac{2}{\pi}k\frac{-30\sin(3\zeta-\pi\beta)-15\sin(3\zeta-2\pi\beta)+60\sin(\zeta+\pi\beta)}{384}$$

$$+\frac{2}{\pi}k\frac{-60\sin(\zeta-\pi\beta)+120\pi\beta\cos\zeta}{384}$$

A.6 The coefficients I_{iq}^{q} and I_{id}^{q} of Eqs.(2.23) to (2.26) for the case $\zeta > \frac{\pi}{2}(1-\beta)$

$$I_{0q}^{q} = \frac{2}{\pi}k\left(\int_{-\frac{\pi}{2}}^{-\beta\frac{\pi}{2}}\cos(\theta-\zeta)\sin(\theta)d\theta + \int_{\beta\frac{\pi}{2}}^{\frac{\pi}{2}}\cos(\theta-\zeta)\sin(\theta)d\theta\right)$$

$$= -\frac{2}{\pi}k\frac{\cos(\zeta+\pi\beta)-\cos(\zeta-\pi\beta)+(2\pi\beta-2\pi)\sin\zeta}{4}$$

$$I_{1q}^{q} = \frac{2}{\pi}k\left(\int_{-\frac{\pi}{2}}^{-\beta\frac{\pi}{2}}\left[-\cos^2(\theta-\zeta)\right]\sin(\theta)d\theta + \int_{\beta\frac{\pi}{2}}^{\frac{\pi}{2}}\cos^2(\theta-\zeta)\sin(\theta)d\theta\right)$$

$$= \frac{2}{\pi}k\frac{\cos\left(\frac{4\zeta+3\pi\beta}{2}\right)-3\cos\left(\frac{4\zeta+\pi\beta}{2}\right)-3\cos\left(\frac{4\zeta-\pi\beta}{2}\right)}{12}$$

$$+\frac{2}{\pi}k\frac{\cos\left(\frac{4\zeta-3\pi\beta}{2}\right)+12\cos\left(\frac{\pi\beta}{2}\right)}{12}$$

$$I_{2q}^{q} = \frac{2}{\pi}k\left(\int_{-\frac{\pi}{2}}^{-\beta\frac{\pi}{2}}\cos^3(\theta-\zeta)\sin(\theta)d\theta + \int_{\beta\frac{\pi}{2}}^{\frac{\pi}{2}}\cos^3(\theta-\zeta)\sin(\theta)d\theta\right)$$

$$= -\frac{2}{\pi}k\frac{\cos(3\zeta+2\pi\beta)-2\cos(3\zeta+\pi\beta)+2\cos(3\zeta-\pi\beta)}{32}$$

$$-\frac{2}{\pi}k\frac{-\cos(3\zeta-2\pi\beta)+6\cos(\zeta+\pi\beta)}{32}$$

$$-\frac{2}{\pi}k\frac{-6\cos(\zeta-\pi\beta)+(12\pi\beta-12\pi)\sin\zeta}{32}$$

$$I_{3q}^{q} = \frac{2}{\pi}k\left(\int_{-\frac{\pi}{2}}^{-\beta\frac{\pi}{2}}\left[-\cos^4(\theta-\zeta)\right]\sin(\theta)d\theta + \int_{\beta\frac{\pi}{2}}^{\frac{\pi}{2}}\cos^4(\theta-\zeta)\sin(\theta)d\theta\right)$$

$$= \frac{2}{\pi}k\frac{3\cos\left(\frac{8\zeta+5\pi\beta}{2}\right)-5\cos\left(\frac{8\zeta+3\pi\beta}{2}\right)-5\cos\left(\frac{8\zeta-3\pi\beta}{2}\right)}{240}$$

$$+\frac{2}{\pi}k\frac{3\cos\left(\frac{8\zeta-5\pi\beta}{2}\right)+20\cos\left(\frac{4\zeta+3\pi\beta}{2}\right)-60\cos\left(\frac{4\zeta+\pi\beta}{2}\right)}{240}$$

$$+\frac{2}{\pi}k\frac{-60\cos\left(\frac{4\zeta-\pi\beta}{2}\right)+20\cos\left(\frac{4\zeta-3\pi\beta}{2}\right)+180\cos\left(\frac{\pi\beta}{2}\right)}{240}$$

$$I_{4q}^{q} = \frac{2}{\pi}k\left(\int_{-\frac{\pi}{2}}^{-\beta\frac{\pi}{2}}\cos^5(\theta-\zeta)\sin(\theta)d\theta+\int_{\beta\frac{\pi}{2}}^{\frac{\pi}{2}}\cos^5(\theta-\zeta)\sin(\theta)d\theta\right)$$

$$= -\frac{2}{\pi}k\frac{2\cos(5\zeta+3\pi\beta)-3\cos(5\zeta+2\pi\beta)+3\cos(5\zeta-2\pi\beta)}{384}$$

$$-\frac{2}{\pi}k\frac{-2\cos(5\zeta-3\pi\beta)+15\cos(3\zeta+2\pi\beta)-30\cos(3\zeta+\pi\beta)}{384}$$

$$-\frac{2}{\pi}k\frac{30\cos(3\zeta-\pi\beta)-15\cos(3\zeta-2\pi\beta)+60\cos(\zeta+\pi\beta)}{384}$$

$$-\frac{2}{\pi}k\frac{-60\cos(\zeta-\pi\beta)+(120\pi\beta-120\pi)\sin\zeta}{384}$$

$$I_{0d}^{q} = \frac{2}{\pi}k\int_{-\beta\frac{\pi}{2}}^{\beta\frac{\pi}{2}}\cos(\theta-\zeta)\sin(\theta)d\theta$$

$$= \frac{2}{\pi}k\frac{\cos(\zeta+\pi\beta)-\cos(\zeta-\pi\beta)+2\pi\beta\sin\zeta}{4}$$

$$I_{1d}^{q} = \frac{2}{\pi}k\left(\int_{-\beta\frac{\pi}{2}}^{-\frac{\pi}{2}+\zeta}\left[-\cos^2(\theta-\zeta)\right]\sin(\theta)d\theta+\int_{-\frac{\pi}{2}+\zeta}^{\beta\frac{\pi}{2}}\cos^2(\theta-\zeta)\sin(\theta)d\theta\right)$$

$$= -\frac{2}{\pi}k\frac{\cos\left(\frac{4\zeta+3\pi\beta}{2}\right)-3\cos\left(\frac{4\zeta+\pi\beta}{2}\right)-3\cos\left(\frac{4\zeta-\pi\beta}{2}\right)}{12}$$

$$-\frac{2}{\pi}k\frac{\cos\left(\frac{4\zeta-3\pi\beta}{2}\right)-16\sin\zeta+12\cos\left(\frac{\pi\beta}{2}\right)}{12}$$

$$I_{2d}^{q} = \frac{2}{\pi}k\left(\int_{-\beta\frac{\pi}{2}}^{-\frac{\pi}{2}+\zeta}\cos^3(\theta-\zeta)\sin(\theta)d\theta+\int_{-\frac{\pi}{2}+\zeta}^{\beta\frac{\pi}{2}}\cos^3(\theta-\zeta)\sin(\theta)d\theta\right)$$

$$= \frac{2}{\pi}k\frac{\cos(3\zeta+2\pi\beta)-2\cos(3\zeta+\pi\beta)+2\cos(3\zeta-\pi\beta)}{32}$$

$$+\frac{2}{\pi}k\frac{-\cos(3\zeta-2\pi\beta)+6\cos(\zeta+\pi\beta)}{32}$$

$$+\frac{2}{\pi}k\frac{-6\cos(\zeta-\pi\beta)+12\pi\beta\sin\zeta}{32}$$

$$I_{3d}^{q} = \frac{2}{\pi}k\left(\int_{-\beta\frac{\pi}{2}}^{-\frac{\pi}{2}+\zeta}\left[-\cos^4(\theta-\zeta)\right]\sin(\theta)d\theta+\int_{-\frac{\pi}{2}+\zeta}^{\beta\frac{\pi}{2}}\cos^4(\theta-\zeta)\sin(\theta)d\theta\right)$$

$$= -\frac{2}{\pi}k\frac{3\cos\left(\frac{8\zeta+5\pi\beta}{2}\right)-5\cos\left(\frac{8\zeta+3\pi\beta}{2}\right)-5\cos\left(\frac{8\zeta-3\pi\beta}{2}\right)}{240}$$

$$-\frac{2}{\pi}k\frac{3\cos\left(\frac{8\zeta-5\pi\beta}{2}\right)+20\cos\left(\frac{4\zeta+3\pi\beta}{2}\right)-60\cos\left(\frac{4\zeta+\pi\beta}{2}\right)}{240}$$

$$-\frac{2}{\pi}k\frac{-60\cos\left(\frac{4\zeta-\pi\beta}{2}\right)+20\cos\left(\frac{4\zeta-3\pi\beta}{2}\right)-256\sin\zeta+180\cos\left(\frac{\pi\beta}{2}\right)}{240}$$

$$I_{4d}^{q} = \frac{2}{\pi}k\left(\int_{-\beta\frac{\pi}{2}}^{-\frac{\pi}{2}+\zeta}\cos^5(\theta-\zeta)\sin(\theta)d\theta+\int_{-\frac{\pi}{2}+\zeta}^{\beta\frac{\pi}{2}}\cos^5(\theta-\zeta)\sin(\theta)d\theta\right)$$

$$= \frac{2}{\pi}k\frac{2\cos(5\zeta+3\pi\beta)-3\cos(5\zeta+2\pi\beta)+3\cos(5\zeta-2\pi\beta)}{384}$$

$$+\frac{2}{\pi}k\frac{-2\cos(5\zeta-3\pi\beta)+15\cos(3\zeta+2\pi\beta)-30\cos(3\zeta+\pi\beta)}{384}$$

$$+\frac{2}{\pi}k\frac{30\cos(3\zeta-\pi\beta)-15\cos(3\zeta-2\pi\beta)+60\cos(\zeta+\pi\beta)}{384}$$

$$+\frac{2}{\pi}k\frac{-60\cos(\zeta-\pi\beta)+120\pi\beta\sin\zeta}{384}$$

Appendix B

Proof of Eqs.(3.1) and (3.2)

In Eq.(3.1), the synchronous reactance in the direct axis is given by the following expression:

$$X_{du} = \frac{\alpha_{q0}}{\sqrt{3}\alpha_{qsc}}. \tag{B.1}$$

According to the IEEE standards [27], the unsaturated synchronous reactance in the direct axis is given by:

$$X_{du} = \frac{V_n}{I_{scn}}, \tag{B.2}$$

where V_n is the nominal terminal voltage per phase, and I_{scn} is the short-circuit armature current which corresponds to the field excitation that produces V_n on the air-gap line.

If the field current which produces the nominal terminal voltage on the air-gap line is I_{fn}, the slope of the air-gap line can be written as:

$$\alpha_{d0} = \frac{V_n}{I_{fn}}. \tag{B.3}$$

The short-circuit current corresponding to the field current I_{fn} can be obtained using the slope α_{dsc} of the short-circuit curve as:

$$I_{dscn} = \alpha_{dsc} I_{fn}. \tag{B.4}$$

Using Eq.(B.3), Eq.(B.4) becomes:

$$\begin{aligned} I_{dscn} &= \alpha_{dsc} I_{fn} \\ &= \alpha_{dsc} \frac{V_n}{\alpha_{d0}}. \end{aligned} \tag{B.5}$$

Thus, the expression of the direct-axis unsaturated synchronous reactance can subsequently be written as:

$$\begin{aligned} X_{du} &= \frac{V_n}{I_{dscn}} \\ &= \frac{V_n}{\alpha_{dsc} \frac{V_n}{\alpha_{d0}}} \\ &= \frac{\alpha_{d0}}{\alpha_{dsc}} \end{aligned} \tag{B.6}$$

If the terminal voltage is plotted using the line-to-line representation, the slope of the direct-axis air-gap line has to be transformed in phase values and will become:

$$\alpha_{d0} = \frac{\alpha_{do}^{L-L}}{\sqrt{3}}. \tag{B.7}$$

Thus, the unsaturated direct-axis synchronous reactance is expressed by:

$$X_{du} = \frac{\alpha_{d0}^{L-L}}{\sqrt{3}\alpha_{dsc}}. \tag{B.8}$$

Similar procedure can be applied to obtain the expression of the quadrature-axis synchronous reactance:

$$X_{qu} = \frac{\alpha_{q0}^{L-L}}{\sqrt{3}\alpha_{qsc}}. \tag{B.9}$$